

**THE PRODUCTION OF FURFURAL FROM  
SUNFLOWER HUSKS USING THE S-SUPRAYIELD  
PROCESS**

**Samantha Rachel Schay**

In fulfilment of the Master of Science in Chemical Engineering, Faculty of Engineering  
University of KwaZulu-Natal

As the candidate's Supervisor I agree/do not agree to the submission of this thesis

September 2010

Supervised by Professor M. Starzak

## DECLARATION

I **Samantha Rachel Schay**.. declare that

- (i) The research reported in this thesis, except where otherwise indicated, is my original work.
- (ii) This thesis has not been submitted for any degree or examination at any other university.
- (iii) This thesis does not contain other persons' data, pictures, graphs or other information, unless specifically acknowledged as being sourced from other persons.
- (iv) This thesis does not contain other persons' writing, unless specifically acknowledged as being sourced from other researchers. Where other written sources have been quoted, then:
  - a) their words have been re-written but the general information attributed to them has been referenced;
  - b) where their exact words have been used, their writing has been placed inside quotation marks, and referenced.
- (v) Where I have reproduced a publication of which I am an author, co-author or editor, I have indicated in detail which part of the publication was actually written by myself alone and have fully referenced such publications.
- (vi) This thesis does not contain text, graphics or tables copied and pasted from the Internet, unless specifically acknowledged, and the source being detailed in the thesis and in the References sections.

Signed:

## ACKNOWLEDGEMENTS

I would like to acknowledge the following people for their invaluable contribution to this work:

- My supervisor Prof. M. Starzak for his invaluable guidance and encouragement and his assistance with the modelling of a complex system
- Prof. D. Arnold for his supervision and assistance
- The technical staff in the school of chemical engineering for their assistance in setting up the experimental apparatus.
- The laboratory staff for providing facilities for the pentosan analysis
- Ronelle Gurney and Dhelia Raman, the two students who assisted in the running of experiments
- My parents and husband for their support, guidance and encouragement

## ABSTRACT

Since the early 1920s, when furfural was first produced, several other processing routes have been developed but none have been able to produce yields comparable to those obtained in the standard TAPPI procedure for xylan which almost completely converts xylan to furfural.

Karl Zeitsch, a German chemist, believed that the key feature of a process which could achieve high yields was rapid removal of the furfural on formation. Zeitsch suggested using gas phase HCl catalysis to produce gaseous furfural from xylan containing material, the process was titled s-Suprayield.

The experimental apparatus heated a water and HCl solution to a superheated vapour phase and then allowed for contact of the vapour and a bed of pentosan-containing material (in this case sunflower husks). The raw material was analysed by the TAPPI procedure for xylose while the product solutions were analysed for HCl, acetic acid and furfural by titration and refractive index.

Tests were performed at four acid concentrations of 0.5, 1.1, 2.2, 4.3% wt and three different temperatures viz. 163°C, 152 °C and 144 °C. The best yields of over 80% were achieved when an acid concentration of 4.3% was used. Temperature did not appear to be as significant a factor as acid concentration in affecting the furfural yield. At an acid concentration of 0.5% the yield was low ranging from 33% to 42%.

The reactor modelling was used to verify the results.

The s-Suprayield process has been demonstrated to be successful at mini-pilot plant scale indicating that a process using gaseous catalysis to produce furfural at moderate temperatures and low acid concentrations can work and that further exploration of this process should be undertaken for potential industrial use. Acid concentration was observed to have a significant effect on the reaction yield while the effect of temperature was not clear from the experimental results.

Further work should focus on understanding the reaction kinetic and the development of a laboratory scale test method for which parameters such as gas flow rate and temperature can be properly controlled. Product analysis should be more rigorous with the use of an HPLC.

## TABLE OF CONTENTS

<b>1. INTRODUCTION.....</b>	<b>1</b>
<b>2. LITERATURE REVIEW.....</b>	<b>3</b>
2.1 FURFURAL – ITS MANUFACTURE AND USES .....	3
2.2 TECHNOLOGY FOR FURFURAL PRODUCTION.....	6
2.3 HEMICELLULOSE STRUCTURE .....	13
2.4 LIQUID PHASE KINETICS OF XYLAN HYDROLYSIS .....	15
2.5 HYPOTHETICAL MECHANISM OF GAS-PHASE CATALYSIS .....	21
2.5.1 <i>HCl dissociation on ice</i> .....	21
2.5.2 <i>The significance of gas phase catalysis to s-Suprayield</i> .....	23
<b>3. THESIS OBJECTIVES.....</b>	<b>24</b>
<b>4. EXPERIMENTAL WORK.....</b>	<b>25</b>
4.1. EQUIPMENT.....	25
4.1.1. <i>Plant description</i> .....	25
4.1.2. <i>Reactor design</i> .....	27
4.1.3. <i>Heating options</i> .....	27
4.1.4. <i>Utilities and control</i> .....	31
4.2. PREPARATION FOR TESTWORK .....	32
4.2.1. <i>Pump calibration</i> .....	32
4.2.2. <i>Raw material and bed characterisation</i> .....	32
4.3. EXPERIMENTAL PROCEDURE.....	36
4.3.1. <i>Sample preparation:</i> .....	36
4.3.2. <i>Start up</i> .....	36
4.3.3. <i>Experimental run</i> .....	36
4.3.4. <i>Shutdown</i> .....	37
4.4. SAMPLE ANALYSIS .....	38
4.4.1. <i>Potentiometric Titration</i> .....	38
4.4.2. <i>Refractive index</i> .....	40
<b>5. RESULTS .....</b>	<b>45</b>
5.1. STATISTICAL TESTS ON DATA .....	52
<b>6. MODELLING .....</b>	<b>54</b>
6.1. PHYSICAL DESCRIPTION OF THE PROCESS.....	54
6.2. SIMPLIFYING ASSUMPTIONS .....	54
6.2.1. <i>The particle model</i> .....	55
6.2.2. <i>The reactor model</i> .....	57
6.3. MODELLING OF THE REACTION MECHANISM .....	57

6.4.	REACTION RATE KINETICS .....	58
6.5.	REACTION STOICHIOMETRY .....	60
6.6.	REACTOR MODELING.....	61
6.6.1.	<i>Gas-phase material balances</i> .....	61
6.6.2.	<i>Solid-phase material balances</i> .....	62
6.6.3.	<i>Calculation of measurables</i> .....	63
6.7.	OPTIMISATION OF MODEL PARAMETERS .....	64
6.8.	MODELLING RESULTS AND DISCUSSION .....	65
<b>7.</b>	<b>CONCLUSIONS AND RECOMMENDATIONS .....</b>	<b>72</b>
7.1.	CONCLUSIONS .....	72
7.2.	RECOMMENDATIONS .....	72
<b>8.</b>	<b>REFERENCES.....</b>	<b>73</b>
	<b>APPENDIX A: CALCULATION METHODS FOR SUPERHEATER .....</b>	<b>76</b>
	<b>APPENDIX B: FURTHER DETAIL ON CALIBRATIONS AND ASSAYS.....</b>	<b>79</b>
	<b>APPENDIX C: TITRATION MATLAB CODE AND CURVES .....</b>	<b>85</b>
	<b>APPENDIX D: SUMMARISED RESULTS TABLES .....</b>	<b>100</b>
	<b>APPENDIX E: SAMPLE RAW DATA SHEET .....</b>	<b>119</b>
	<b>APPENDIX F: STATISTICAL ANALYSIS .....</b>	<b>124</b>
	<b>APPENDIX G: MATLAB CODES FOR MODELLING.....</b>	<b>126</b>
	<b>APPENDIX H: INITIAL MODEL DEVELOPMENT.....</b>	<b>133</b>
	<b>APPENDIX I: DIFFUSION CALCULATION .....</b>	<b>136</b>
	<b>APPENDIX J: MODEL RESULTS – PROFILES FOR EACH RUN .....</b>	<b>138</b>

## LIST OF FIGURES

Figure 1: Furfural molecular structure	3
Figure 2: Post-reaction furfural product refining (Kirk-Othmer Encyclopaedia of Chemical Technology)	6
Figure 3: Furfural-water phase diagram (Zeitsch, 2000a)	11
Figure 4: Fischer projections for d-xylose and arabinose (Hart et al., 1999)	14
Figure 5: Hydrolysis mechanism for depolymerisation of xylan to xylose monomers (Zeitsch, 2000a)	18
Figure 6: Mechanism for the dehydration of xylose to furfural (Antal et al., 1991)	19
Figure 7: Plant diagram	25
Figure 8: Figure showing vapour exit temperature at different nichrome wire coil spacing	28
Figure 9: Superheater temperature profiles at different voltages	29
Figure 10: A temperature/time profile for the QVF® condenser and superheater over 90 minutes	30
Figure 11: Pump calibration curve	32
Figure 12: Percent contribution of each size fraction	33
Figure 13: Titration curve for run 1, sample 1	39
Figure 14: Refractometer calibration curve for concentration in g/L	41
Figure 15: Refractometer calibration curve for concentration in % wt	41
Figure 16: RI for varying mass % of furfural in water at constant (1.2%) acetic acid concentration	42
Figure 17: RI for varying mass % of furfural in water at constant (1.3%) hydrochloric acid concentration	43
Figure 18: RI for varying mass % of HAc in water at constant (1.3%) hydrochloric acid concentration	43
Figure 19: Comparison of furfural production profiles at a reaction temperature of 160°C and a range of HCl concentrations	46
Figure 20: Comparison of furfural production profiles at a reaction temperature of 150°C and a range of HCl concentrations	46
Figure 21: Comparison of furfural production profiles at a reaction temperature 140°C and a range of HCl concentrations	47
Figure 22: Comparison of furfural production profiles at 4%HCl	48
Figure 23: Comparison of furfural production profiles at 2%HCl	48
Figure 24: Comparison of furfural production profiles at 1%HCl	49
Figure 25: Comparison of furfural production profiles at 0.5%HCl	49
Figure 26: Furfural yield (%) versus temperature at different acid concentrations	50

Figure 27: Furfural yield (%) versus acid concentration at different temperatures	50
Figure 28: HCl concentration in product solution over time	51
Figure 29: Comparison of experimentally determined concentration and that determined by the model for (a) furfural, (b) acetic acid and (c) hydrochloric acid	66
Figure 30: Contribution of each run to the total error (performance index)	66
Figure 31: Comparison of experimentally determined concentration versus time profiles (shown in red) and predicted profiles (shown in green) for furfural, acetic acid and hydrochloric acid for each run	70
Figure 32: Concentration profiles	71



**LIST OF TABLES**

Table 1: Products of xylose decomposition in water at high temperatures	5
Table 2: Hydrolysis products of hemicellulose from different plant material (Slavianskii, 1962) (translated from the Russian)	6
Table 3: Industrial processes for furfural production	9
Table 4: Furfural yield at the temperatures and acid concentrations tested	52
Table 5: Table of statistical data	52
Table 6: Relevant $F_0$ values at various levels of significance	53
Table 7: Tested $k_{gw}$ values and corresponding $y(x_c)$ values	56
Table 8: Modelling results with reaction rate constants calculated at 160°C	65

## 1. INTRODUCTION

Furfural is a useful chemical particularly as a raw material for the production of furan resins for which there are several industrial applications. It is also advantageous that the raw material for furfural production is found in the waste products after the processing of food crops.

Furfural is produced from the acid catalysed dehydration of D-xylose, a pentose sugar. D-xylose occurs as a significant member of hemicellulose, a polymer which forms part of plant cell walls in association with cellulose and lignin. Hemicellulose exists predominantly in the structural components of plants e.g. the hulls of sunflower seeds and oat husks and it can also occur in sugarcane bagasse which remains after the sugar has been extracted.

Furfural has been produced since the early 1920's when Quaker Oats first went into production. The furfural was produced in order to diminish waste volumes and to generate income from the leftover oat hulls from their animal feed plant. Furfural was originally produced in a high temperature, high pressure process, using high concentrations of sulphuric acid. These conditions resulted in a high cost of production of furfural from both a capital perspective, due to having to account for the high corrosiveness of the sulphuric acid, and an operational perspective, due to the high pressures and temperatures which had to be maintained. The Quaker Oats process had low yields of the order of 53%, was also detrimental to the environment and was also a batch process and therefore was not an ideal means by which to produce furfural.

Several other methods have been developed in subsequent years but none of them has been able to obtain very high yields, particularly when one considers that the TAPPI analytical procedure for furfural is able to achieve close to 100% theoretical conversion of pentose sugars to furfural. If it can be achieved in a bench scale test, it should be possible to achieve yields close to this in industrial applications. Karl Zeitsch, a German chemist, proposed a method of furfural production based on his understanding of the standard Tappi procedure for pentosan determination.

According to Zeitsch, the key factor to the success of this process is the rejection of furfural to the vapour phase. It is generally recommended that the furfural be removed from the reaction zone rapidly to minimise loss reactions such as resinification and condensation which occur between the furfural produced and the intermediates in the furfural production process. Producing furfural directly in the gas phase aids its rapid removal by the carrier gas.

Based on this thinking and studies on ozone depletion, Zeitsch developed the s-Suprayield process for furfural production. In s-Suprayield, as for other furfural producing process, furfural is produced from the hydrolysis and subsequent dehydration of hemicellulose. Unlike the other processes which use liquid phase acid catalysts, the catalyst used for s-Suprayield is gas phase HCl. Since ozone depletion in stratospheric ice crystals has been observed to be catalysed by gas phase HCl, it was assumed that due to the structural similarities of the ice crystals and hemicellulose, the catalysing properties of HCl in the gas phase could also be applicable to hemicellulose. Thus a gas phase reaction for furfural production is possible.

It has previously been thought that a process such as s- Suprayield, which relies on gaseous acid catalysis, is not possible at moderate temperatures and pressures since this type of catalysis relies on ionisation of the acid – a process which typically occurs in the gas phase at over 1000°C. Studies of ozone depletion reactions in the stratosphere however have indicated that there may be a possibility of acid dissociation occurring at low pressures and temperatures as a result of it being catalysed by ice crystals in polar stratospheric clouds.

## 2. LITERATURE REVIEW

### 2.1 Furfural – its manufacture and uses

Furfural has the chemical formula  $C_5H_4O_2$  with the cyclical structure shown in Figure 1:

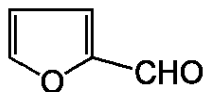


**Figure 1: Furfural molecular structure**

Furfural is produced when hemicellulose contained in plant matter is subjected to acid conditions at high temperatures and often high pressures. The xylan polymer breaks down into pentose sugars (xylose) which are subsequently dehydrated to furfural.

Furfural has many uses as an intermediate product and is “the most economical source of furans” (Lázaro et al., 1986). It is one of the few carbohydrates from biomass sources which can compete with hydrocarbon chemicals without subsidies (Wondu Business and Technology Services, 2006).

Furfural itself is of limited use but it is employed as the raw material for the synthesis of other chemicals (Zeitsch, 2000a, Win, 2005, Wondu Business and Technology Services, 2006). Furfural’s main use as an intermediate product is in the manufacture and production of furan resins which among other uses finds application as a binding agent in foundry technologies. Furfural also finds use to a lesser degree in the manufacture of specialist adhesives, plastics, nylons, flavourants, pesticides, fungicides and nematocides. Furfural itself is also used as a selective solvent in the petroleum industry for the production of lubricants as well as a butadiene extractant and a refining solvent in the manufacture of synthetic rubber. Furfural’s usefulness also lies in its thermosetting properties, physical strength and corrosion resistance (Dias et al., 2005a, Win, 2005, Wondu Business and Technology Services, 2006, Zeitsch, 2000a, Dias et al., 2005b). Reference has also been made to its use in cigar manufacture, perfume, as a food preservative and even as a fuel (Peters, 1948).

Furfural was first produced in 1832 by Dobreiner (Peters, 1948). Furfural has many uses and can be made from diverse sources including olive pips (Montane et al., 2002) and dairy manure (Liao et al., 2004).

The production of furfural on an industrial scale was initiated by the Quaker Oats company at Cedar Rapids, Iowa (Brownlee and Miner, 1948). This company frequently had an abundance

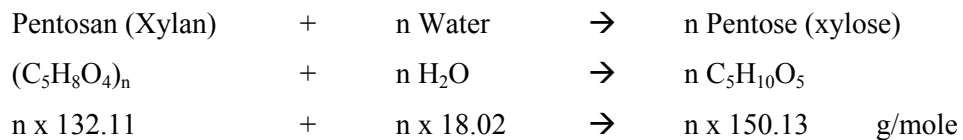
of oat hulls for which there was no market. The company initially tried to dispose of the waste as animal feed, and in a quest to increase digestibility and palatability found that acid treatment of the hulls produced furfural. A process was developed based on laboratory experiments and the availability of unused iron pressure cookers at the f plant. There was no pilot plant phase and no attempt to design specific equipment that would produce the highest possible yield.

The production of furfural falls within the concept of biomass refining. This is a process which involves the use of chemical treatments to separate raw material into its main polymeric components, viz. cellulose, hemicellulose and lignin, which can then be recovered separately either as polymers or as decomposition products. These decomposition products may then be converted into saleable end products. (Mylerly et al., 1981) as referred to by (Parajó et al., 1995).

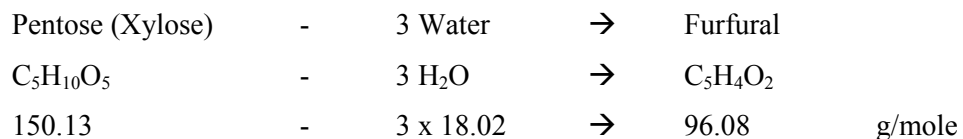
Furfural production from hemicellulose is a two step process. The first step is a rapid, high yield, acid catalysed hydrolysis of hemicellulose to pentose sugars. This is followed by a second step involving dehydration of the resulting pentose sugars to produce furfural. (Mansilla et al., 1998)

The stoichiometry for furfural production from hemicellulose is as follows (Zeitsch, 2000a):

Hydrolysis:



Dehydration:



From this stoichiometry the theoretical yield can be determined:  $Y_{th} = 96.082/132.114 = 72.7\%$

These reaction deals only with the dehydration of the xylose to furfural; however during this reaction the hemicellulose can also form other products which result from the exposure of xylose and other hemicellulose components to water at high temperatures and this is summarised by Antal et al (1991) in the Table 1:

**Table 1: Products of xylose decomposition in water at high temperatures**

	<b>Isomerisation</b>	<b>Dehydration</b>	<b>Fragmentation</b>	<b>Condensation</b>
			Formic acid	
			Lactic acid	
<b>Major</b>	Lyxose	2-Furaldehyde	Dihydroxyacetone	
			Glyceraldehyde	
			Acetol	
			Glycolaldehyde	
			Formaldehyde	
<b>Minor</b>		Reductic Acid	Acetaldehyde	Resin
			Crotonaldehyde	

These products result from the reaction of furfural with intermediates in the furfural formation process leading to losses in the furfural produced from the reaction in the liquid phase (Antal et al., 1991). In addition to the reactions and products described in the table, chlorination, nitration and sulphonation may also occur as a result of interaction with the strong acids generally associated with furfural production (Zeitsch, 2000a).

Furfural has been and is currently produced using a range of different methods but all furfural production methods use a similar process whereby raw material is placed in a reaction vessel which is heated with high pressure steam. Enough excess steam is used to drive the furfural away from the reaction zone in the vapour phase to limit the occurrence of loss reactions. The furfural rich vapour leaving the reactor is first condensed before being fed into a stripping column. The stripping column produces an enriched furfural-water distillate mixture from overhead. The distillate mixture is condensed and then passes into a decanter from which the water layer containing +/- 8% furfural is removed and recycled back to the stripper column. The furfural layer from the decanter is then fed to a dehydrating column before going for further distillation (Kirk-Othmer Encyclopaedia of Chemical Technology). This is shown in Figure 2:

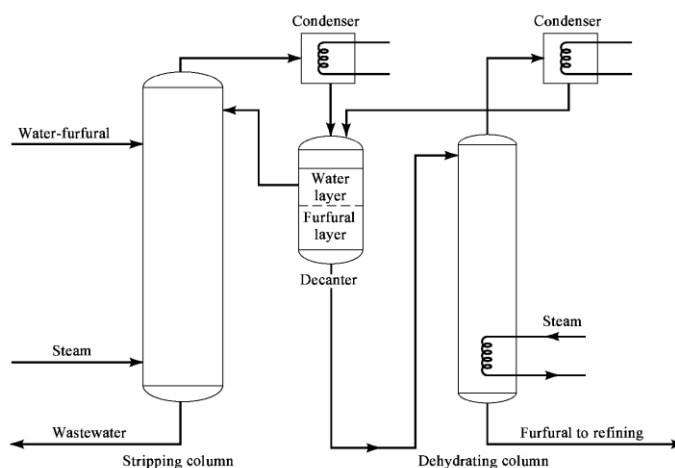


**Figure 2: Post-reaction furfural product refining (Kirk-Othmer Encyclopaedia of Chemical Technology)**

## 2.2 Technology for furfural production

Different methods of furfural production have been developed for two reasons. On the one hand different processes have arisen to deal with the lignocellulosic waste products from different industries e.g. sugarcane bagasse, oat hulls, sunflower husks, wood pulp etc. Different methods have also been developed in an effort to find more cost effective means of furfural production.

Hemicellulose is the key component of the raw material from which furfural is produced as it is the xylose monomers found in the hemicellulose which are dehydrated to furfural. Hemicellulose is also more reactive than the cellulose and lignin with which it is associated. Different feed stocks not only have different amounts of hemicellulose in them but the nature of the hemicellulose itself can vary in terms of composition and structure (See 2.3). A breakdown of the different hydrolysis products of hemicellulose is shown in Table 2:

**Table 2: Hydrolysis products of hemicellulose from different plant material (Slavianskii, 1962) (translated from the Russian)**

Type of Material	Reducing Part %(m/m) Dry Material	Reducing Components of Hemicellulose Hydrolysate, %(m/m)					
		Acetic Acid	Uronic Acid	Xyloses	Arabinoses	Galactoses	Glucoses
Corn "waste"	42	9.5	11.0	72.0	7.0	3.0	7.0
Cotton husks	26	13.5	15.0	75.0	5.0	2.0	3.0
Sunflower husks	23	13.7	29.0	56.0	9.5	3.5	2.1
Reed	23	10.0	16.0	61.0	10.0	4.0	4.0
Oat hulls	38	6.4	12.0	76.0	7.0	3.0	2.0
Oak wood (an ode - Bina)	20	16.0	18.0	67.0	4.0	6.0	5.0

Table 2 shows how the amount of hemicellulose (reducing part) varies from 42% in corn waste to 20% in oak wood. Of further interest is the variation in the xylose concentration which despite being the major component of the hemicellulose in all material ranges from 76% of the hemicellulose in oat hulls to only 56% of the hemicellulose in sunflower husks.

In Table 2 it was also observed that the sum of the mass fractions of the reducing components exceeds 100% by the amount of acetic acid. It was therefore assumed that the xylose mass fraction included the acetyl groups attached to the xylose and therefore acetic acid is accounted for twice.

Several processes for furfural production exist (McKillip and Zeitsch, 2002):

- The Quaker Oats Batch Process in which the raw material is soaked in dilute sulphuric acid before being placed in spherical or cylindrical reactors capable of rotation around a horizontal axis. Steam is then passed through these reactors and the product vapour collected. The acid is diluted so that a moisture content of 42% is achieved after heating.
- The Chinese Process is similar to the Quaker Oats process as it also uses raw material soaked in dilute sulphuric acid but this process uses vertical cylindrical batch reactors.
- The Agrifurane/Petrol Chimie Process uses several vertical, cylindrical, batch reactors operated in series with steam passing from one reactor to the next. The steam entering the first reactor increases the reactor temperature to 177°C then passes into the second reactor. Some primary steam is added to the second reactor to make up for the pressure lost in the first reactor. This is repeated for the third, fourth etc. reactors. In order to maintain a pressure drop to ensure flow of the steam the temperature to the last reactor is only 161 °C. An intricate pipe and valve system is required to ensure, that although run at different temperatures, the raw material charge in each reactor has the same reaction time. The reactor residue is dewatered and the 1% sulphuric acid solution is recycled to prepare a slurry of the fresh raw material at a solid-to-liquid ration of 1:6 by weight.
- The Continuous Quaker Oats Process uses bagasse as a raw feed. The raw material is pretreated with steam prior to being fed into a horizontal reactor by means of an auger press. The auger press serves as both a feeder and a pressure lock. The equipment is made with mild steel but the reactor itself is also lined with acid resistant bricks. The raw material is propagated through the reactor using stainless steel transport paddles and the dilute sulphuric acid (0.8%) is introduced by multiple spray nozzles. The solid and vapour phase flow co-currently. The steam is introduced to maintain a moisture content of 40 to 45% and maintain a temperature of 184°C. Discharge of the product vapour and solid residue is achieved through the use of a double lock ram valve system and product and residue separation is by means of a cyclone.
- The Escher Wyss Process uses a fluidised bed reactor system in which raw material is fed intermittently into a vertical reactor where steam is introduced continuously from the bottom to maintain a fluidised bed, to provide heating and to strip the bed. The



residue is ejected intermittently from the bottom whereas the steam, flowing counter-currently exits from the top. Either sulphuric acid is added to the process or the innate acetic and formic acids are used as catalysts. The reaction temperature is 170°C while the reaction time is 45 min when sulphuric acid is used. This process is no longer used as the fluidised bed process is not suitable due to the characteristic wide range in residence times.

- The Rosenlew Process uses a similar procedure to the Escher Wyss process as raw material is also fed intermittently into the top of a vertical reactor, while the residue is ejected intermittently from the bottom. Steam is used for both heating and stripping as with many of the other processes and it is fed continuously at the bottom of the reactor so that steam flows counter currently to the raw material. In this case however the bed is not fluidised. The acetic acid formed during the reaction acts as the acid catalyst.

Table 3 presents a summary of the features of the main industrial processes used for furfural production. It should be noted that the yield is reported as a percentage of theoretical yield and therefore is on the basis of pentosan and not total biomass.

**Table 3: Industrial processes for furfural production**

<b>Process</b>	<b>Acid</b>	<b>Temperature /Pressure</b>	<b>Residence Time</b>	<b>Reactor</b>	<b>Yield (Percentage of Theoretical)</b>
<b>Quaker Oats (Batch)</b>	Sulphuric Acid (2.25kg acid per 100kg dry raw material)	153°C	5 hours	Rotating, spherical or cylindrical, carbon bricks to control corrosion	52.3%
<b>Chinese Batch</b>	Sulphuric Acid	6.1-7.1 bar	4-5 hours	Mild steel cylinders, walls 50mm thick to control corrosion	~50%
<b>Petrol Chimie</b>	Sulphuric Acid	Initial: 177°C (9.35 bar)		Series of reactors including a costly valve control system and belt filters.	
<b>Quaker Oats (Continuous)</b>		650°C 11.0 bar	1 hour		55%
<b>Escher Wyss</b>	Sulphuric Acid (3%)	170°C	45 minutes	Fluidised bed reactor	
<b>Rosenlew</b>	Innate acids	180°C 10 bar	120 minutes		
<b>Supratherm</b>		200-240°C			
<b>Stake</b>	Innate acids	230°C	6.3 minutes		66%

The first process in Table 3, the Quaker Oats batch process, has been discussed in detail in Section 2.1; however an additional disadvantage not discussed previously is the fact that it is a batch process as are the Chinese process and the Petrol Chimie process. The Chinese process is very similar to the Quaker Oats process and therefore obtained similar results, although in this method thick mild steel walls were used to offset corrosion compared to the use of carbon bricks in the Quaker Oats process. The Petrol Chimie process used higher temperatures and pressures than the Quaker Oats and Chinese processes and required the use of a complex valve system which was expensive. The Quaker Oats continuous process used even higher temperatures of 650°C and pressures of 10 atmospheres resulting in a reduced residence time of 1 hour (reduced from the 4-5hours of the batch and Chinese process). The Escher Wyss process used a reaction temperature of only 170°C and a reduced reaction time of 45 minutes; however the fluidised bed used for this process was not suited to the process. Both the Rosenlew and Stake methods had the cost saving advantage of using innate acids (i.e. the acetic acid arising from the hemicellulose hydrolysis). The Rosenlew process had a more typical reaction time of

120minutes while the Stake process resulted in a rapid reaction with a residence time of only 6.3minutes and a yield of 66%.

The researchers mentioned below are pursuing laboratory scale testwork to find further means of improving the selectivity and yield of furfural. If any of these methods is found to be successful, the process will be scaled up for industrial application. As the common trend is to remove the furfural from the reaction environment as soon as it is formed, many of the newer procedures have utilised liquid-liquid equilibria to remove the furfural to another liquid phase rather than removing it by vaporisation.

Moreau et al (1998) studied the option of using H-form zeolites as an alternative to the mineral acids commonly used for hemicellulose hydrolysis. It was found that a high selectivity to furfural could be attained at 170°C as long as the conversion is kept low. The process was investigated in a liquid-liquid, water/methylisobutylketone mixture as well as a water/toluene mixture. The organic phase acted as an extraction solvent for the furfural. In this way the furfural formed was removed from the aqueous acid solution and thus condensation and resinification could be minimised. More recently Dias et al (2005b) attempted the use of Keggin-type heteropolyacids as a catalyst but achieved yields of under 70% in 8 hours at 140°C. Again a liquid-liquid solvent was used to extract the furfural to the organic phase. It is important that the organic solvent used be one with which the furfural will not react. The authors claim that heteropolyacids have many advantages over mineral acids such as their low volatility and corrosiveness, their high flexibility and safe handling. Another advantage is that they result in no sulphonation, chlorination or nitration, which generally results in furfural losses when strong mineral acids are used.

In another study, Dias et al. (2005a) have attempted the use of surfactant templated microporous silicas possessing sulphonic acid groups as catalysts. This is another variation of heterogeneous solid catalysis. In this instance the less ordered the microporous hybrid material, the lower the furfural selectivity. Using a MCM-41-SO<sub>3</sub>Hc catalyst was found to give a furfural yield of 70% with the selectivity remaining reasonably high at high conversions unlike the case of zeolites which could only produce good selectivity at low xylose conversions (Moreau et al., 1998). The success of this particular method is assumed to be related to the porous structure of the catalyst which allows the furfural to diffuse rapidly out of the catalyst. The problem with this process is that there is not yet a method for regeneration of the catalyst and the process will not be viable until the catalyst can be recycled.

The TAPPI procedure for complete conversion of xylose to furfural was developed by Hughes and Acree (1938) and involves the use of 12% hydrochloric acid saturated with sodium chloride. This process is known as the 'analytical procedure'. If this process is known to have yields of 100%, one must ask why no other industrial process has been able to exceed 66 % yields?

It is suggested by Zeitsch (2000a) that the high yield in the analytical process is the result of the furfural being rejected into the vapour phase as it is formed. This is due to the reaction taking place at a temperature of 110°C as result boiling point elevation caused by the dissolved solute and the fact that the processes takes place under continuously boiling conditions. The situation is explained in the T-X-Y diagram shown in Figure 3 below.

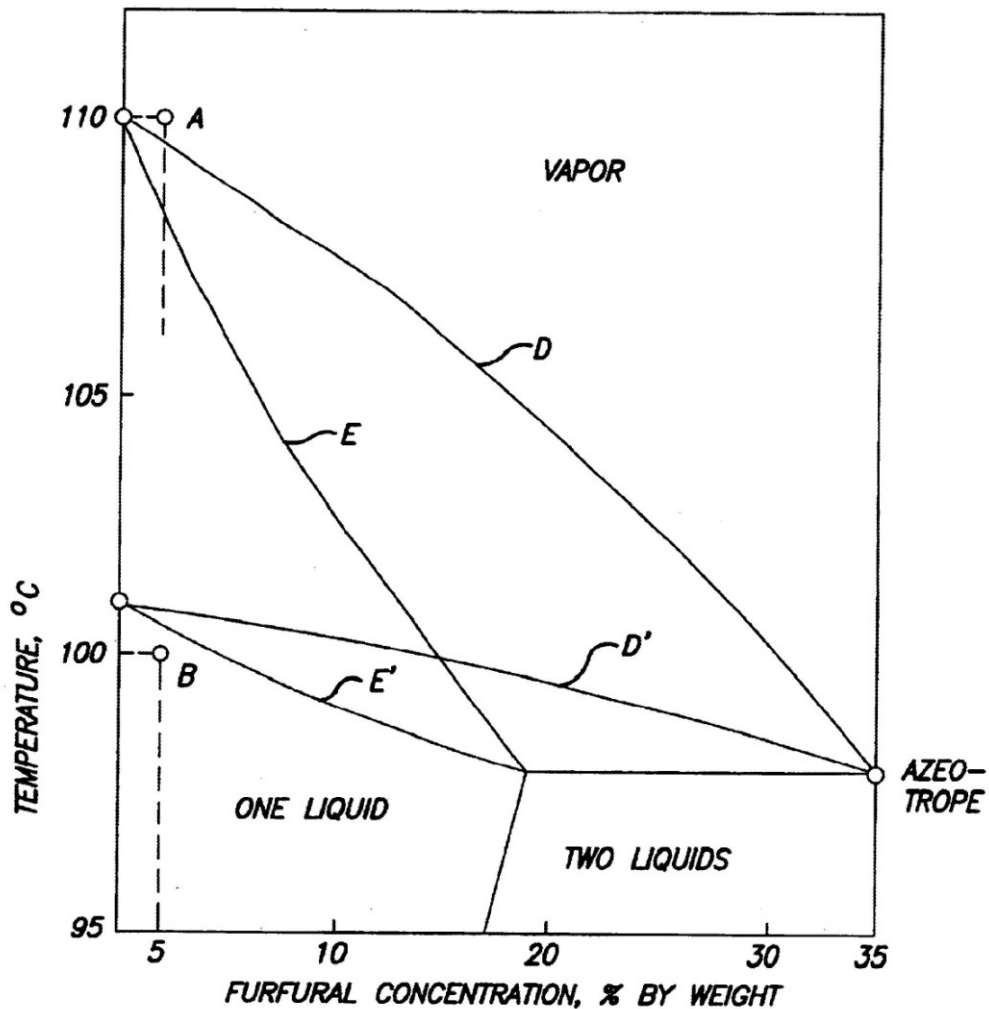


Figure 3: Furfural-water phase diagram (Zeitsch, 2000a)

In Figure 3 the lines D and E are the dew point and vapour point curves respectively for a 12% HCl solution saturated with sodium chloride with small amounts of dissolved furfural as for the analytical process. This shows that the boiling point of this solution is 110°C. A low concentration of furfural produced in such a solution maintained at boiling point is produced in the vapour phase as shown by point A on the diagram. Producing furfural in the vapour phase limits the interaction with itself and intermediates under conditions favourable for loss reactions. On the other hand the lines D' and E' shows the dew point and vapour point curves for an aqueous solution of furfural and water with a boiling point of 101°C which is typical of industrial processes using steam injection. In industrial processes, heated by condensing steam, furfural is produced at point B which is in the liquid phase and will therefore undergo 'loss reactions' with the intermediates in the liquid phase.

All of the laboratory methods being developed indicated a move toward the removal of newly formed furfural from the reacting system as it is believed that if the furfural is removed from the reaction solution it is unable to undergo loss reactions (McKillip and Zeitsch, 2002)

Based on the discovery of ice catalysed dissociation of HCl, which will be discussed in section 2.5.1, Zeitsch proposed that a similar dissociation could take place on hemicellulose – the raw material from which furfural is produced.

Zeitsch (2001) claims that when the process was attempted at a temperature of 155°C by placing comminuted raw material in a reactor and exposing it to superheated steam into which a small quantity of vaporised HCl had been dispersed, a product stream containing furfural, low boiling compounds and carboxylic acids was produced. No quantitative data were provided with this document.

Not only does this process have the potential to produce furfural at high yields, it also has several other advantages over existing technology such as (Zeitsch, 2001):

1. The process runs at atmospheric pressure
2. The temperatures are moderate.
3. It is likely to be simpler to recover the acid from the gas than from the liquid residues produced in other processes.

One of the most notable disadvantages is that the highly corrosive HCl and steam combination would require special materials to combat corrosion; however this is common to many of the other methods.

The use of steam and hydrogen chloride gas to produce furfural from hemicellulose is not entirely new. In 1921 it was discovered that by passing dry steam in the presence of hydrogen chloride vapour through a preheated hemicellulose bed, acetic acid, furfural and methyl alcohol could be produced (Pringsheim, 1921).

### 2.3 Hemicellulose structure

In order to better understand this section the following terms should be understood:

- Hemicellulose: A structural component of cell walls made up of pentosan polymers
- Pentosan: A polymer consisting of pentose (5 –Carbon) sugars predominantly xylan and araban
  - Xylan: Consists mainly of xylose monomers
  - Araban: Consists of xylose and arabinose monomers terminating in an arabinose molecule
- Pentose: 5-Carbon sugar
  - Xylose
  - Arabinose

Hemicellulose may be defined as the name given to the water-insoluble polysaccharides that are usually found with celluloses (Hagglund, 1951) or it may be defined as those components of the cell wall which are found to dissolve readily in hot, dilute mineral acids (Wise, 1952).

Hemicellulose is a structural component of plant cell walls, accounting for one third of the material in plants (Chaikumpollert et al., 2004). It is connected with lignin by covalent bonds and may be connected to other plant cell components by chemical bonds (Yang et al., 2006) as well as hydrogen bonds (Sun et al., 2004b). The strands of cellulose (hexose) chains are reported to be surrounded by thin layers of pentosan chains in the cell wall (Voss et al., 1938, Ott et al., 1952, Klauditz, 1941).

Hemicellulose has a macromolecular structure (Wise, 1952) and is generally amorphous (Percival, 1953, Sun et al., 2004a) however it can become more crystalline and thermally stable with lower branching (Chaikumpollert et al., 2004). Cellulose on the other hand is crystalline (Sun et al., 2004a).

Xylan is the predominant component of hemicellulose but other components such as araban, acetyl groups and uronic substituents are present in smaller quantities (Garrote et al., 2004). D-galactose and D-glucose monomers may also be found to a lesser extent in the polymers

constituting hemicellulose from some plants (Chaikumpollert et al., 2004). The polymers consist mainly of xylose monomers with arabinose being the second major component (Sun et al., 2004a). The chains consist of xylose units (Wise, 1952) linked by  $\beta$ -1,4-linkages (Vierhuis et al., 2001, Percival, 1953) as opposed to cellulose which consists of  $\alpha$ -1,4-glycosidic linkages between glucose molecules (Wise, 1952). The xylan chains terminating with arabinose are termed araban (Garrote et al., 2004, Ott et al., 1952).

The composition of hemicellulose varies for different species of plant (Vierhuis et al., 2001). The compositional differences arise mainly due to the manner of substitution of the principle xylan chain (which is related to the arabinose to xylose ratio) and the manner and sequence of linkages between arabinose and xylose. The composition affects the macro-structure of the hemicellulose because the number of branch points can be correlated to the arabinose concentration (Chaikumpollert et al., 2004).

At this point, for the sake of process chemistry it is necessary to look at the various components making up the hemicellulose chain:

- Firstly xylose, the most predominant component of the hemicellulose, and arabinose have the same chemical formulae of  $C_5H_{10}O_5$ . The molecules are diastereomers of each other each with the Fischer projections shown in Figure 4:

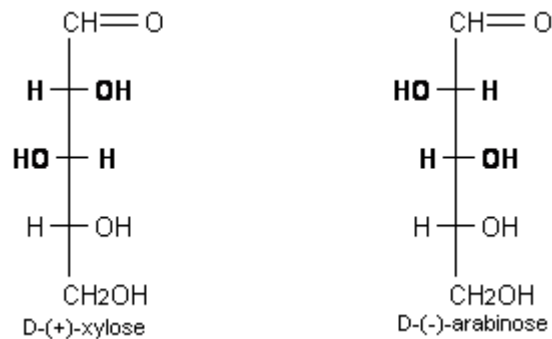


**Figure 4: Fischer projections for d-xylose and arabinose (Hart et al., 1999)**

Although arabinose sugars are released as part of the hydrolysis reaction more quickly even than xylose, these sugars do not decompose under conditions which result in xylose decomposition to furfural (Rodriguez-Chong et al., 2004) and it was therefore assumed that arabinose decomposition products would not form a significant part of the product solution.

- The next most predominant species are uronic acids. An uronic acid is a sugar acid which has both a carbonyl functional group and a carboxylic acid functional group. An example of this is glucuronic acid.

The uronic acid–xylose bonds are very resistant to acid hydrolysis when compared to the acetyl and xylosidic bonds which cleaved more easily (Johnson, 2003).

- Glucose and galactose have the same chemical formula of  $C_6H_{12}O_6$  (Hart et al., 1999). Rodriguez-Chong et al.(2004) reported in their experiments on sugar cane bagasse using nitric acid that while the glucose was released as a hydrolysis product there was no detection of the decomposition product hydroxymethylfurfural.

It is necessary to determine the molar ratio of the acetyl groups to the xylose in order to determine the reaction stoichiometry. From Table 2, it was assumed that the acetic acid arises from the acetyl groups on the xylose members. The molar mass of acetyl-containing xylose was therefore:

$$MM_{xylose} + X \times MM_{acetyl}$$

where  $MM_{xylose}$  is the molar mass of xylose (g/mol)  
 $X$  is the mole fraction acetyl groups per mole of xylose  
 $MM_{acetyl}$  is the molar mass of the acetyl group ( $C_2H_2O-$ )

This calculation was used together with the mass ratio of 13.7% acetic acid to 56% xylose to determine  $X$  to be 0.74. This means that 0.74 moles of acetic acid would be produced per mole of xylose for sunflower husks.

## 2.4 Liquid phase kinetics of xylan hydrolysis

Plant material is resistant to biological and chemical attack due to the existence of bonds between hemicellulose and other cell wall components (Rodriguez-Chong et al., 2004, Vierhuis et al., 2001) as well as branching groups in the hemicellulose structure (Yang et al., 2006). Lignin, which is one of the components to which hemicellulose may bond, is hydrophobic and therefore hinders proton access to the hemicellulose (Rodriguez-Chong et al., 2004). These factors inhibit reactions of the hemicellulose and therefore extraction of hemicellulose is required to allow reactions to take place. This extraction takes place by the hydrolysis of the ester linkages which form between the different cell wall components (Yang et al., 2006). Under alkaline conditions, alkaline hydrolysis of the ester or ether linkages takes place thus liberating hemicellulose from the lignocellulosic matrix and extracting them into aqueous media (Sun et al., 2004b). Strong alkali solutions are required for this (Vierhuis et al., 2001).



Hemicellulose is much more susceptible to hydrolysis than cellulose (Maloney et al., 1985) and it is soluble in hot, dilute mineral acids (Wise, 1952). The rate of hemicellulose hydrolysis is strongly influenced by acid concentration and temperature while the cellulose degradation, although also dependent on hydrolysis conditions proceeds at a much slower rate. This means that when both substrates are present in the system, first hemicellulose hydrolysis proceeds, then cellulose degradation occurs only after the xylan conversion is underway (Maloney et al., 1985).

The araban side chains are highly susceptible to hydrothermal degradation and the formation of intermediate reaction products in the path to furfural production (Garrote et al., 2004). Under harsh conditions furfural can be produced from the pentose sugars arising from both xylose and arabinose.

Many analyses have found that the xylan hydrolysis rate is not uniform and at a conversion of about 70% the rate slows (Maloney et al., 1985). Several different reasons for this have been suggested:

- Mass and energy transport effects which are affected by structure and accessibility (Maloney et al., 1985, Garrote et al., 2004, Rodriguez-Chong et al., 2004). This is particularly important when particle size is large and when there is a high solids concentration (Rodriguez-Chong et al., 2004)
- Different intrinsic reactivity of the different xylose fractions (Maloney et al., 1985)
- If the reaction occurs at the xylan water interface, the changing xylose structure may cause a problem (Maloney et al., 1985) as a result of a variation in particle size and available surface area (Garrote et al., 2004) or as a result of changes in the interphase water-hemicellulose surface along the reaction (Rodriguez-Chong et al., 2004). The fraction susceptible to hydrolysis is therefore dependent on the reaction conditions (Garrote et al., 2004).
- The fraction of hemicellulose which reacts quickly is dependent on the type of plant material used (Garrote et al., 2004). This is because the fraction of hemicellulose which easily undergoes hydrolysis is a function of the uronic acid content as this component has a lower reactivity than xylose and will be present in differing amounts and because the fraction of hemicelluloses directly linked to the lignin may also react differently (Rodriguez-Chong et al., 2004).
- Product inhibition arising from a decreasing  $H^+$  concentration with reaction time as a result of the furfural's ability to act as a Brønsted base which reacts with  $H_3O^+$  to form stable, protonated furfural. This causes the acid concentration to decrease and the reaction rate to drop (Antal et al., 1991).

- The degree of polymerization may have an effect on the rate since research has also shown the existence of an easily soluble xylan, with a degree of polymerisation (weight average) of 150, and a sparingly soluble xylan with a degree of polymerisation of 157 (weight average). (Hagglund, 1951)

Having to account for faster and slower hydrolysis rates for xylan has caused difficulties in reaction modelling for kinetic studies and some researchers have chosen to split xylan into two theoretical fractions, an “easy-to-hydrolyse” fraction and a “hard-to-hydrolyse” fraction (Lavarack et al., 2002). Taking this approach resulted in two parallel reactions viz. a fast hydrolysis and a slow hydrolysis which required data fitting to two separate first order reactions. The amounts of the “hard-to-hydrolyse” and “easy-to-hydrolyse” fractions, have been quantified for a xylan sample by Lavarack et al. (2002). The experimental method involved combining xylan containing material with 4wt% H<sub>2</sub>SO<sub>4</sub> at 90°C (initial acid temperature and reaction temperature as maintained in a water bath). Samples were removed at intervals and the xylose concentration was measured. The rate is initially high as the “easy-to-hydrolyse” fraction undergoes hydrolysis but drops off as this fraction is used up and the “hard-to-hydrolyse” fraction is left. The fraction of “hard-to-hydrolyse” material is then determined by extrapolating the steep section of the rate curve backward to time zero.

Lavarack et al. (2002) tested several different schemes for xylose formation and it was found that the simplest scheme:



gave the best fit to the experimental data. In the hydrolysis of xylan, the concentration of xylose initially rose as it formed faster than it is consumed.

Sugar polymer hydrolysis reactions are very complex (Aguilar et al., 2002) therefore due to the difficulty in modeling these processes, empirical models have been developed. The production of soluble xylan was found to fit the mixed order Michaelis-Menton equation for a dry steaming process and fast and slow floating xylan data could be fitted to two separate first order models (Yang et al., 2006).

Where both selectivity to furfural and generation of furfural are high however, xylan hydrolysis can be accounted for by a simple unimolecular reaction (Moreau et al., 1998).

In previously used acid catalyzed hemicellulose hydrolysis processes, the reactant is in the solid phase while the catalyst is in the liquid phase. The steps for liquid/solid catalysis can be outlined as follows:

- (i) “Diffusion of protons through the wet lignocellulosic matrix
- (ii) Protonation of the oxygen of a heterocyclic ether bond between the sugar monomers
- (iii) Breaking of the ether bond
- (iv) Generation of a carbo-cation as intermediate
- (v) Solvation of the carbo-cation with water
- (vi) Regeneration of the proton with cogenesis of the sugar monomer, oligomer or polymer depending on the position of the ether bond
- (vii) Diffusion of the reaction products in the liquid phase if it is permitted for their form and size
- (viii) Restarting of the second step.” (Aguilar et al., 2002)

The mechanism of hemicellulose hydrolysis is shown in Figure 5:

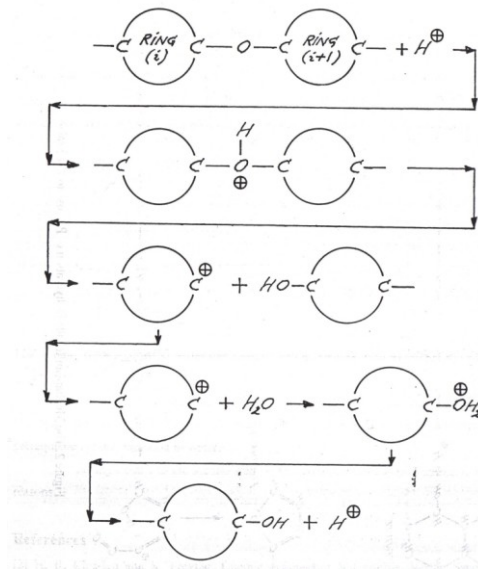


**Figure 5: Hydrolysis mechanism for depolymerisation of xylan to xylose monomers (Zeitsch, 2000a)**

Paraphrasing from Zeitsch (2000a): The process begins with protonation of the oxygen link, the oxygen then has excess positive charge and cleavage of an oxygen-carbon bond occurs resulting in a carbo-cation on one side of the original bridge and an hydroxyl group on the other. The oxygen of a water molecule is attracted to the carbo-cation and forms a bond with it. This again results in oxygen with excess positive charge and a hydrogen ion is liberated. The process requires an acid catalyst and a water molecule for each oxygen bridge.

The xylose monomers produced by hydrolysis have three different forms – acyclic, xylofuranose and xylopyranose. According to Antal et al (1991) furfural arises from the xylofuranose monomers only. It is assumed by Antal et al (1991) that xylofuranose is the

residual xylose which still remains after long reaction times as it is relatively stable, while the acyclic monomers produce pyruvaldehyde and therefore a 100% theoretical yield of furfural yield cannot be achieved. For this dissertation the calculated furfural yield is not based on the residual xylose measurement.

Antal et al. (1991) recorded the existence of two proposed mechanisms from the literature and undertook to fit experimental data to each mechanism to determine which was correct. Their conclusion was that dehydration of pentose to furfural takes place by an acid catalysed sequence proceeding through a 2,5 anhydride intermediate as shown in Figure 6 rather than via open chain intermediates.

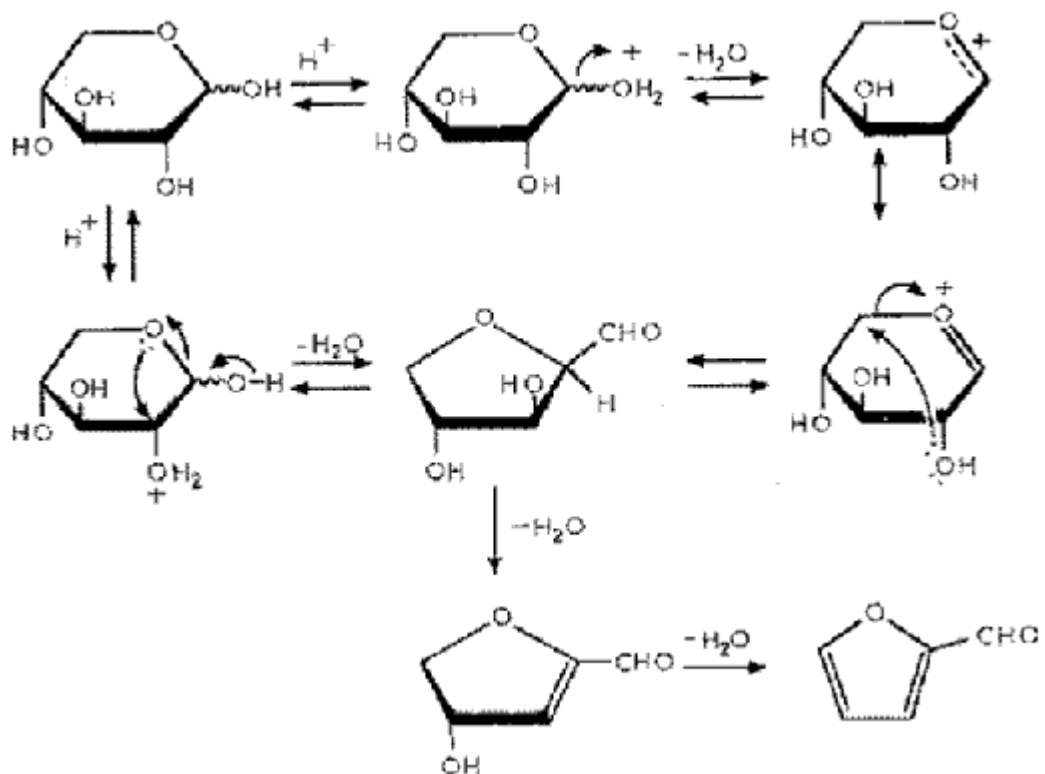


**Figure 6: Mechanism for the dehydration of xylose to furfural (Antal et al., 1991)**

Heterogeneous catalysis with a solid catalyst and a gaseous reactant is common practice; however in this particular instance the roles are reversed with the solid as the reactant and the gas as the catalyst. It is assumed that despite this many of the features of these 'normal' heterogeneous reactions will be present in this particular reaction.

There are several factors which affect the production of furfural from xylan-containing hemicellulose such as the initial xylose concentration, feed flow rate or residence time, the acid catalyst concentration and reaction temperature are important variables (Lázaro et al., 1986).

In studies of the acid hydrolysis of sugarcane it was found that high temperatures and pressures were necessary to soften the lignin wall to allow acid attack and due to this the rate of the reaction was found to increase with an increase in these variables (Lavarack et al., 2002). An increase in steam temperature would increase the soluble xylan concentration and hence increase furfural production (Yang et al., 2006) however some authors have suggested that pentosans are released better at slightly lower temperatures (Cunningham et al., 1982). It is important to keep in mind the negative effect that temperature has on the rate of adsorption of the gaseous reactants onto the solid reactant surface (Zeitsch, 2000b). The temperature of the steam should also not be in excess of 40 to 50°C superheat (at 1 atmosphere) as above this the pentosan containing material may char (Wells and Preston, 1977).

Decreasing the solid to liquid mass ratio decreases the rate of decomposition of xylan (Lavarack et al., 2002, Polakovic et al., 2001) since a low solid to liquid mass ratio is also a low reactant concentration (Lavarack et al., 2002); however some authors found that the initial reactant concentration had minimal effect on the rate of xylose disappearance (Antal et al., 1991).

The particle size does have an effect on reaction rate but the effect is very small (Lavarack et al., 2002).

It has been shown that increasing the acid concentration has a strong effect of increasing the rate of hydrolysis and xylose decomposition (Lavarack et al., 2002, Antal et al., 1991). The lignocellulosic material itself may have a neutralizing effect on the acid due to the buffering effect of the mineral salts contained in the wood particularly at low hydronium ion concentrations (Springer and Harris, 1985, Parajó et al., 1995).

The type of acid does not affect the kinetics (Polakovic et al., 2001) however it does have an effect on the reaction rate since the type of acid would affect the concentration of  $H^+$  ions (Lavarack et al., 2002). Hydrochloric acid has been found to be less effective than sulphuric acid because of the lower number of protons per mole of acid (Lavarack et al., 2002). The use of hydrochloric acid for hemicellulose hydrolysis and subsequent degradation to furfural is not common because it is volatile and large losses are assumed to take place at the temperatures and concentrations used in 'normal' furfural processes (Wells and Preston, 1977).

It is assumed for the s-SUPRAYIELD process that there is a need for high steam flow rates to remove the furfural as it is formed in order to prevent the reactant from becoming saturated with furfural and reaching an equilibrium (which may lead to condensation of the furfural). The

vapour superficial velocity would not however affect catalytic activity of the reaction. (Zeitsch, 2000b).

There are several other processes which exist that make use of steam hydrolysis or gaseous acid catalysis:

- The pre-treatment process developed by Yang et al. (2006) in which corncobs were first pretreated with dilute sulphuric acid then filtered, washed, trickled to remove bulk water before being steamed without the use of extra water. Their process involved placing a bucket containing lignocellulosic materials with no bulk water in an electrically heated autoclave.
- Another example of a gaseous catalysis is the patent registered by Gernon et al. (2005) which uses a tertiary amine gaseous catalyst for a phenolic urethane cold box (PUCB) process as a means of curing premixed sand, polyol and polyisocyanate. The PUCB process is used in the production of moulds and cores for metal castings.
- Ruf et al. (1999) have patented a process for the production of formaldehyde by dehydrogenation of methanol in the presence of a gaseous catalyst.
- In 1990 Mensinger et al. (1990) studied the effect of gas phase catalysts on the rate of bituminous coal char gasification.
- The Noguchi-Chisso process of cellulose hydrolysis uses anhydrous HCl which passes through a damp, fluidized bed of particles in order to allow the HCl to be absorbed by the particles. Subsequently the HCl is removed by heating the particles to volatilize the HCl gas (Higgins and Ho, 1982).
- In 1977 Wells patented a process (Wells and Preston, 1977) for the manufacture of furfural by passing steam and HCl gas through a bed of hemicellulose containing material of minimum water content.

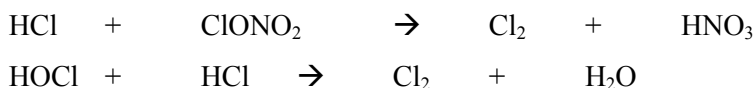
s-Suprayield is unique in that the process involves *dry* superheated steam and a dry bed with all residual moisture removed.

## **2.5 Hypothetical mechanism of gas-phase catalysis**

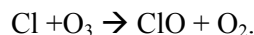
### **2.5.1 HCl dissociation on ice**

Historically it has been believed that gaseous acids cannot act as catalysts, this being due to the difficulty with which they ionize, a feature demonstrated by their property of being perfect insulators. There is generally no significant thermal ionization below 2500 °C for water and below 5000 °C for HCl (Zeitsch, 2001). This belief has been debunked by recent studies into the processes associated with ozone depletion. These studies have shown that hydrochloric acid vapour ionizes on stratospheric ice crystals.

Ozone depletion is said to involve the following reactions (Bolton and Petterson, 2001):



Ozone depletion reactions are initiated by active chlorine gas (Gertner and Hynes, 1996) which arises either from the reaction between chlorine atoms (radicals) (Baceleo et al., 1999, Voegele et al., 2002) or from chlorine anions reacting with other atmospheric chlorine-containing gases (Bolton and Petterson, 2001). The seasonal ozone hole is related to the disappearance of polar stratospheric clouds (PSC) in the spring. The diatomic chlorine trapped in the PSCs is photolysed by sunlight allowing the following reaction to take place (Isakson and Sitz, 1999):



The formation of this chlorine molecule must begin with the ionisation of HCl, a process which is catalysed by the ice surfaces found in PSCs (Bolton and Petterson, 2001). The PSCs have thin layers of mobile water molecules with which the HCl may interact (Baceleo et al., 1999). In order for reactions to take place between ionised HCl and chlorine, the chlorine 'reservoir' (inert) species should be in large amounts in close proximity to the surface (Gertner and Hynes, 1996).

There are two types of PSCs, type I consisting mainly of nitric acid trihydrate (NAT) and type II predominantly ordinary ice (Gertner and Hynes, 1996). Recent research (Aguzzi et al., 2003) has shown that the ice surfaces of type II PSCs are not the only ones capable of catalysing heterogeneous atmospheric reactions, in the troposphere both cirrus clouds and aviation trails may also be possible sites for such reactions.

HCl ionisation is only a part of the process which occurs on PSCs. The HCl acts as a proton donor to HOCl to form a transition state complex:  $\text{H}_2\text{OCl}^+\text{Cl}^-$  which is followed by a decomposition of the intermediate product to  $\text{H}_2\text{O}$  and  $\text{Cl}_2$ . Research has shown that three water molecules which form part of an hexagonal shaped ice surface are sufficient to catalyse the process (Voegele et al., 2002).

Unfortunately it is almost impossible to obtain experimental data as the stratospheric conditions are extremely difficult to create - thus many of the studies performed are by computer simulation (Mantz et al., 2001).

### **2.5.2 The significance of gas phase catalysis to s-Suprayield**

The similarity was drawn based on the dangling OH- and H-groups found on the hemicellulose structure which is discussed in section 2.3. In this way the hydrochloric acid vapour could catalyse the hydrolysis of hemicellulose to pentoses and the subsequent dehydration to furfural. The catalytic ability of the HCl vapour is hence limited by the existence of the hemicellulose structure and therefore it cannot catalyse any furfural destruction reactions. In this process a solution of hydrochloric acid is superheated to form a superheated steam/HCl vapour mixture which is passed through a dry bed of pentosan containing material.



### 3. THESIS OBJECTIVES

No conclusive evidence has been presented in the literature as to the feasibility of s-Suprayield and no testwork has been done to explore factors affecting the furfural yield which would help in process optimisation. If s-Suprayield could be used successfully for furfural production it could provide a more cost effective means by which the industry could efficiently utilise a range of agricultural process waste material to produce a useful chemical.

The objective of the work presented in this thesis was therefore:

- To show that s-Suprayield is a viable process by which furfural can be produced from hemicellulose containing material by means of gas phase catalysis by HCl.
- To determine the effect of the HCl concentration and the reaction temperature on the furfural yield.

In order to achieve these objectives a mini-pilot plant rig was set-up by careful down-scaling of the larger pilot-plant available. The plant also had to be operated in a manner which gave consistent results within the limits of the equipment available.

In order to fully interpret the data, a model was developed and the data was used to fit the model parameters which were the pre-exponential factor and the activation energy for reaction rate constants for the different reactions taking place.

## 4. EXPERIMENTAL WORK

### 4.1. Equipment

A pilot plant set-up was already available which had been used to meet the requirements for a previous funding grant. The original reactor was 100mm in diameter and 1m in length and it required an entire day for a complete reaction. For the experimental work planned for this MSc programme several modifications had to be made in order to facilitate the performance of multiple reactions per day. The main modification required was therefore to diminish the size of the reactor which in turn required changes to the heating and pumping system to allow for the smaller fluid flowrates. The reduced fluid flow rates were necessary to maintain acceptable superficial velocities. Consideration was also given to the materials used in the construction of the plant as they had to be able to withstand high temperatures and corrosive acidic conditions.

#### 4.1.1. Plant description

The flowsheet for the experimental testwork is shown in Figure 7. The design decisions which resulted in this flowsheet are discussed in the sections that follow.

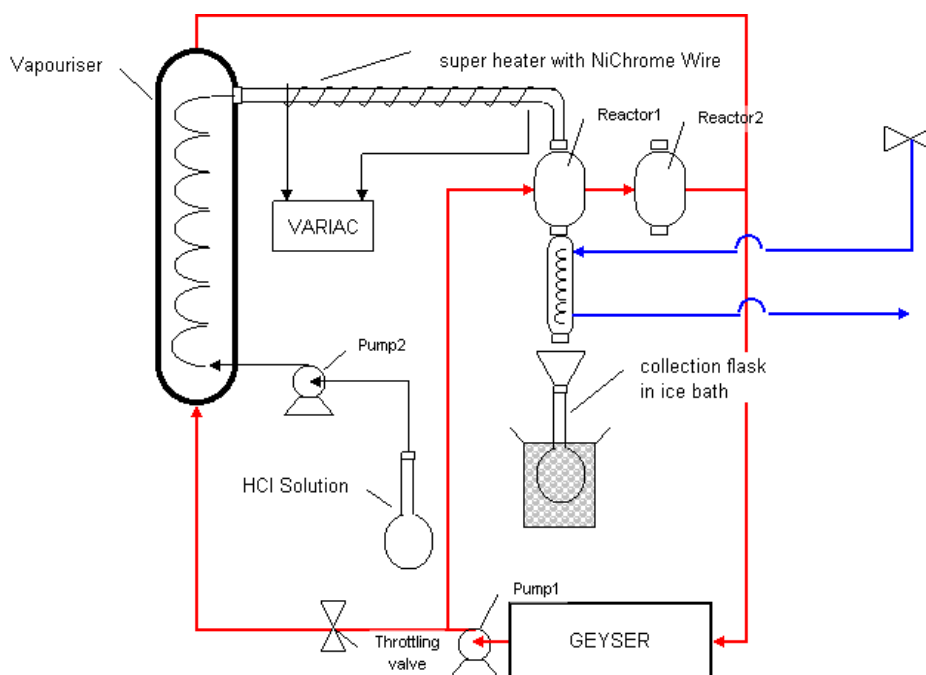


**Figure 7: Plant diagram**

Two reactors were connected to the hot oil supply to feed their heating jackets, however only one reactor at a time could be connected to the reactant gas flow. The reason for this was to decrease the changeover time to enable two experimental runs to be performed per day i.e. while one reaction was nearing completion in the first reactor, the second reactor could be loaded and once the second reactor was already in place, the first reactor could be unloaded.

Liquid was initially pumped in silicone tubes from either an acid solution container or a water container by a peristaltic pump (labelled Pump 2 in the diagram), into the coils of a QVF® condenser which had hot oil from the geyser flowing on the shell side. The QVF® condenser thereby acted as a vapouriser resulting in a gaseous stream which exited the coils of the condenser and passed into the superheater through a Teflon connector. The superheater consisted of a 5mm outer diameter (OD) glass tube wrapped in nichrome wire windings with 10mm spacing. The power was supplied to the nichrome wire by means of a Variac. The now superheated vapour passed from the superheater into the packed bed reactor that consisted of a jacketed, Pyrex vessel with a point for the insertion of a thermometer. Prior to starting the experiment, the reactor had been filled with glass Raschig rings and dried hemicellulose containing material (sunflower hulls), which was held up by a glass plug that was attached to the reactor by means of springs. The glass Raschig rings were used to ensure that the reactor contents were located in the jacketed section of the reactor and not in the unheated section. Once the vapour had come into contact with the bed and had passed through it, the product vapour passed into a Graham condenser which was supplied with cooling water from the mains passing through the coils. The condensate leaving the condenser was then collected in a flask over ice.

The larger equipment was supported on a dexian frame and retort clamps were used to support the smaller equipment.

#### *4.1.1.1. Materials of construction*

Since the acid solution was superheated, the system had a high potential for corrosion because hot acid solutions would come into contact with the walls of the pipes and vessels. This somewhat limited the range of materials which could be used in the system to very expensive metals, such as Monel or Titanium or to the much cheaper option of glass or Pyrex. Pyrex was chosen as the construction material although it had the disadvantage of being sensitive to thermal stresses arising from the thermal gradients.

Another issue was the material that was to be used for the connections between glassware and glassware and between glassware and the copper tubes since some flexibility was required. Silicon tubes, with a high melting point, were used where a flexible connection was required, such as for connecting the oil supply to the reactors. Unfortunately these tubes were found to rupture from manipulation and pressure build-ups and therefore had to be carefully monitored for wear. If significant wear was observed the pipes were replaced. Where customised

connections between glassware and glassware were required, Teflon connectors fitted with Viton O-rings to create a seal, were used.

Copper pipes were used to carry the oil through the system except where braided Teflon tubes were used to make flexible connections.

A peristaltic pump was used to pump the material because this type of pump does not make any contact with the liquid and is therefore safe from corrosion. Silicone tubing of a very narrow bore was used in the peristaltic pump in order to achieve a very slow flow rate.

#### **4.1.2. Reactor design**

The new reactors, made of Pyrex, were designed with a diameter of 50 mm and length of 100 mm which gave a cross sectional reactor area of  $6.25 \times 10^{-4} \text{ m}^2$  and a volume of  $5.25 \times 10^{-5} \text{ m}^3$ . The length to diameter ratio (L/D) of the new reactors was two. This was reduced from 10 as it was desired to maintain a low superficial velocity for the smaller reactor and this was achieved by increasing the reactor diameter relative to the length. It had also been observed, when testing smaller diameter reactors, that condensation occurred in narrower vessels. The short reactor length and small volume allowed for the reactor to be modelled as a differential bed for the modelling.

The reactors were surrounded by an oil heating jacket and glass wool to maintain the reaction temperature. Despite being insulated, the top of the reactor and the thermometer opening were areas of heat loss. In order to prevent condensation, additional heating was supplied by nichrome wire which was wrapped around these areas. An alternate Variac, to the one used for the superheater, was used to supply power to the nichrome wire. The bottom of the reactor was fitted with a glass plug which was attached to the reactor with glass hooks and springs and was used to support the bed. In order to ensure that the reaction took place in the jacketed section of the reactor, the plug and the bottom part of the reactor were filled with glass Raschig rings which supported the bed.

#### **4.1.3. Heating options**

A decision was taken to retain the QVF condenser which had been used in the previous plant at higher velocities to vaporise the gas, since its large available surface area was in excess of that required to heat the new plant's lower velocity stream. The disadvantage of using the QVF condenser as a vaporiser was that the glassware's thermal gradient tolerance restricted the oil

temperature to 150°C. Due to the large heat transfer area, this unit acted as a total vapouriser completely vaporising the HCl solution so that the concentration of HCl in the gas exiting the vapouriser was the same as that of the liquid solution that was pumped into the vapouriser.

The superheater used in previous testwork was replaced by a 5 mm (OD) glass tube which was wrapped in nichrome wire with 10 mm spacings. Unfortunately there was no automatic control on heat supplied to the nichrome wire and it was therefore controlled manually using a pt 100 temperature probe to measure the external temperature and a Variac to regulate the voltage.

The optimum spacing for the nichrome wire was determined through calculation; if the spacing was too wide the heat loss between the coils would be high and the vapour would lose heat more rapidly than it would gain it. If the windings were too close, the temperature would rise too high. Simulations were performed in MATLAB to determine the coil spacing which would provide sufficient heating surface while ensuring that the superheater was not overly sensitive to the change in variac voltage. Figure 8 shows the vapour exit temperature predicted at different coil spacing and different voltages. The equations used to determine the plots for this graph and the MATLAB code for this simulation can be found in Appendix A. It must be noted that the decrease in temperature is a result of the lack of heating in the final section of the tube and that the calculations are based on 2 m of wire which covers different tube lengths depending on the coil spacing.

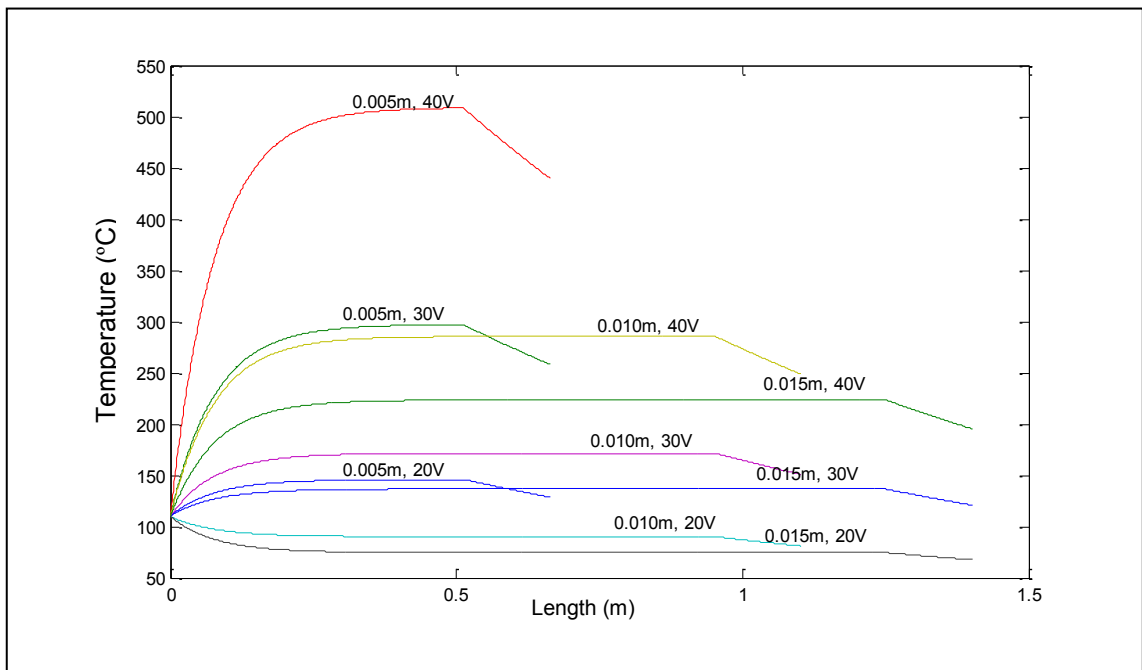


**Figure 8: Figure showing vapour exit temperature at different nichrome wire coil spacing**

From Figure 8 it was apparent that coil spacings of 5 mm lead to gas temperatures which were strongly dependent on the voltage, reaching temperatures of 150, 300 and 500°C as the voltage increased. While the 15 mm spacing did not show the large changes obtained when a coil spacing of 5 mm was used, the temperatures achieved would not have been high enough to prevent condensation of the gas phase. A spacing of 10 mm was selected as the temperature change was not as sensitive to voltage as the 5 mm spacing but it also achieved high enough temperatures to maintain a temperature above the saturated temperature of steam when voltages of 30V and higher were used.

It was concluded that the voltage provided to the superheater wire could successfully be used to control the temperature of the superheater glass and therefore the gas outlet temperature. This was demonstrated experimentally as shown in Figure 9 which shows the variation in the superheater glass temperature with time. When the Variac was set to 20V, a stable temperature approaching 120°C could be achieved and when the Variac supply was changed to 30V the temperature increased steadily. The voltage could therefore be used to control the superheater temperature, which in turn set the reactor gas outlet temperature.

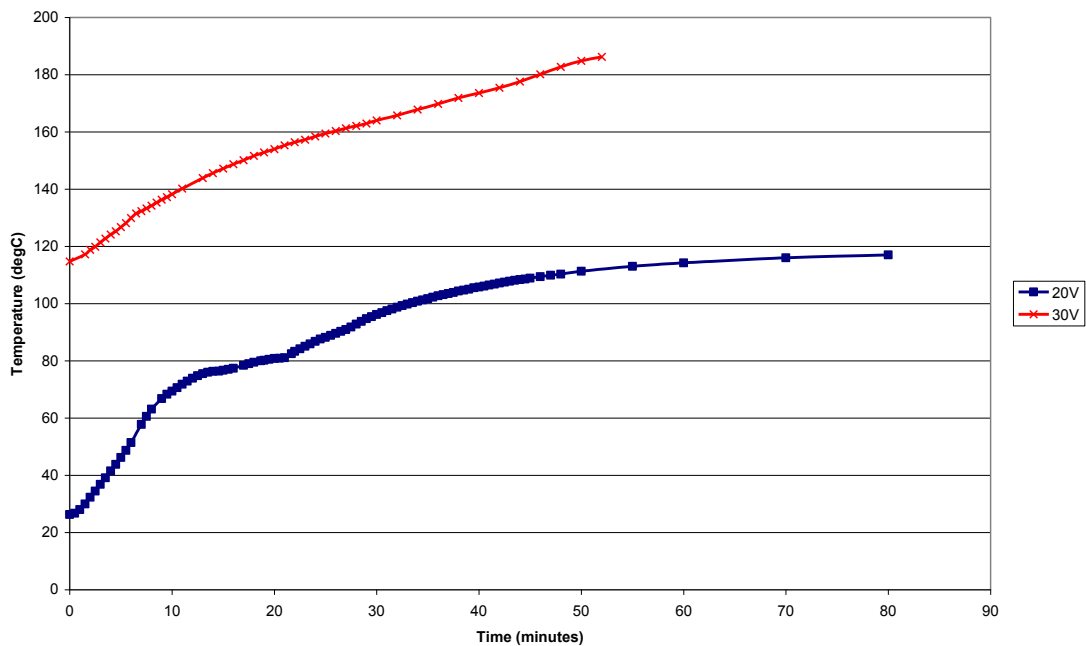


**Figure 9: Superheater temperature profiles at different voltages**

The entire heating system was verified experimentally as follows: The QVF® condenser was put in place and connected so that the oil flowed into the bottom of the shell and out the top. The water / acid solution was pumped into the condenser's coil inlet using a Teflon and glass connector, where it vaporised completely during its passage up the condenser. Thereafter the vapour exited the condenser via another Teflon plug which connected onto the superheater. The

vapour then passed through the superheater's glass tube which was surrounded by the nichrome wire coils and was well insulated. By regulating the voltage across the nichrome wire, the gas exit temperature could be controlled. Finally, the exit vapour was directed to the reactor and then through the condenser, where it was collected. The temperatures of the superheater, steam exit and oil exit were measured over a 90 minute period. The profiles are plotted in Figure 10.

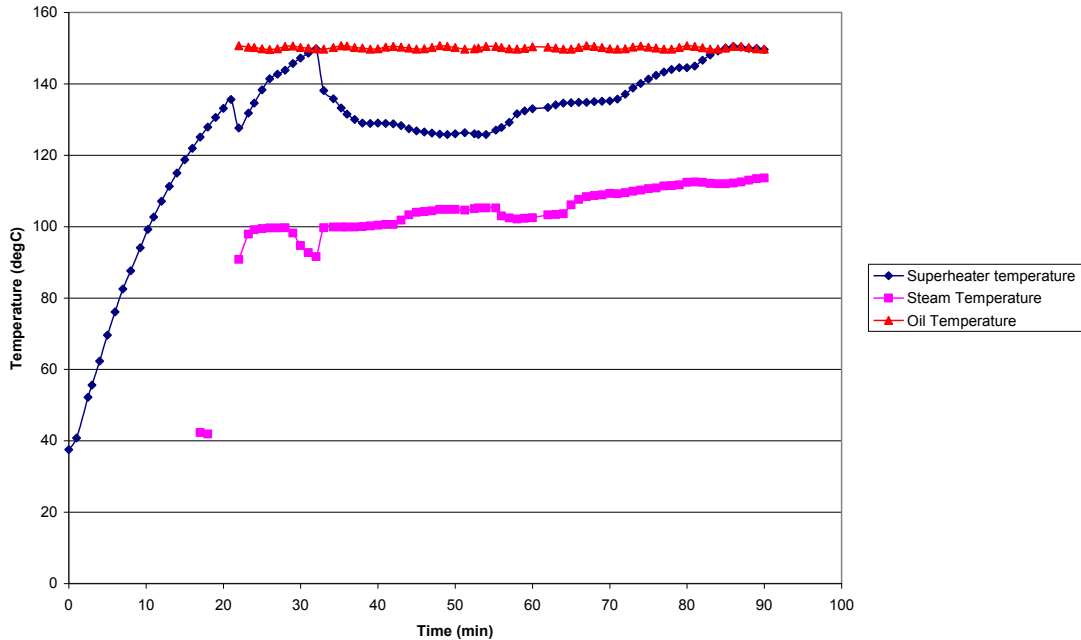


**Figure 10: A temperature/time profile for the QVF® condenser and superheater over 90 minutes**

Figure 10 indicated that the temperature reached in the reactor (steam temperature) was at the desired level, i.e. in excess of 100°C, which is the saturated temperature of steam at atmospheric pressure.

This experiment showed that this equipment set-up, using the QVF® condenser from the previous plant as a vapouriser and a thin glass tube wrapped with nichrome wire as a superheater, was a feasible option for producing steam at the desired reaction conditions.

Difficulty with this set-up arose as there was no fine control on the Variac. The inability to source an acid resistant pt100 temperature probe meant that control was manual and based on the reading of a thermometer.

#### 4.1.4. Utilities and control

In the plant description in section 4.1.1, reference is made to the heating and cooling utilities which were used in the plant. This section further elaborates on the choice and use of those utilities as well as the methods put in place to control their conditions.

There were two main heat sources used on the plant:

- Heat transfer oil (which was heated in an electric geyser)
- Nichrome wire supplied by a Variac(electric)

The temperature of the oil was controlled by a proportional–integral–derivative (PID) temperature controller with the PT100 temperature sensor located between the geyser outlet and the pump.

The geyser was fitted with a safety trip switch which cut the power supply to the geyser when the oil temperature was in excess of the safety cut off temperature. In this way ignition of the oil could be prevented.

The oil chosen for the testwork was Texatherm 46 which had a flashpoint of 230°C (COC) and had very few safety and health risks associated with it.

The hot oil from the geyser was pumped in copper tubes by a gear pump (Pump 1) to the plant. The flow of the oil was split, with a portion being directed to the reactor jacket and a portion being directed to the vapouriser. From this point the oil was carried in silicon tubes to the reactor jacket inlet. The reactor jacket outlet stream flowed into the second reactor with the second reactor jacket outlet being linked by silicon tubes to the copper pipes. The link between the copper pipes and the silicon tubing was achieved by means of connectors which were of ‘snap-on’ type. These connectors sealed the ends of the pipes when the connection was broken, enabling the reactor section to be removed if required. The copper pipes then merged with the vapouriser oil outlet returning to the geyser to reheat the hot oil stream. The stream leading to the vapouriser passed through a ball valve, which acted as a throttle, then through the vapouriser then returning to the geyser. The purpose of the throttling valve was to increase the pressure drop in the vapouriser stream so as to allow some of the oil to flow to the reactors jackets.

There was no controller on the superheater outlet but the reaction temperature was measured using a thermometer inserted into the reactor. Because of this, some manual intervention was



required to actually control the reaction temperature and this was achieved through the use of a Variac.

All heat supply lines and hot vessels were insulated using glass tape and/or ceramic wool.

The condenser cooling water was supplied from the mains supply and was fed to the Graham condenser in silicon tubes.

## 4.2. Preparation for testwork

Further details for this section can be found in Appendix B.

### 4.2.1. Pump calibration

Water was used to calibrate the pump by measuring the mass of water collected in a fixed time period at a given pump setting. The calibration curve is shown in Figure 11. Each point on the graph was measured in duplicate. Although the lowest flowrate possible was required, it was decided that it would be prudent not to work at the minimum speed setting of 0.6 but rather to perform the testwork at the higher speed of 0.75 which gave a flow rate of  $2.16 \times 10^{-5}$  kg/s.

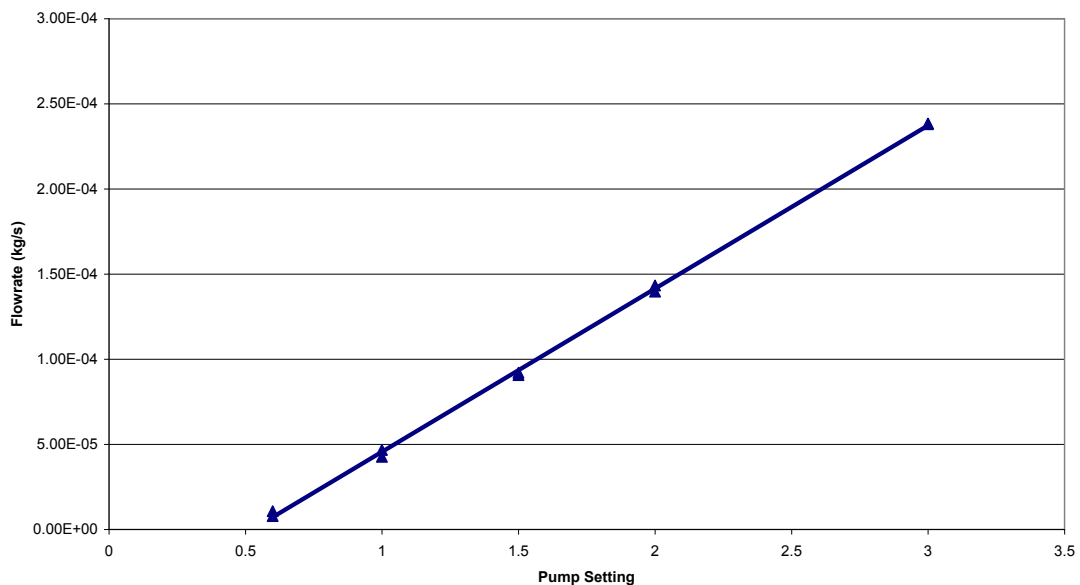


Figure 11: Pump calibration curve

### 4.2.2. Raw material and bed characterisation

Gupta and Das (1997) studied the physical properties of sunflower seeds and determined physical properties for seed and kernel as a function of moisture content. The density of the

hull itself at a moisture content of 9.4% d.b. was found to be  $1443 \text{ kg/m}^3$ . Unfortunately no dependence on moisture content for the hull exclusively was determined in their work and this value was used in bed density calculations. The seed length of unmilled sunflower husks was found to be  $9.52 \pm 0.7 \text{ mm}$ . Although the experimental work done in this project used milled sunflower husks, this length measurement was still applied as it was assumed that the particle width would be affected by milling more than the particle length. The bed voidage of the material determined in the work of Gupta and Das (1997) was not valid for the milled sunflower hulls as the milling would result in more closely packed particles than if whole hulls were used.

#### 4.2.2.1. Sunflower husk sizing and density

A narrow size range of sunflower husks was selected for the testwork. In order to determine which size fraction was most abundant, the milled material was subjected to dry screen sizing.

Samples of approximately 150 g were split from the bulk sample using a riffle splitter to ensure even distribution of all size fractions in the sample. An approximate root two series of sieve screen sizes was used. Each sieve was weighed before being stacked in descending mesh size order. The sample was then added to the top sieve and the lid was placed on top of it. The sieve stack was then placed on a sieve shaker for 40 minutes. Each sieve was then reweighed with the oversize material. The difference between the weight of the empty sieve and that of the sieve including the oversize material gave the mass of each size fraction and therefore the mass percent contribution of each size fraction could be determined. The size distribution is shown in Figure 12:

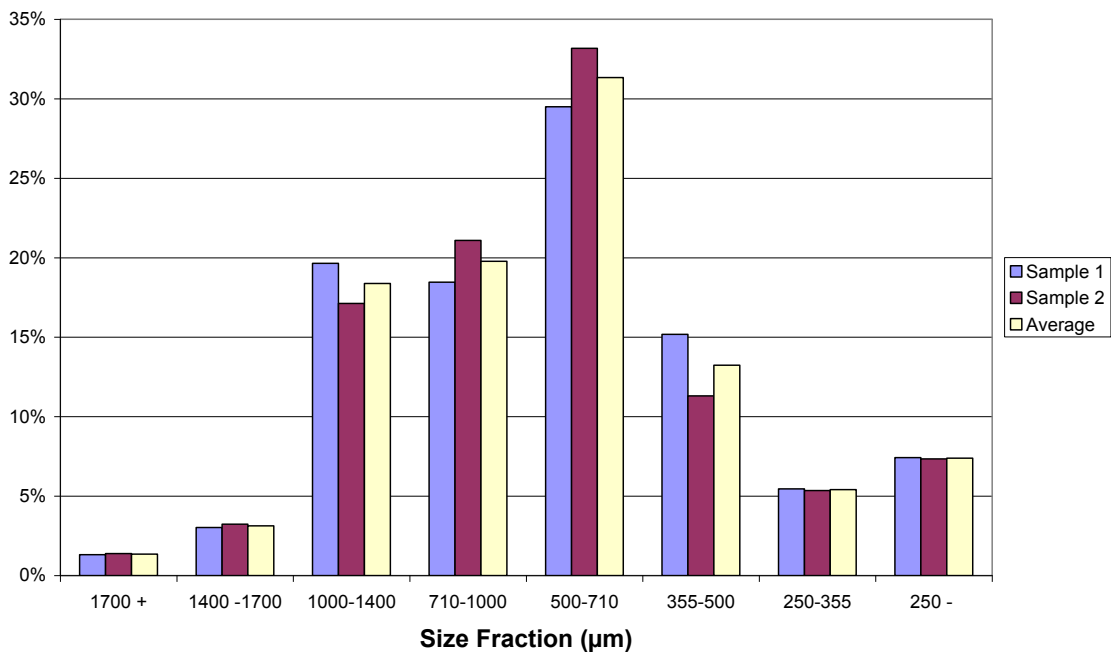


**Figure 12: Percent contribution of each size fraction**

From Figure 12, it was observed that a majority of the mass was in the range of sizes between 1400 and 500 $\mu\text{m}$ . The -710+500  $\mu\text{m}$  fraction was chosen for the testwork as it was the most abundant. Using the root mean square method to determine an average size, it was found that the average size of the particles was 596  $\mu\text{m}$ . This was assumed to be representative of the diameter of the particles.

As an approximation, the seed length determined by Gupta and Das (1997) for ungraded sunflower seeds was used as the material length (9.52 mm). Even though the material used for this project was milled, it was assumed that the effect of milling was to change the raw material width rather than the length and therefore this length could be applied to the milled material.

Also of interest for calculating the modelling parameters was the sunflower husk density. The material was shown by Gupta and Das (1997) to have a density of 1443  $\text{kg/m}^3$  at a 9.4% d.b. moisture content. Although the material used for experiments would have been dried, the change in density arising from the moisture content has not been accounted for.

Unfortunately the bed porosity ( $\varepsilon$ ) was not measured but according to Gupta and Das (1997) the porosity of the unmilled seed was 0.32 for a 0% d.b. moisture content and this was assumed to be the porosity for this testwork. This would give a bulk density of:

$$\rho_B = (1 - \varepsilon)\rho_{solid} + \varepsilon\rho_{air} \quad 1$$

$$\rho_B = (1 - [0.32])[1443] + [0.32][1.205] = 981 \text{ kg/m}^3$$

#### 4.2.2.2. *Pentosan analysis*

This test was performed according to the TAPPI method (Hughes and Acree, 1938) which was as follows:

Firstly the sample was ground and left in a beaker overnight to air dry. 0.3 +/- 0.0005 g of the sample was added to a round bottom flask with 20 g NaCl, 100 ml of 3.85 M Hydrochloric acid and a few boiling stones. The round bottom flask was then placed in a preheated heating mantle and attached to a condenser which would condense the resulting vapour. In order to maintain the liquid level in the round bottom flask, 250 ml of Hydrochloric acid was added drop-wise over the period from a separating funnel above the flask. Distillate was collected in 250 ml volumetric flasks over a 90 (+/- 5 minute) period during which time approximately 225 ml of distillate was collected. After the distillation procedure the volumetric flasks were topped up to

the 250 ml mark with 3.85 M Hydrochloric acid. 5 ml of distillate was added to two 50 ml flasks respectively to which 25 ml of orcinol reagent was added. The resulting solutions were placed in a water bath at 25°C for 60 minutes and then topped up to the 50 ml mark with 95% ethanol. The flasks were thereafter returned to the water bath for a further 60 minutes. The absorbance of each of these solutions was then determined. The blank for the absorbance measurement was prepared by performing the entire procedure outlined above but without adding any pentosan containing material to the round bottom flask. The resulting distillate was used as a blank.

The absorbance measurements were then converted to the equivalent mass of xylan present in the sample using a calibration curve relating absorbance to the mass of xylose. The calibration curve can be found in Appendix B. The calibration curve was prepared by performing the test procedure using fixed masses of pure D-xylose and determining the corresponding absorbance. A plot of absorbance versus xylan concentration was then plotted ( $\text{xylan} = \text{xylose} \times 0.88$  based on the ratio of molar masses). The xylan concentration was found to be 25.23% which corresponds with the concentration of 25% found in the literature (Wondu Business and Technology Services, 2006).

In order to standardise the readings a moisture analysis was performed so that the percent pentosan could be determined on a dry mass basis. The moisture analysis was performed by weighing an empty sample vial which had been heated to 105°C and then cooled. 0.5 – 1 g of a sample of material was then added to the empty sample vial. The full vial was then placed in the oven for one hour at 105°C, cooled in a dessicator and then reweighed. The sample was repeatedly placed in the oven for one hour periods and weighed until the mass remained constant (dry mass).

The concentration of pentosan in the different size fractions was determined as it was initially unclear whether or not this information would be relevant in determining the reaction model. As the process turned out to be reaction controlled rather than diffusion controlled due to the slow reaction rate, only the -710+500 $\mu\text{m}$  fraction was used for the testwork and no further investigation of the pentosan concentration in different size fractions was performed.

The full results and discussion of the pentosan analysis can be found in the Appendix B.

### 4.3. Experimental Procedure

#### 4.3.1. Sample preparation:

Sunflower seed husks were used as raw material for the reaction. The husks were first screened in order to obtain a size fraction of  $-710+500\ \mu\text{m}$  and thereafter sub-samples of approximately 18 g were placed in the oven overnight to ensure that there was no residual moisture. Once the reactors were preheated, the gas flow was shut off and the reactor was filled with 14 g of glass Raschig rings. The oven dried sample was then weighed and placed in the reactor. When filling the reactor, care was taken to ensure that any material which spilt or fell through the plug was collected and put back into the reactor.

A hydrochloric acid solution was made up to the test concentration by diluting a set amount of 37% HCl with water in a 1 L volumetric flask. The composition of the acid was checked prior to the test by performing a titration with NaOH using bromothymol blue as an endpoint indicator. The mass of the solution was also noted prior to the reaction.

#### 4.3.2. Start up

On the day prior to the run, time switches were set to switch on the oil pump and thereafter the geyser. In addition the trip switch was reset and the oil set point was adjusted to  $150^{\circ}\text{C}$ . The following steps were performed when commencing a run:

- All power sources were switched on and all temperatures were noted.
- The variac was switched on to supply 50 V to the Nichrome wire.
- A collecting flask was placed at the condenser exit.
- The condenser cooling water flow was switched on.
- The feed line was placed in a water container and the peristaltic pump was set to 0.75 which would give a gas flow rate of  $0.2 \times 10^{-4}\ \text{kg/s}$ .
- The pump was then switched on to start the flow of water (which was converted to steam).
- In order to check the steam temperature, the flow had to be directed through the second reactor (initially empty).
- When the steam reached the desired temperature the runs could commence.

#### 4.3.3. Experimental run

The experiments were performed in the following manner:

- The peristaltic pump was momentarily switched off and the inlet pipe was transferred from the water container to the acid container.
- The raw material was collected from the oven.

- The digester through which gas was not flowing was detached from the plant and the screw-on seal was removed.
- The digester was then loaded with approximately 18 g of the required raw material, the screw on seal was then replaced and the digester was reattached to the plant.
- The thermometer was inserted into the reactor.
- The peristaltic pump was re-started.
- A two minute period was allowed for the flow of HCl to commence before a new collecting flask in an ice bath was placed at the condenser outlet.
- The collecting flask was replaced at 35 minute intervals for a total of 210minutes (i.e. 6 concentrates were collected). The condensate collected over each 35 minute period was analysed for furfural, acetic acid and HCl by titration and refractive index measurements as described in 4.4.
- The peristaltic was again switched off and the inlet pipe was transferred to a water container and the pump was switched on again. The purpose of this was to pump water through the system in order to purge the line and the reactor of any residual HCl. During this time, a collecting flask was placed at the collector outlet.
- After several minutes when the condensate ran clear, the peristaltic pump was switched off.
- The reactor was then removed and the entire residual bed, having been stripped of xylose, was emptied into a flask to be weighed.

Two runs were performed per day.

#### **4.3.4. Shutdown**

After the completion of the second run, the plant was shutdown as follows:

- Pump 1 was switched off to change the flow from acid to water.
- All the controller set points were reset.
- After 10 to 15 minutes of water flowing through the system, the pumps could be switched off.
- When there was no longer condensed steam leaving the condenser, the water supply to the condenser was switched off.
- Lastly all power switches to the plant were switched off.

#### **4.4. Sample analysis**

The amount of pentosan in the raw material was determined as described in 4.2.2.2. Subsequently, the reaction product samples were analysed for furfural, acetic acid and HCl.

From the hemicellulose structure described in 2.3, it may appear that there are many other constituents that may form part of the product solution; however many of the components that make up hemicellulose can be safely assumed to remain in the solid state as it is only the more volatile components i.e. furfural, water, HCl and acetic acid which will form part of the product solution. Furthermore the carboxylic ions which form part of the uronic acid do not enter the product solution as they are not in the free form and therefore are not easily hydrolysed (Azarov et al., 1999). They therefore do not influence the pH of the final solution.

In order to determine the amounts of each component in the product solution, the solutions were firstly assumed to consist only of HCl, acetic acid, furfural and water. The more suitable and accurate method of using High Pressure Liquid Chromatography (HPLC) was not available. Through the use of a potentiometric titration, the concentrations of acetic acid and HCl could be determined. The Refractive Index (RI) of the solution was then read as it was assumed that the RI contributions of each component would be linearly additive and that, knowing the RI of distilled water and being able to relate the HCl and acetic acid concentrations to their contributions to the overall RI, the furfural contribution to the overall RI could be calculated. This could be related to the actual furfural concentration.

##### **4.4.1. Potentiometric Titration**

The first part of the analysis required the titration of a 25 ml aliquot of the product solution with 1M sodium hydroxide. A potentiometric titration was performed as two endpoints had to be determined with the first equivalence point being indicative of the HCl concentration (HCl is a strong acid), while the second equivalence point was due to the weaker acetic acid. The titration was performed by adding small amounts of sodium hydroxide to the solution and noting the pH reading after each addition. A plot of pH vs. volume of NaOH addition was then used to determine the volume of NaOH added at each end point. In order to demonstrate how the points were read off the graph the titration curve for run 1, sample 1 is shown in Figure 13.

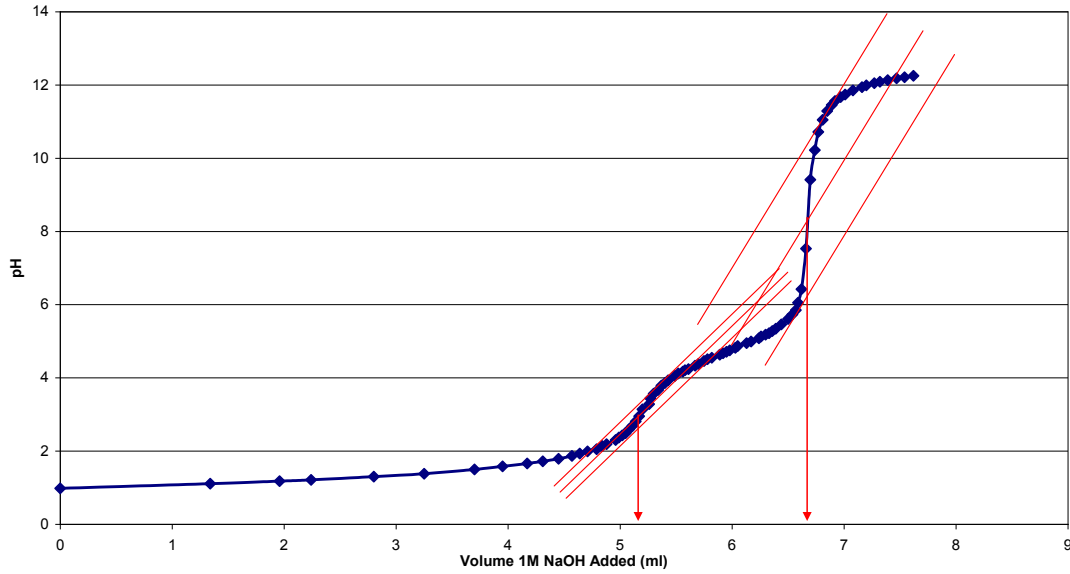


**Figure 13: Titration curve for run 1, sample 1**

Figure 13 shows that the end points were located by first drawing two parallel lines tangential to the inflection points, a line was then drawn parallel to these lines to bisect the space between the two lines. The intercept between this line and the titration curve was determined to be the end point. The lines for determining the end points are shown in red. In this case the first endpoint was found at 5.20 ml NaOH while the second endpoint was found at 6.69 ml NaOH.

Once the volume of NaOH addition at the titration endpoint had been determined, the concentrations of HCl and acetic acid were determined as shown in Equations 2 and 3:

$$C_{HCl} \left[ \frac{g}{L} \right] = \frac{vol_{NaOH,1} [L] \cdot M_{NaOH} \left[ \frac{mol}{L} \right] \cdot MM_{HCl} \left[ \frac{g}{mol} \right]}{vol_{aliquot} [L]} \quad 2$$

$$C_{HAc} \left[ \frac{g}{L} \right] = \frac{(vol_{NaOH,2} [L] - vol_{NaOH,1} [L]) \cdot M_{NaOH} \left[ \frac{mol}{L} \right] \cdot MM_{HAc} \left[ \frac{g}{mol} \right]}{vol_{aliquot} [L]} \quad 3$$

In order to confirm these values, simulation of the titration curve and regression of the concentration values was performed in MATLAB and a good correlation between the graphically determined values and those determined from MATLAB were found. The MATLAB code performed a mass balance for the reaction between NaOH and the acids in the test solution for a series of NaOH additions. From the mass balance, the  $H_3O^+$  ion concentration could be determined and thus pH could be calculated for a range of NaOH additions. The change in the  $H_3O^+$  ion concentration is due to its reaction with the  $OH^-$  ion coming from the base to form water which is neutral:





For HCl, a strong acid, it is assumed that the acid dissociates completely in water and therefore the  $H_3O^+$  ion concentration is equivalent to the HCl concentration in the solution. For acetic acid the reaction with NaOH and calculation of the  $H_3O^+$  ion concentration is complicated by the fact that it is a weak acid and therefore it does not fully dissociate in water but dissociates according to its dissociation constant at 25°C:

$$K_a = \frac{[H_3O^+][CH_3COO^-]}{[CH_3COOH]} = 1.75 \times 10^{-5} \text{ (Skoog et al., 1997)} \quad 5$$

This corresponds to a  $pK_a$  value of 4.76.

During the first part of the titration, the HCl dominates as the  $H_3O^+$  concentration is high limiting the dissociation of acetic acid. It is only once the HCl has been neutralised that the acetic acid begins to dissociate and can be neutralised. This accounts for the two endpoints found on the titration curve.

The MATLAB code can be found in Appendix C along with the tabulated graphically determined endpoint values and the corresponding MATLAB generated values.

#### 4.4.2. Refractive index

The refractive index readings were taken using a refractometer. The refractive index for each of the exit stream samples collected over 35 minutes was determined at  $20.0^\circ\text{C} \pm 0.2^\circ\text{C}$ .

The refractive index measurement was repeated twice per sample in order to minimise the error by taking an average reading.

Before the testwork started, a binary calibration curve was determined for each component in water, i.e. for HCl/water, acetic acid/water and furfural/water. The calibration curve was measured using different concentrations of each solution and measuring the RI in duplicate for each solution of known concentration. A plot of RI v/s concentration was produced as shown in Figure 14 and Figure 15:

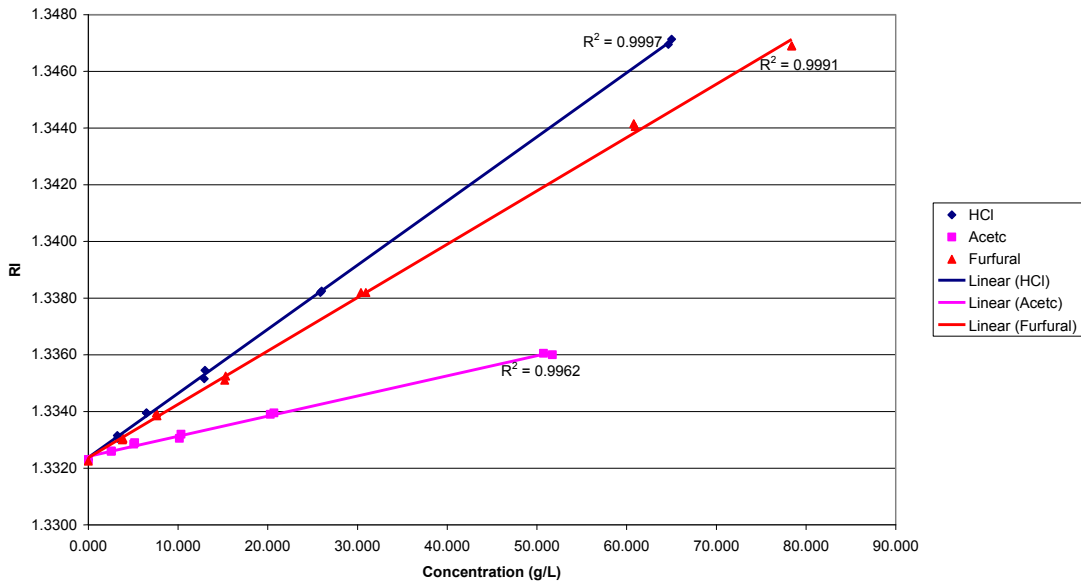


Figure 14: Refractometer calibration curve for concentration in g/L

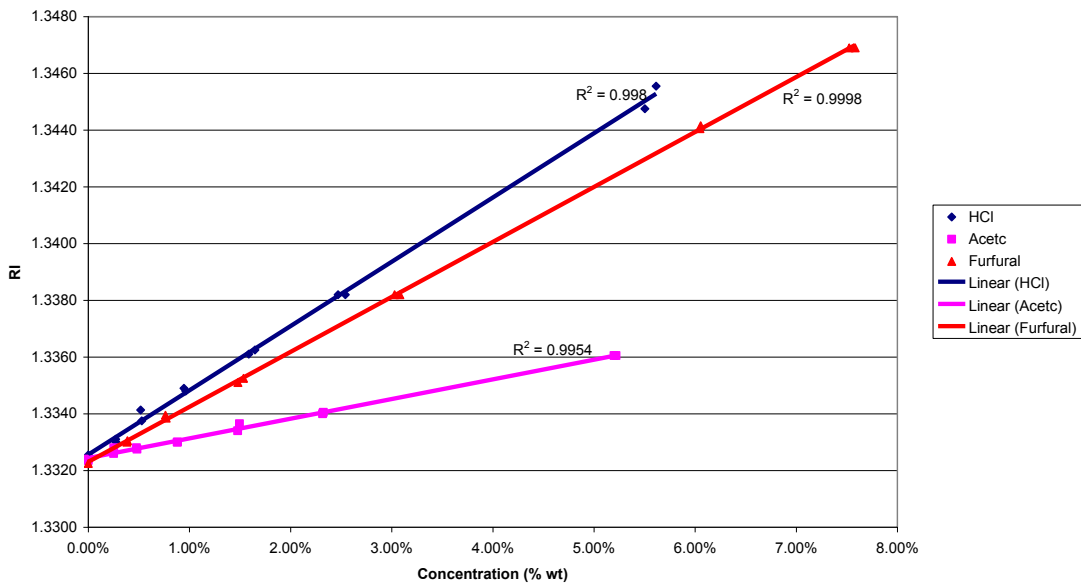


Figure 15: Refractometer calibration curve for concentration in % wt

Figure 14 and Figure 15 show rectilinear relationships and the intercept of these curves were dependent on the RI of distilled water but the gradient was considered unique for each component. It was assumed that the contribution from each component in a ternary or quaternary solution would be linearly additive as is the case for binary solutions when applying the Arago and Biot rule described by Aminabhavi (1984). This rule is only applicable for cases where there is no volume change of mixing which is generally the case when solutions are dilute as is the case here. The use of this assumption is described in Equation 6 and Equation 7:

$$RI_{measured} = RI_{Water} + \sum_n RI_{Contribution_n} \quad 6$$

where:  $RI_{Contribution, n}$  contribution of component 'n' to the RI

$$RI_{Contribution} = m_{RI, n} \times C_n \quad 7$$

where:  $m_{RI, n}$  is the gradient of the RI versus concentration curve for component  $n$

$C_n$  is the concentration of component  $n$

The concept of linearity and additivity for the refractive index of mixtures was also described by Glover and Goulden (1963). In their discussion they stress that this only applies in the case of concentration measured on a per unit volume basis rather than on a mass percent basis however at low concentrations, their curve produced an approximately linear curve with respect to mass percent. For this dissertation mass percent was found to give smaller errors than a mass per volume basis.

Tests were done to determine the RI of ternary solutions of known concentration to test this assumption and the results are shown in Figure 16 to Figure 18.

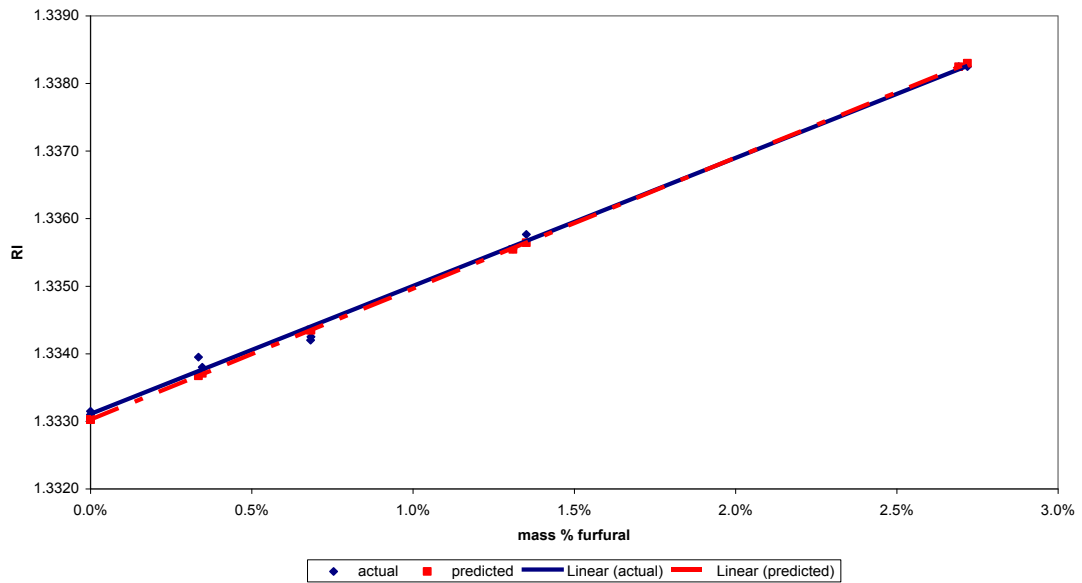
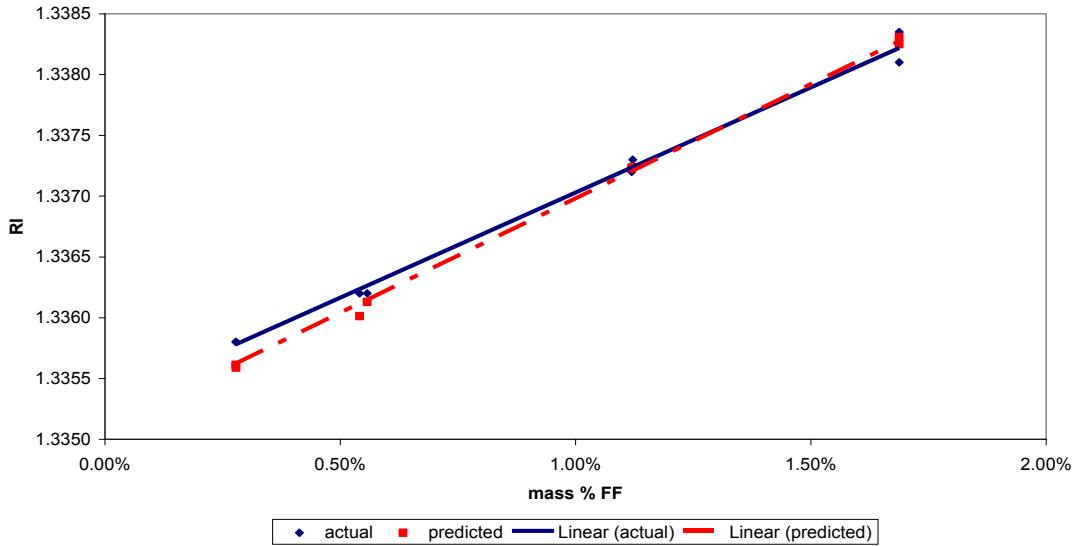
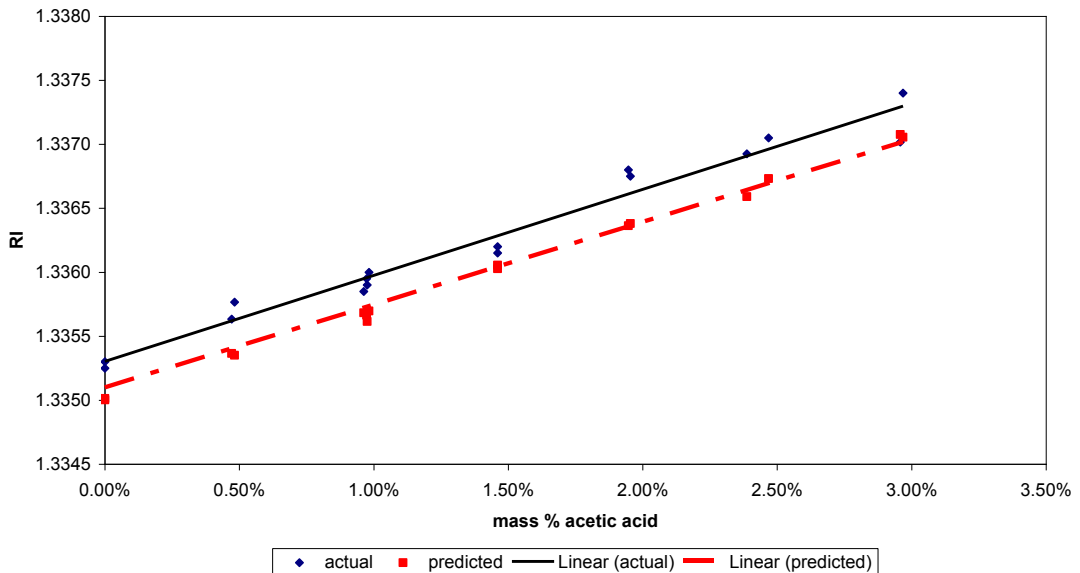


Figure 16: RI for varying mass % of furfural in water at constant (1.2%) acetic acid concentration



**Figure 17: RI for varying mass % of furfural in water at constant (1.3%) hydrochloric acid concentration**



**Figure 18: RI for varying mass % of HAc in water at constant (1.3%) hydrochloric acid concentration**

Figure 16 and Figure 17 show that there is good correlation between the RI measured for a particular solution and that predicted by linear addition. Figure 18 however, indicates that there could be an over-estimation of the amount of furfural in the solution when using this method. The over-prediction of furfural would be 0.14 %wt on average. When one considers that the mass of furfural collected per test solution is of the order of 350 g, this translates to 0.5 g of furfural which is a 9 % over prediction of the final yield. It was assumed that as all ternary combinations had been tested, a quaternary mixture need not be tested.

Unfortunately no HPLC, which is the commonly used equipment for analysis for furfural, was available for doing the analysis.

Appendix B shows the data and method for preparing the calibration curves.

## 5. RESULTS

The furfural concentration was determined from the steps described in 4.4 and since both the mass and volume of solution had been measured during the experiments, the mass of furfural collected for each 35 minute interval for each run could be determined. In order to calculate the furfural yield, the mass of furfural was divided by the starting mass of pentosan and adjusted by the theoretical maximum yield from section 2.1:

$$\text{Furfural Yield} = \frac{\text{mass furfural}}{\text{mass pentosan} \times 0.727} \times 100\% \quad 8$$

The furfural production rate was determined on a kmol per second basis by converting the mass of furfural produced in each 35 minute time step to moles (using the molar mass) and then dividing by the number of seconds in each time step to determine an average rate.

Summarised tables for the results for each run can be found in Appendix D and a sample of the raw data sheets can be found in Appendix E.

Figure 19 to Figure 25 show the furfural production profiles. For some of the runs it was observed that the maximum furfural production was sometimes shifted along the time axis indicating that there may have been problems with the gas flow in the system. This may have resulted in different total reaction times resulting in different furfural yields and hence contributing to the scatter in the experimental data. Figure 19 to Figure 21 show furfural production profiles for comparing runs at the same temperature but different acid concentrations.

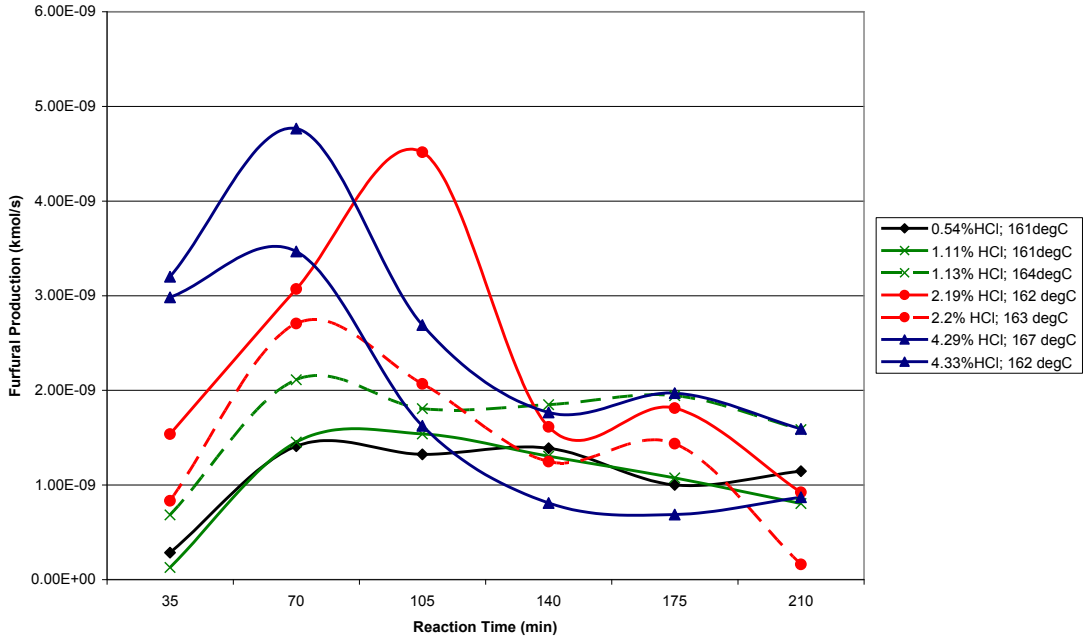


**Figure 19: Comparison of furfural production profiles at a reaction temperature of 160°C and a range of HCl concentrations**

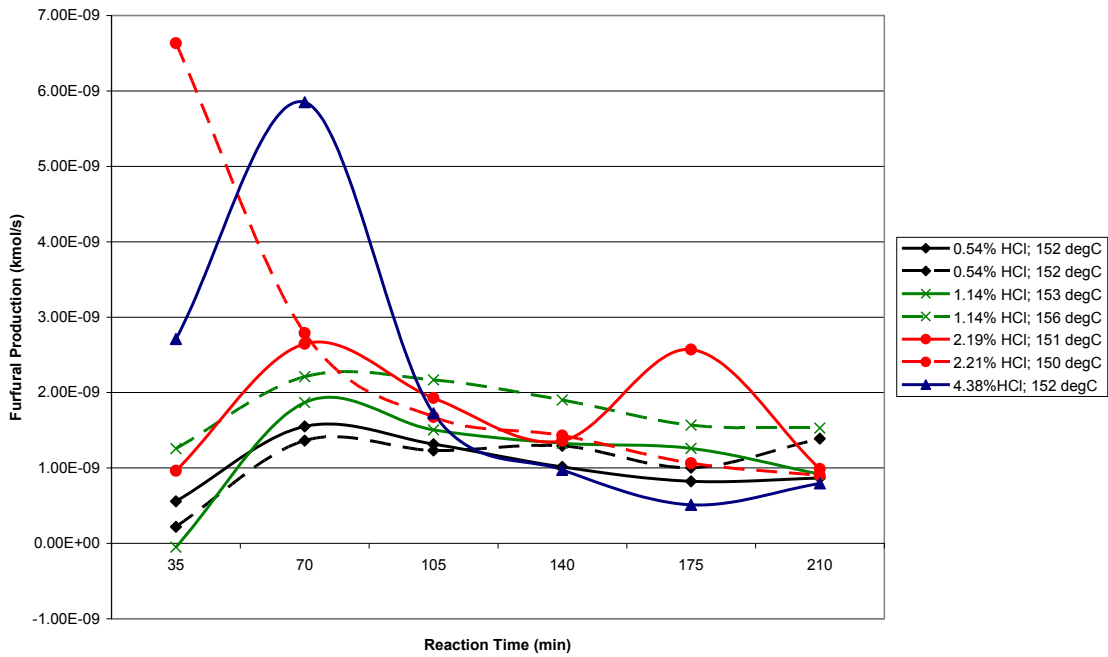


**Figure 20: Comparison of furfural production profiles at a reaction temperature of 150°C and a range of HCl concentrations**

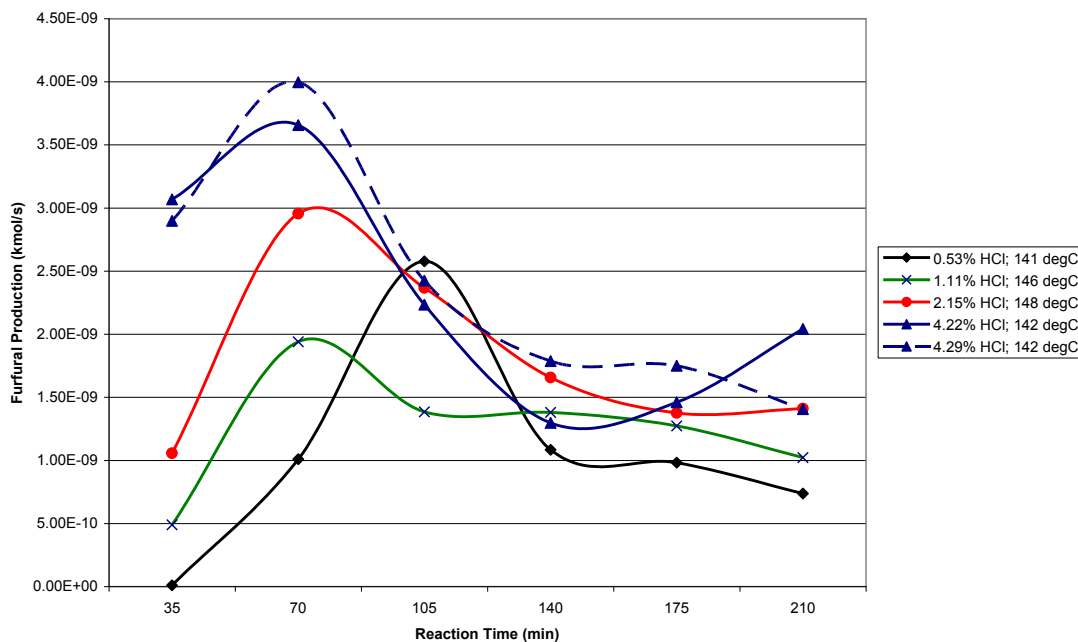


**Figure 21: Comparison of furfural production profiles at a reaction temperature 140°C and a range of HCl concentrations**

From Figure 19 to Figure 21 it was observed that the maxima for each profile generally increased with increasing acid concentration.

In Figure 19, the curve for the test performed at 162°C and 2.19% acid is seen to display a maximum at a different time to the other values. This is most likely because of variations in overall gas flow rate. Particularly, as was observed in some reactions, there was a delay in the time for the flow of liquid to restart. The reaction ‘start-time’ was taken to be 2 minutes after the pump was switched on. It was however observed that the pump behaved slightly differently for the start of each run and that this time would better have been measured as 2 minutes from the first appearance of liquid in the condenser outlet. This ‘shift’ would result in very different final furfural yields as is seen in Figure 26 and Figure 27. The same may be said of the 161°C and 1.11% HCl run in Figure 19 as well as the 150°C and 2.21% HCl run shown in Figure 20.

Figure 22 to Figure 25 show the furfural production profiles comparing runs at the same HCl concentration.



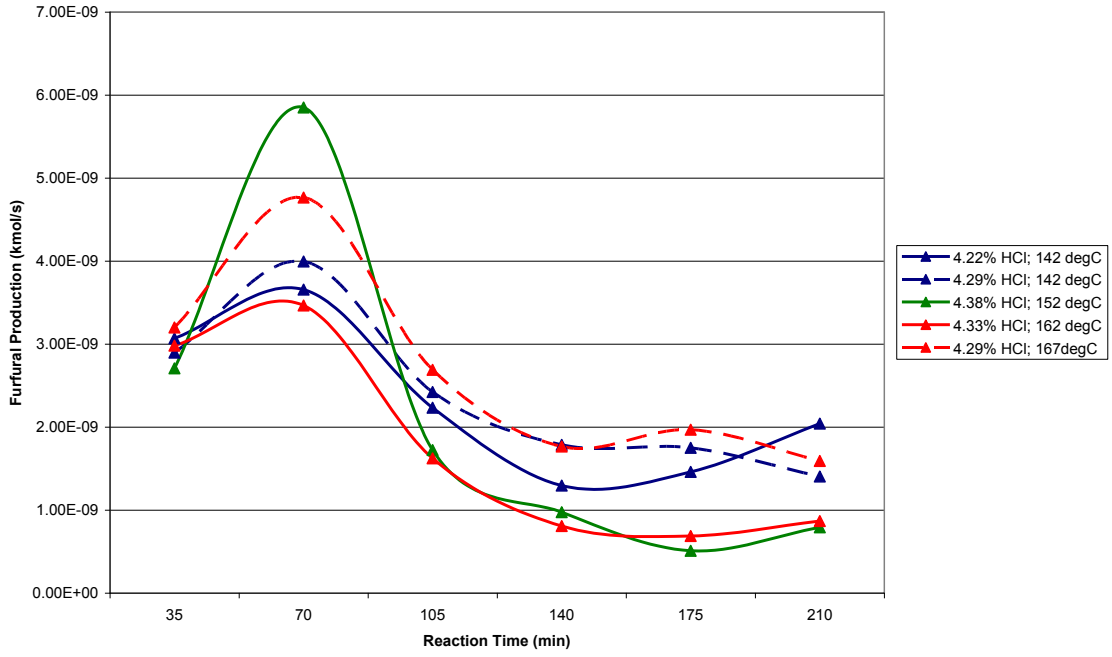


Figure 22: Comparison of furfural production profiles at 4%HCl

Figure 22 shows that increasing temperature resulted in a higher maximum furfural production value for the run.

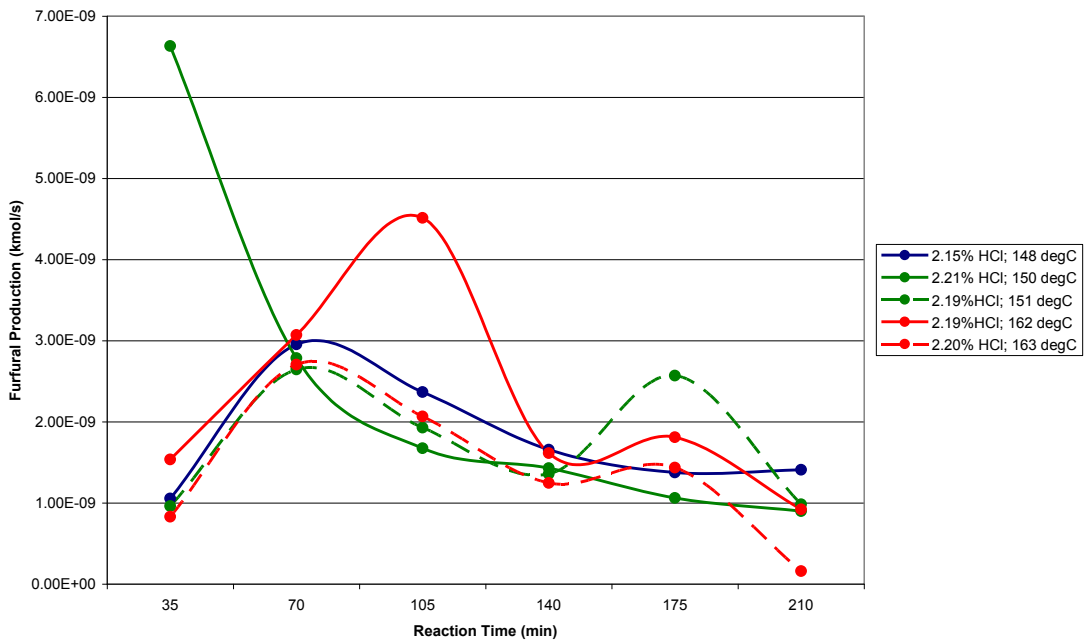
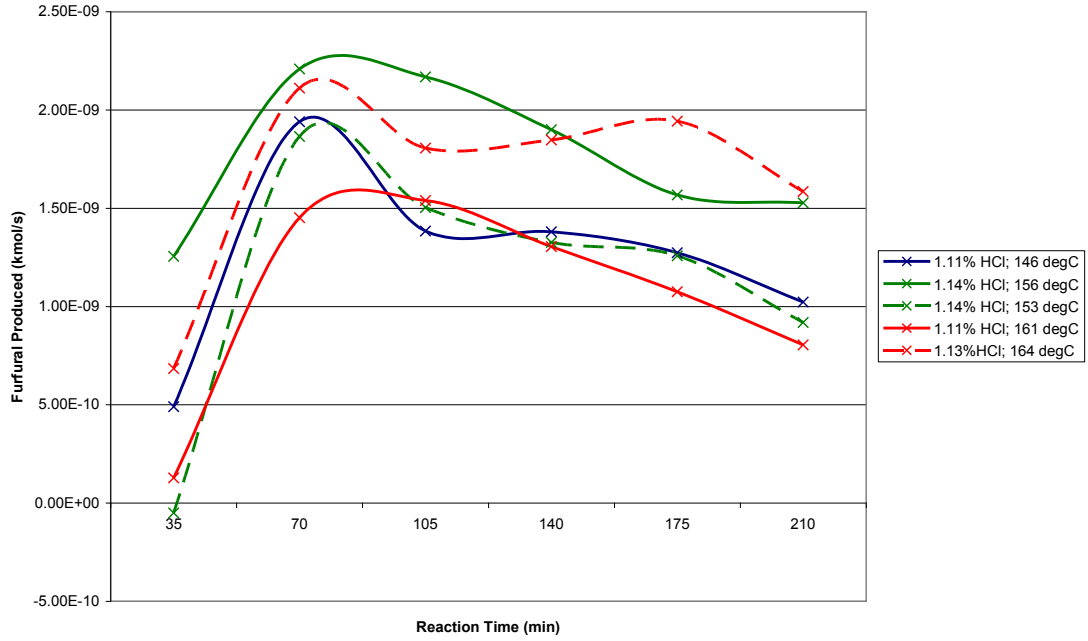
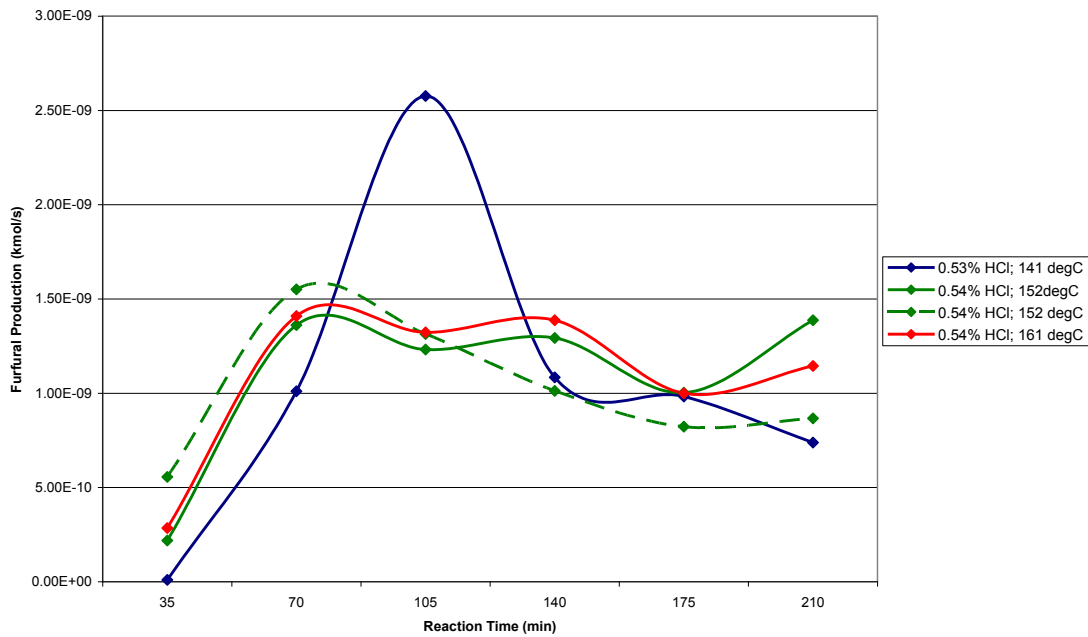


Figure 23: Comparison of furfural production profiles at 2%HCl



**Figure 24: Comparison of furfural production profiles at 1% HCl**

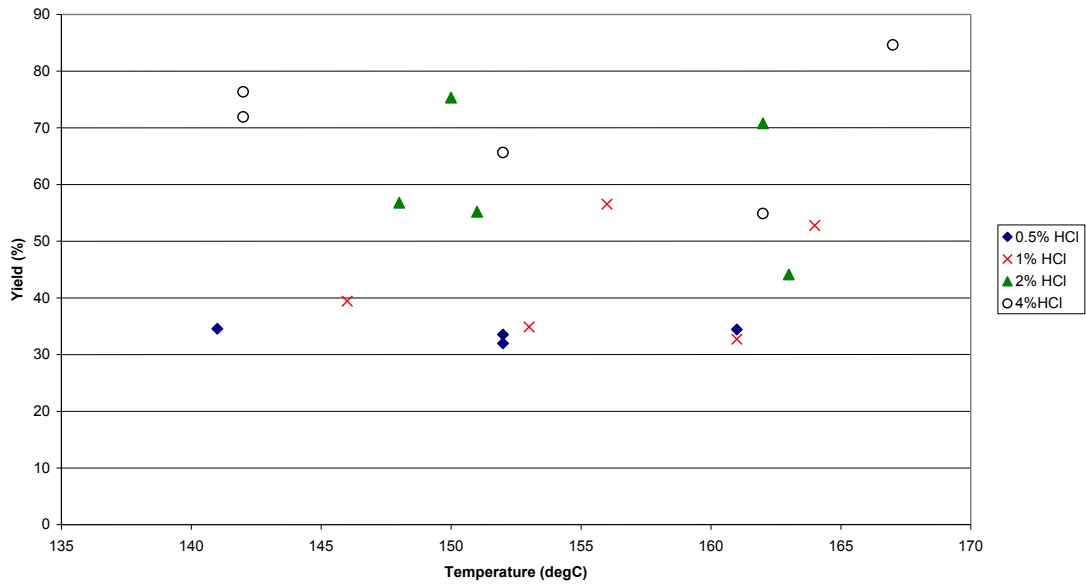


**Figure 25: Comparison of furfural production profiles at 0.5% HCl**

For Figure 23 to Figure 25 the dependence of the maximum furfural production rate on temperature was not apparent (see the discussion of Figure 26).

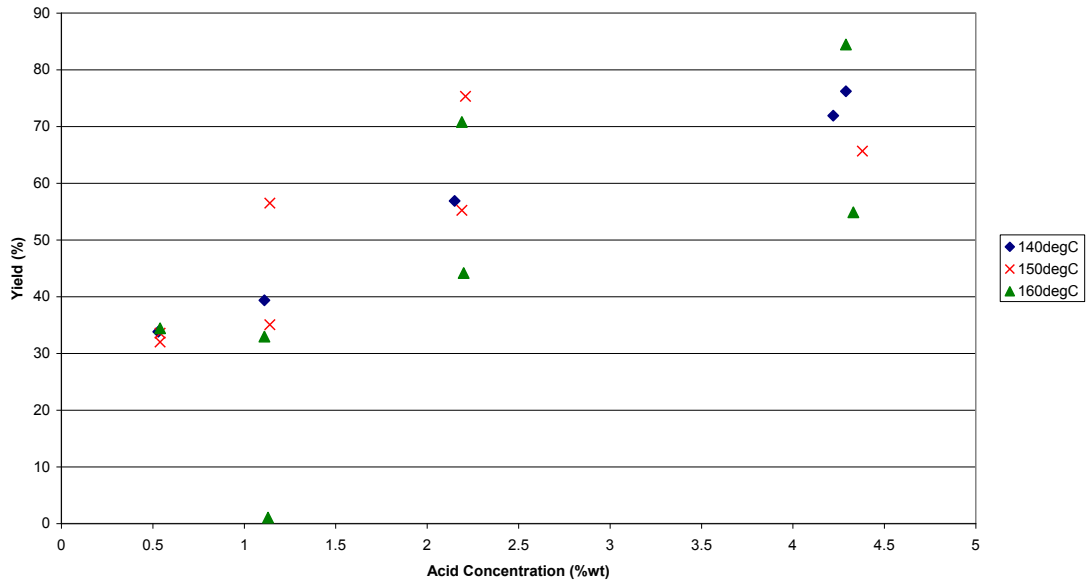
The yield results from the tests performed at each acid concentration and temperature are shown in Figure 26 and Figure 27. Figure 26 shows the effect of increased temperature when the acid

concentration is constant while Figure 27 shows the effect of increased HCl concentration when the reaction temperature is constant.



**Figure 26: Furfural yield (%) versus temperature at different acid concentrations**

Figure 26 shows that there does not appear to be any correlation between the furfural yield and the temperature. This result however needs to be viewed in context of the poor temperature control and measurement and is therefore not conclusive.



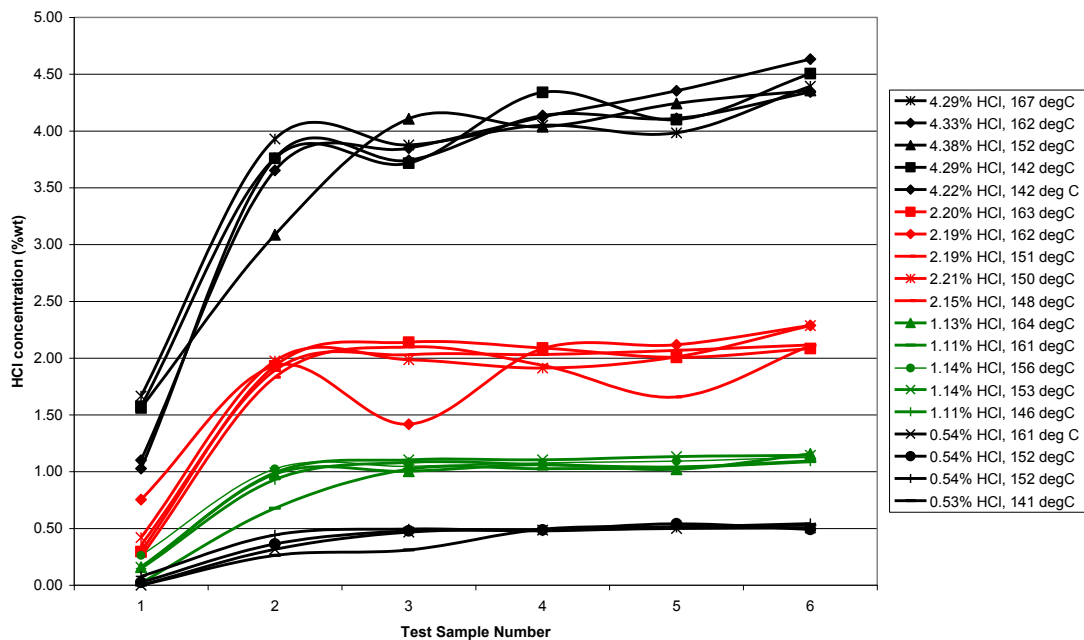
**Figure 27: Furfural yield (%) versus acid concentration at different temperatures**

Figure 27 shows that there did appear to be a relationship between the HCl concentration and the furfural yield with the furfural yield increasing with increasing acid concentration. It was

observed that despite the scatter in some of the replicate points, the yield values ranged from over 30% to over 80% and several of these values were over 60% yield. This indicated that the gaseous HCl catalysed s-Suprayield process was able to produce furfural despite gaseous catalysis being previously thought to be impossible and that the yields achieved were similar to and in some cases higher than those achieved in other processes.

Typically, the main source of error in reaction testwork is the analytical method; however the testwork data indicates that temperature control and measurement may have had a more significant contribution to the error in this instance.

Figure 28 shows the HCl concentration profiles in the product solutions as a function of time.



**Figure 28: HCl concentration in product solution over time**

What is apparent from Figure 28 is that there is an initial dilution of the HCl which may have been a result of the time taken for the HCl to travel from the supply flask to the reactor exit. Although the reactor residence time is short, the time taken for the acid to pass through the vapouriser and the superheater is longer and dilution by the steam initially present in the system may also have occurred. Since there seems to be a proportional relationship between the acid concentration and the furfural yield from Figure 27, the low furfural concentration in the sample collected in the first 35 minutes may be a result of the lower initial acid concentration. The low initial HCl concentration may however be related to the initial adsorption of HCl onto the pentosan molecules with the HCl only reaching a stable concentration once the adsorption

reaction has reached equilibrium. This would result in low initial furfural production while the adsorption reaction takes place.

### 5.1. Statistical tests on data

An analysis of variance was performed on the experimental data to confirm that there exists a statistically significant relationship between the acid concentration and furfural yield (Figure 27) whereas the experimental data shows no clear relationship for temperature and furfural yield (Figure 26). The calculation methods for the statistical data are described in Appendix F.

Table 4 shows the total furfural yield results for the different tests. The average value is shown for tests performed in duplicate.

**Table 4: Furfural yield at the temperatures and acid concentrations tested**

		Acid Concentration (%wt)			
		0.54%	1.12%	2.19%	4.30%
Reaction Temp (°C)	163	34%	43%	58%	70%
	152	33%	46%	65%	66%
	144	35%	39%	57%	74%

Based on this data, an analysis of variance was performed to determine the significance of the effect of each of the two factors on the reaction yield and the significance of any interaction between each factor. The Mean Square Error (MSE) was determined based on the replicated data points. The effect of each factor was then determined from a table consisting of only one data point per condition i.e. replicate data points were averaged.

The calculated  $F_0$  values are as follows:

**Table 5: Table of statistical data**

Effect	$v_1$	$v_2$	$F_0$
<b>A</b>	2	7	0.011
<b>B</b>	3	7	3.799
<b>Interaction</b>	6	7	0.075

In Table 5, effect A and B refer to the effect of temperature the effect of acid concentration respectively while  $F_0$  is the F-test statistic. The parameters  $v_1$  and  $v_2$  are the numerator and denominator degrees of freedom as explained in Appendix F.

**Table 6: Relevant  $F_0$  values at various levels of significance**

<b>0.05</b>	<b>0.025</b>	<b>0.01</b>
4.74	6.54	10.92
4.35	5.89	9.78
3.87	5.12	8.47

Therefore at all levels of significance the interaction effect as well as the effect of temperature was insignificant. At a 5% level of significance, the effect of HCl concentration was found to be significant which confirms what was inferred from the graph.

Despite the statistics indicating that the effect of temperature is not significant, it was felt that these results may have been due to the inconsistencies in the temperature measured and therefore this result should be viewed with caution. More experiments using a better means of temperature control should be performed to verify this result. In the assumptions made in the modelling section, the effect of temperature is still considered.

## 6. MODELLING

The modelling of the process was attempted several times, the details of the most successful model are fully documented. The MATLAB code for the model can be found in Appendix G.

The earlier model assumed that the system could be modelled using only two reactions, the hydrolysis of pentosan chains to pentose monomers and the subsequent dehydration of xylose to furfural. This earlier model also used the assumption that the unreacted core model could be applied to the reaction. This model was unable to adequately predict the experimental data and therefore a new model was sought which also accounted for the acetic acid produced during hydrolysis.

It was found that the modelling of the process required a fairly complex approach for which many parameters, such as the structure of hemicellulose, were not fully studied. It is therefore believed that in order to complete this modelling process, further testwork needs to be done to generate more data and study more parameters and more importantly the structure of the individual players needed to be subjected to further analysis.

### 6.1. Physical description of the process

A stream of superheated steam containing a small amount of hydrogen chloride was fed into the top of a packed bed tubular reactor. The bed consisted of haphazardly packed needle-shaped, milled sunflower husks which consisted of structural components (lignin) and pentosan chains. It was assumed that HCl from the gas phase adsorbed onto the pentosan chains to catalyse the steam hydrolysis in order to produce pentose monomers. The resulting complex then underwent a three-stage dehydration mechanism to produce furfural. As the pentosan chains in different raw materials are to various extents substituted with acetyl, formyl and other such groups, formation of acetic acid occurs during the production of furfural as a product of the hydrolysis of the pentosan chains.

### 6.2. Simplifying assumptions

In order to model this process as a whole, there were two sub-models which fitted into each other viz. the particle reaction and the reactor as a whole. This had the potential to devolve into a fairly complex system of equations but the following assumptions were made in order to simplify the model as much as reasonably possible.

### 6.2.1. The particle model

In a heterogeneous reaction system there are several processes occurring which can affect the reaction rate.

For a heterogeneous reaction the following steps typically occur:

1. Diffusion of the reactant (and in this case the catalyst) to the particle surface
2. Diffusion of the reactant and catalyst into the particle by means of intra-particle diffusion
3. Reaction with solid reactant
4. Diffusion of product and catalyst away from the reaction site
5. Diffusion of the product and catalyst into the bulk gas

In the case of s-Suprayield the process is reversed with the catalyst in the gas phase diffusing to the reactant surface; however the principle remains that the overall reaction rate must take into account extra-particle and intra-particle particle diffusion as well as the reaction rate itself. It may occur that the rate of one of these steps listed above occurs at a significantly slower rate than the other processes in which case it is considered rate limiting and the overall reaction rate is then dependent on the rate of this process only.

In an earlier model described in Appendix H, it was found that this was the case and that the reaction occurs very much more slowly than the diffusion processes and therefore can be considered rate limiting. The diffusion effect can then be ignored. In this model, which used a shrinking core approach to particle modelling, a dimensionless variable ( $\alpha$ ) relating the gas phase mass transfer coefficient to the reaction rate constant was generated. It was calculated as shown in 9:

$$\alpha = \frac{k_{gW}}{2k_1} \quad 9$$

where  $k_{gW}$  is the gas phase mass transfer coefficient for water (m/s)

$k_1$  is the reaction rate constant (here in m/s because of the surface reaction assumed for the shrinking core model)

Using dimensionless numbers the change in the water for the shrinking core model concentration was dependent on  $\alpha$  as shown:



$$y(x_c) = \frac{\alpha}{x_c Sh \ln x_c - x_c + \alpha} \quad 10$$

- where  $x_c$  is ratio of the reactive core radius to the total particle radius  
 $y(x_c)$  is the ratio of the water concentration at the reaction surface to the water concentration in the bulk gas  
 $\alpha$  is a dimensionless variable relating the gas phase mass transfer coefficient to the reaction rate constant  
 $Sh$  is the Sherwood Number

When the gas phase mass transfer coefficient of water was much greater than the reaction rate constant, i.e.  $k_{gw} \gg k_l$ ,  $\alpha \gg (x_c Sh \ln x_c - x_c)$  and:

$$y(x_c) \approx \frac{\alpha}{\alpha} = 1 \quad 11$$

It can therefore be assumed that the water concentration at the solid reaction surface is the same as in the bulk gas. This implies that extraparticle diffusion resistance can be ignored in the overall process rate.

Using a reaction rate constant,  $k_l$ , of  $5 \times 10^{-7}$  m/s which gave a reasonable approximation of conversion, a range of values for the mass transfer coefficients were tested to determine a value at which the assumption in Equation 11 would no longer be valid. The results are shown in Table 7.

**Table 7: Tested  $k_{gw}$  values and corresponding  $y(x_c)$  values**

$k_{gw}$	$y(x_c)$
1E-01	1.00
1E-02	1.00
1E-03	1.00
1E-04	1.01
5E-05	1.03
1E-05	1.15
5E-06	1.35

Table 7 shows that the assumption that  $y(x_c) \approx 1$  is no longer valid for  $k_{gw}$  values of the order of  $10^{-5}$  m/s and lower. The determination of  $k_{gw}$  for this application is shown in Appendix I and was found to be 0.74 m/s which is very much greater than  $10^{-5}$  m/s indicating that  $y(x_c) \approx 1$  and the effects of extra particle diffusion can thus be ignored in the overall process.

For modelling purposes this also negates the dependence of the reaction rate on the position within the particle and therefore spatial dependencies can be ignored resulting in only one variable, time.

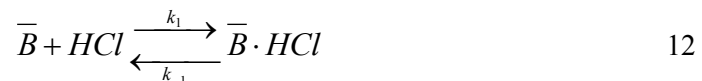
### 6.2.2. The reactor model

Since the reactor and particularly the bed volume is very small, the residence times in the reactor become very short when compared to the characteristic reaction time and therefore changes in the ‘z’ (reactor length) domain can be ignored. It is also assumed that the gas disperses radially and therefore the assumption of perfect mixing can be made. Ultimately spatial domains can be ignored and only the time domain need be considered as a result of the gas composition being dependent upon the reaction in the individual particles.

Using the assumed bulk density of 981 kg/m<sup>3</sup> from 4.2.2.1, the volume of 18 g of sunflower hulls was calculated to be 1.83x10<sup>-5</sup> m<sup>3</sup>. Using the pumping mass flow rate in Section 4.2.1 of 2.16x10<sup>-5</sup> kg/s and a superheated steam density at 160°C of 0.51kg/m<sup>3</sup> (from the Chemical Logic Steam Table Companion (2003)) the gas volumetric flow rate was 4.24 x10<sup>-5</sup> m<sup>3</sup>/s resulting in a gas residence time of approximately 0.4 seconds.

### 6.3. Modelling of the reaction mechanism

The reaction mechanism was modelled assuming a three-step chemical reaction process. In the first step, a single pentose monomer in the pentosan chain attached to an HCl molecule to form an intermediate  $\overline{B} \cdot HCl$  complex as shown in Equation 12. It was assumed that the adsorption process was reversible.  $\overline{B}$  is the hemicellulose which takes into account the non-xylose groups as per the hemicellulose description in section 2.3. This species has a molar mass of 163.22 kg/kmol (132.11 kg/kmol for the xylan monomer + 0.74\*42.04 kg/kmol for the acetyl groups). It was assumed that the TAPPI method is used to determine the total pentosan concentration i.e. “the combined polysaccharides of xylose monomers and arabinose” (Lavarack et al., 2002). This implied that the concentration of only the pentose sugars was determined from this method and therefore it was adjusted to account for the non-pentose groups as shown in Equation 12:



The resulting complex exhibited much higher reactivity than the original pentosan monomer and therefore reacted readily with water resulting in depolymerisation of the pentosan chain and the formation of a pentose molecule. This pentose molecule however was assumed to remain attached to the HCl molecule. A side reaction involving hydrolysis of the acetyl groups on the pentosan chain also took place resulting in the production of acetic acid. In order to simplify the modelling, it was assumed that both the hydrolysis of the pentosan monomers and the acetyl groups took place at the same rate and that the reaction system can be described as follows:



The hydrolysis was assumed to be followed by dehydration of a pentose molecule and the simultaneous desorption of the HCl to produce furfural:



This proposed reaction scheme excluded the occurrence of the side reactions described in section 2.1.

The following sub-scripts for the reaction components will be used in the sections that follow:

- B – Monomer in the pentosan chain
- W – Water
- F – Furfural
- A – Acetic Acid
- H - Hydrogen chloride
- BH – Pentose monomer and HCl complex
- PH – Pentose sugar and HCl complex

#### 6.4. Reaction rate kinetics

The system was heterogeneous and it was therefore necessary to account for the processes occurring in individual solid particles as well as those occurring in the gas phase. It was assumed that the unreacted solid material was porous enough to be penetrated by the reactant gas through the mechanism of intraparticle diffusion. For this reason the model of progressive conversion was considered to be more applicable to this system than the popular unreacted core model. In addition the progressive conversion model could be simplified further, since for slow reactions, the diffusion process could be believed to be fast enough to constantly replenish the reactant losses due to reaction. As a result the gas composition inside the particle would remain practically the same as that at the external surface of the particle. It has been discussed in 6.2.1 that the extra-particle mass transfer resistance could be ignored as well and therefore the gas composition within the particle remains uniform and identical to that of the corresponding bulk composition of the gas phase. It was also assumed that the porosity of the sunflower husks does not change with increasing conversion of xylan. These conditions were considered to be valid for the entire duration of the reaction.

Since there were three independent reactions in the proposed reaction mechanism, three independent rate expressions were sufficient to describe the reaction kinetics. If one assumes that the reactions are elementary then:

$$r_1 = k_1 C_B C_H - k_{-1} C_{BH} \quad 15$$

$$r_2 = k_2 C_{BH}^S C_W^G \quad 16$$

$$r_3 = k_3 C_{PH}^S \quad 17$$

where  $r_1 - r_3$  are the three reaction rates

$k_1 - k_3$  are the reaction rate constants

$C_j$  is the concentration of component  $j$  (in kmol/m<sup>3</sup>)

The superscripts  $S$  and  $G$  refer to solid and gas phase respectively

Through the use of the equilibrium constant  $K = k_1/k_{-1}$ , Equation 15 can be rewritten as:

$$r_1 = k_1 C_B C_H - \frac{k_1}{K} C_{BH} \quad 15a$$

All the reaction rates were defined in the conventional way i.e. per unit volume of the porous solid material. The solid phase volume includes that of pentosan, its complexes as well as lignin and cellulose. The raw solid material contained 25.2% pentosan by mass and the remaining material was considered to be made up of non-reactive lignin and cellulose. Although finally all the products were in the vapour phase, it was assumed that the change in the solid volume over the course of the reaction was negligible.

When developing the material balances for the reactor, it became apparent that for convenience, matrix-vector notation should be used. In this new notation, the reaction rate vector  $\mathbf{r} = [r_1, r_2, r_3]^T$  is a function of the gas-phase concentration vector  $\mathbf{C}^G = [C_F^G, C_A^G, C_W^G, C_H^G]^T$  as shown in Equation 18:

$$\mathbf{r} = \Lambda_1 \mathbf{C}_G + \Lambda_0 \quad 18$$

where  $\Lambda_1$  and  $\Lambda_0$  are defined as follows:

$$\Lambda_1 = \begin{bmatrix} 0 & 0 & 0 & k_1 C_B^S \\ 0 & 0 & k_2 C_{BH}^S & 0 \\ 0 & 0 & 0 & 0 \end{bmatrix} \quad 19$$

$$\Lambda_0 = \begin{bmatrix} \frac{k_1}{K} C_{BH}^S \\ 0 \\ k_3 C_{PH}^S \end{bmatrix} \quad 20$$

## 6.5. Reaction stoichiometry

The stoichiometry of the proposed system of three reactions has been reflected in the net formation rate equations written for individual reaction species in terms of the rates  $r_1$ ,  $r_2$  and  $r_3$ :

$$R_B = -r_1 \quad 21$$

$$R_{BH} = r_1 - r_2 \quad 22$$

$$R_{PH} = r_2 - r_3 \quad 23$$

$$R_A = 0.74r_2 \quad 24$$

$$R_F = r_3 \quad 25$$

$$R_W = -1.74r_2 + 3r_3 \quad 26$$

$$R_H = -r_1 + r_3 \quad 27$$

The set of rate equations described in Equation 21 to Equation 27 can be written using an equivalent matrix notation as:

$$\mathbf{R} = \mathbf{S}^T \mathbf{r} \quad 28$$

where the stoichiometry matrix

$$\mathbf{S} = \begin{bmatrix} 0 & 0 & 0 & -1 & -1 & 1 & 0 \\ 0 & 0.74 & -1.74 & 0 & 0 & -1 & 1 \\ 1 & 0 & 3 & 1 & 0 & 0 & -1 \end{bmatrix} \quad 29$$

For convenience, the net formation rate vector  $\mathbf{R}$  has been broken into two parts,  $\mathbf{R}_G = [R_F, R_A, R_W, R_H]^T$  and  $\mathbf{R}_S = [R_B, R_{BH}, R_{PH}]^T$ , corresponding to gas-phase species (furfural, acetic acid, water and HCl) and solid-phase species (pentosan, pentosan-HCl complex and pentose-HCl complex), respectively

$$\mathbf{R} = \begin{bmatrix} \mathbf{R}_G \\ \mathbf{R}_S \end{bmatrix} \quad 30$$

An analogous partition has been performed on the stoichiometry matrix:

$$\mathbf{S} = [\mathbf{S}_G \quad \mathbf{S}_S] \quad 31$$

where

$$\mathbf{S}_G = \begin{bmatrix} 0 & 0 & 0 & -1 \\ 0 & 0.74 & -1.74 & 0 \\ 1 & 0 & 3 & 1 \end{bmatrix} \quad 32$$

$$\mathbf{S}_S = \begin{bmatrix} -1 & 1 & 0 \\ 0 & -1 & 1 \\ 0 & 0 & -1 \end{bmatrix} \quad 33$$

## 6.6. Reactor modeling

In principle, the process was unsteady and the reactor, i.e. the solid and gas phase, could be classified as a distributed-parameter system. Due to the characteristic reaction time being much larger than the gas residence time, several simplifying assumptions regarding the operation of the reactor could be made. Firstly, it was noted that the system operates in semi-batch mode as the solid phase constituted a closed (batch) system while the gas phase was an open (flow) system. In other words, the reactor bed operated as a differential bed under unsteady state conditions. For the same reason the accumulation of species in the gas phase present in the reactor could also be neglected. These assumptions allowed for the application of the pseudo-steady-state assumption to the gas phase. It could not be considered as entirely steady state as the gas phase still operated under non-steady state conditions, which was a result of the constant kinetic interaction with the solid phase which is inherently transient.

### 6.6.1. Gas-phase material balances

Following the above discussion it was decided to neglect both the accumulation terms as well as axial concentration gradients from the material balances of the gas phase. This resulted in algebraic rather than differential material balances for each component in the gas phase.

The material balance equation without accumulation is:

$$in - out + generation = 0$$

Using the equation above, the material balance for component  $j$  is:

$$F_{j,0} - qC_j + R_jV_s = 0 \quad 34$$

- where  $F_{j,0}$  is the feed molar flow rate of component  $j$  (in kmol/s)  
 $q$  is the total gas flow rate (in m<sup>3</sup>/s)  
 $C_j$  is the molar concentration of component  $j$  in the gas phase (in kmol/m<sup>3</sup>)  
 $R_j$  is the net formation rate of component  $j$  per unit of volume of solid (in kmol/(m<sup>3</sup>s))  
 $V_s$  Volume of solid (in m<sup>3</sup>)

Since the equations are the same for all gas phase components, the vectors and matrices determined in 6.4 and 6.5 can be used to write the set of material balance equations in matrix notation as follows:

$$\mathbf{F}_0 - q\mathbf{C}_G + \mathbf{R}_G V_S = \mathbf{0} \quad 35$$

where  $\mathbf{F}_0 = [F_{F0}, F_{A0}, F_{W0}, F_{H0}]^T$  is the vector of molar feed flow rates  
 $q$  is the total gas volumetric flowrate  
 $\mathbf{C}_G$  is the vector of component concentrations in the gas phase  
 $\mathbf{R}_G$  is the net formation vector for the gas phase components only  
 $V_S$  is the solid volume

By substituting Equation 18 into Equation 28 one obtains for the net formation rate:

$$\mathbf{R} = \mathbf{S}^T (\mathbf{\Lambda}_1 \mathbf{C}_G + \mathbf{\Lambda}_0) \quad 28_a$$

then taking only the gas phase components would give:

$$\mathbf{R}_G = \mathbf{S}_G^T (\mathbf{\Lambda}_1 \mathbf{C}_G + \mathbf{\Lambda}_0) \quad 28_b$$

$\mathbf{R}_G$  can then be substituted into 35:

$$\mathbf{F}_0 - q\mathbf{C}_G + \mathbf{S}_G^T (\mathbf{\Lambda}_1 \mathbf{C}_G + \mathbf{\Lambda}_0) V_S = \mathbf{0} \quad 36$$

Equation 36 can then be rearranged as follows to solve for the vector  $\mathbf{C}_G$ :

$$\begin{aligned} \mathbf{F}_0 + \mathbf{S}_G^T \mathbf{\Lambda}_0 V_S &= q\mathbf{C}_G - \mathbf{S}_G^T \mathbf{\Lambda}_1 \mathbf{C}_G V_S \\ \mathbf{F}_0 + \mathbf{S}_G^T \mathbf{\Lambda}_0 V_S &= \mathbf{C}_G (q\mathbf{E}_4 - \mathbf{S}_G^T \mathbf{\Lambda}_1 V_S) \\ \mathbf{C}_G &= (q\mathbf{E}_4 - \mathbf{S}_G^T \mathbf{\Lambda}_1 V_S)^{-1} (\mathbf{F}_0 + \mathbf{S}_G^T \mathbf{\Lambda}_0 V_S) \end{aligned} \quad 37$$

Note that the 4x4 identity matrix  $\mathbf{E}_4$  is introduced so that the scalar  $q$  can be applied to the matrix equation.

As the reaction is non-equimolar, the gas phase volumetric flow rate,  $q$ , changes during the course of reaction; however the variation of  $q$  was ignored since a large excess of steam was used in the feed stream so the change could be considered negligible.

If the change in  $q$  were to be calculated, it could be done by imposing on  $\mathbf{C}_G$  the requirement of a constant total molar gas concentration under isobaric conditions since the pressure drop is expected to be negligible due to the short bed length.

### 6.6.2. Solid-phase material balances

As the solid bed operates in a batch mode, it is more convenient to describe its behavior in terms of the absolute number of moles rather than molar concentrations. Since the solid phase

represents a batch system it is inherently in unsteady-state but axial gradients can still be ignored. In a similar manner to Equation 35 the set of equations for each component can be written in matrix notation as follows:

$$\frac{d\mathbf{N}}{dt} = \mathbf{R}_S V_S = \mathbf{S}_S^T \mathbf{r} V_S \quad 38$$

where  $\mathbf{N} = [N_B, N_{BH}, N_{PH}]^T$  is the vector of the absolute number of moles of the solid phase species

The initial value of  $\mathbf{N}$  at time zero is:

$$N(0) = [N_{B0}, 0, 0]^T$$

Equation 38 is nonlinear due to nonlinear kinetics and can only be solved numerically. It has to be considered together with Equation 37 as the solid-phase kinetics depends on the gas-phase concentrations.

### 6.6.3. Calculation of measurables

Since the model had to predict the values determined experimentally in order to fit the model parameters, these were calculated as follows:

- mass concentration of furfural in a liquid sample (g/L)

$$\bar{C}_F(t_i, t_{i-1}) = M_F \frac{n_F(t_i) - n_F(t_{i-1})}{V_{Li}} \quad 39$$

- mass concentration of acetic acid in a liquid sample (g/L)

$$\bar{C}_A(t_i, t_{i-1}) = M_A \frac{n_A(t_i) - n_A(t_{i-1})}{V_{Li}} \quad 40$$

- mass concentration of hydrogen chloride in a liquid sample (g/L)

$$\bar{C}_H(t_i, t_{i-1}) = M_H \frac{n_H(t_i) - n_H(t_{i-1})}{V_{Li}} \quad 41$$

where  $n_j$  ( $j=F, A, H$ ) is the number of moles of species  $j$  which left the reactor since the beginning of the experiment

$M_j$  is the molecular mass of species  $j$ ,

$t_i$  is the current time instant

$t_{i-1}$  is the previous time instant

$V_{Li}$  is the volume of sample collected at this time instant

The functions  $n_j(t)$  can be evaluated either by direct integration as:



$$n_j(t) = \int_0^t qC_j^G dt \quad 42$$

or by solving an additional differential equation:

$$\frac{dn_j}{dt} = qC_j^G, \quad n_j(0) = 0 \quad 43$$

## 6.7. Optimisation of model parameters

It was necessary to find the model parameters which gave the best fit between the model generated concentrations and the experimental data. In order to achieve this, a performance index was evaluated which compared the values of the experimentally measured concentrations to the corresponding value generated by the model.

Firstly the error was calculated for each run (n) and each component as shown in Equation 44:

$$\mathbf{E}_j^n = \frac{\mathbf{c}_{j,\text{mod}}^n - \mathbf{c}_{j,\text{exp}}^n}{\bar{\mathbf{c}}_{j,\text{exp}}^n} \quad 44$$

where  $\mathbf{E}_j^n$  is the error for component  $j$  and run 'n'

$\mathbf{c}_{j,\text{mod}}^n$  is the vector of concentrations for component  $j$  predicted by the model

$\mathbf{c}_{j,\text{exp}}^n$  is the vector of concentrations for component  $j$  measured in the experiment

$\bar{\mathbf{c}}_{j,\text{exp}}^n$  is the average concentration for component  $j$  measured during the experiment.

The performance index was then determined as shown in Equation 45:

$$I = \sqrt{\frac{\sum_n \left( \sum_j E_j^n \right)^2}{N}} \quad 45$$

where  $I$  is the performance index and  $N$  is the total number of runs

$N$  is the total number of analyses from all runs

The reaction rate constants used for the modelling were assumed to conform to the Arrhenius equation which is shown in equation 46:

$$k_i = k_{i,0} \exp \left[ \frac{-E_i}{R} \left( \frac{1}{T_R} - \frac{1}{T_A} \right) \right] \quad 46$$

where  $k_{i,0}$  is the pre-exponential factor  
 $E_i$  is the activation energy  
 $R$  is the universal gas constant  
 $T_R$  is the reaction temperature in K  
 $T_A$  is the ambient temperature in K

Analogously the equilibrium constant may be written as:

$$K = K_0 \exp \left[ \frac{-DH}{R} \left( \frac{1}{T_R} - \frac{1}{T_A} \right) \right] \quad 47$$

where  $DH$  is a randomly assigned name for the variable analogous to the activation energy

A built-in MATLAB optimisation search function was used to determine the best fit for the experimentally generated data by determining the values of  $k_{i,0}$  and  $E_i$  which would give the minimum value for 'I'.

## 6.8. Modelling results and discussion

The modelling resulted in the following results which gave a performance index of 0.62.

**Table 8: Modelling results with reaction rate constants calculated at 160°C**

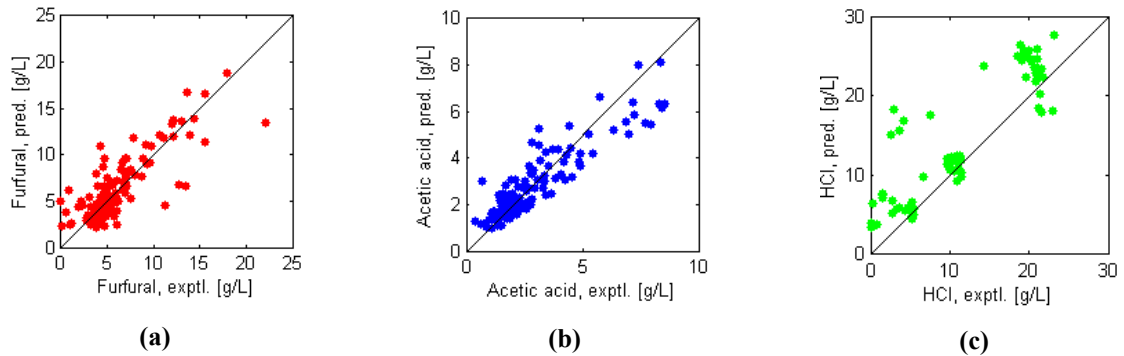
$k_{10}$ [m <sup>3</sup> /(kmol.s)]	151.83	$E_1/R$ [K]	5121.63	$k_1 =$ [m <sup>3</sup> /(kmol.s)]	0.72
$K_0$ [m <sup>3</sup> /kmol]	2385.11	$DH/R$ [K]	79.25	$K =$ [m <sup>3</sup> /kmol]	2195
$k_{20}$ [m <sup>3</sup> /(kmol.s)]	17.48	$E_2/R$ [K]	717.82	$k_2 =$ [m <sup>3</sup> /(kmol.s)]	8.25
$k_{30}$ [1/s]	20.69	$E_3/R$ [K]	870.05	$k_3 =$ [1/s]	8.33

The values of the reaction rate constant for each step indicated that reaction 1 proceeded slowest while reaction 2 and reaction 3 occurred at more or less the same rate. The large value of  $K$

indicated that reaction 1 occurred more rapidly in the forward direction than in the reverse direction.

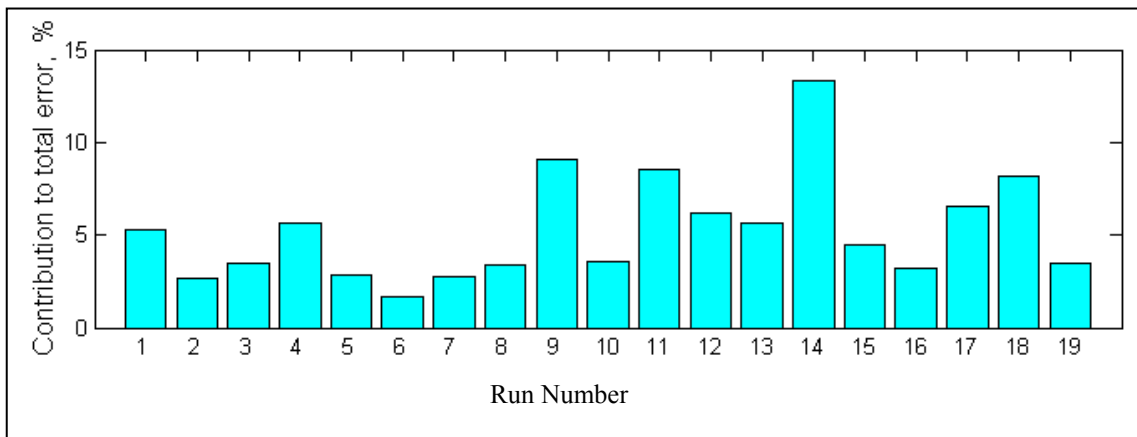
This fit may not be the optimal solution as it is a complex problem to find an optimal solution for 8 different variables.

The scatter of the data is shown in Figure 29 and Figure 30



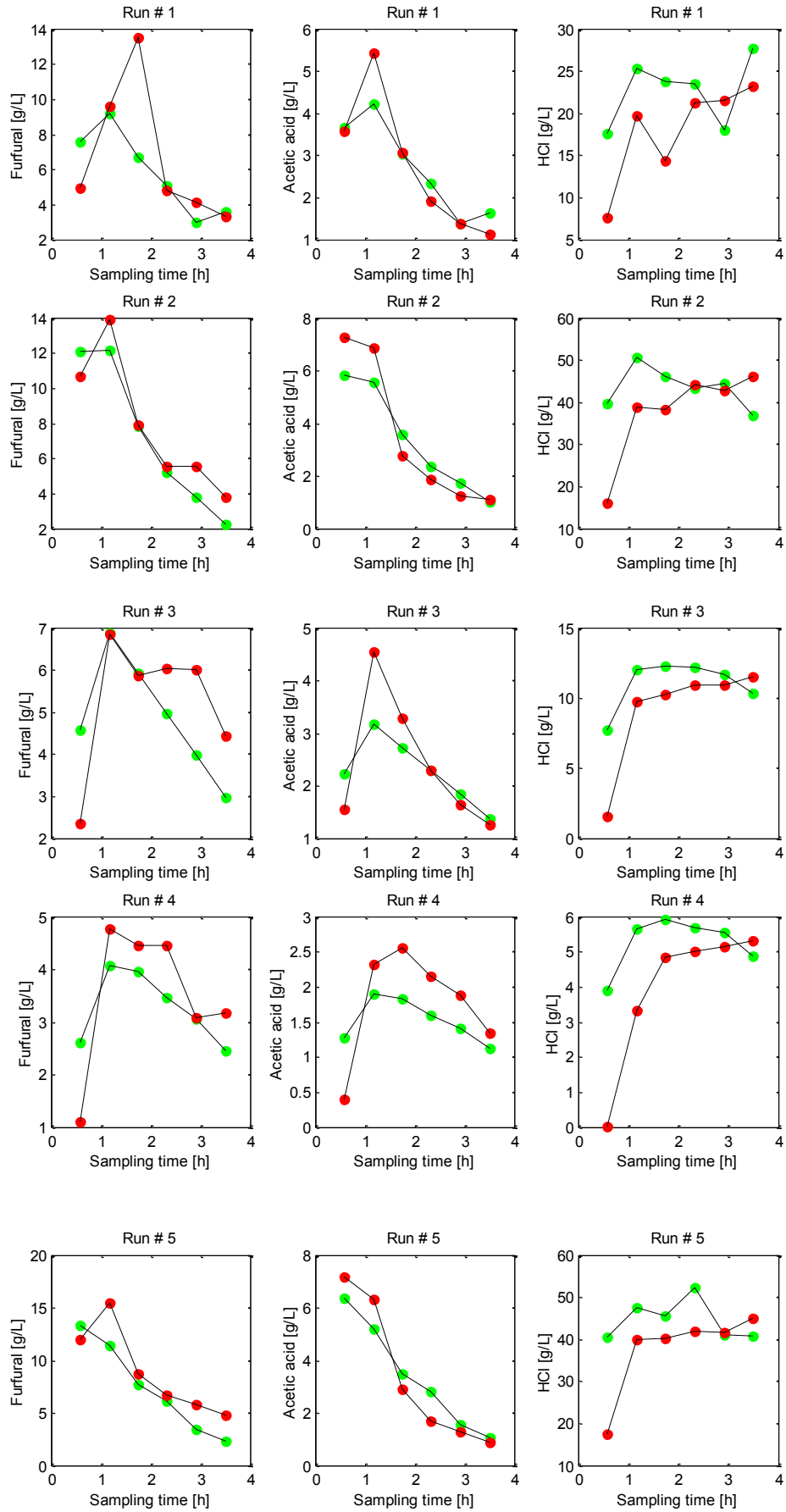
**Figure 29: Comparison of experimentally determined concentration and that determined by the model for (a) furfural, (b) acetic acid and (c) hydrochloric acid**

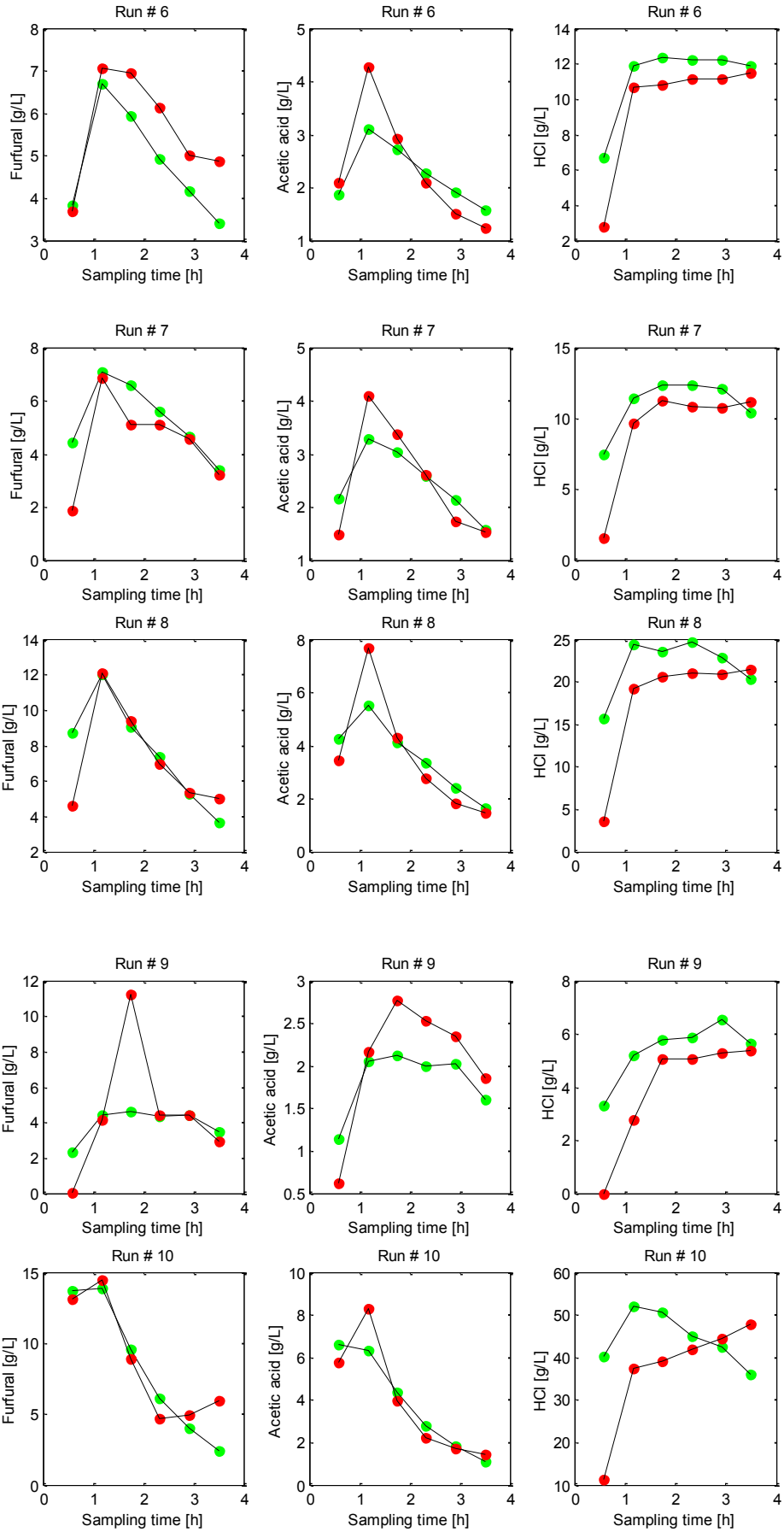
From Figure 29 it was apparent that while reasonable fit of the furfural and acetic acid data could be achieved, the HCl tended to be over-predicted.

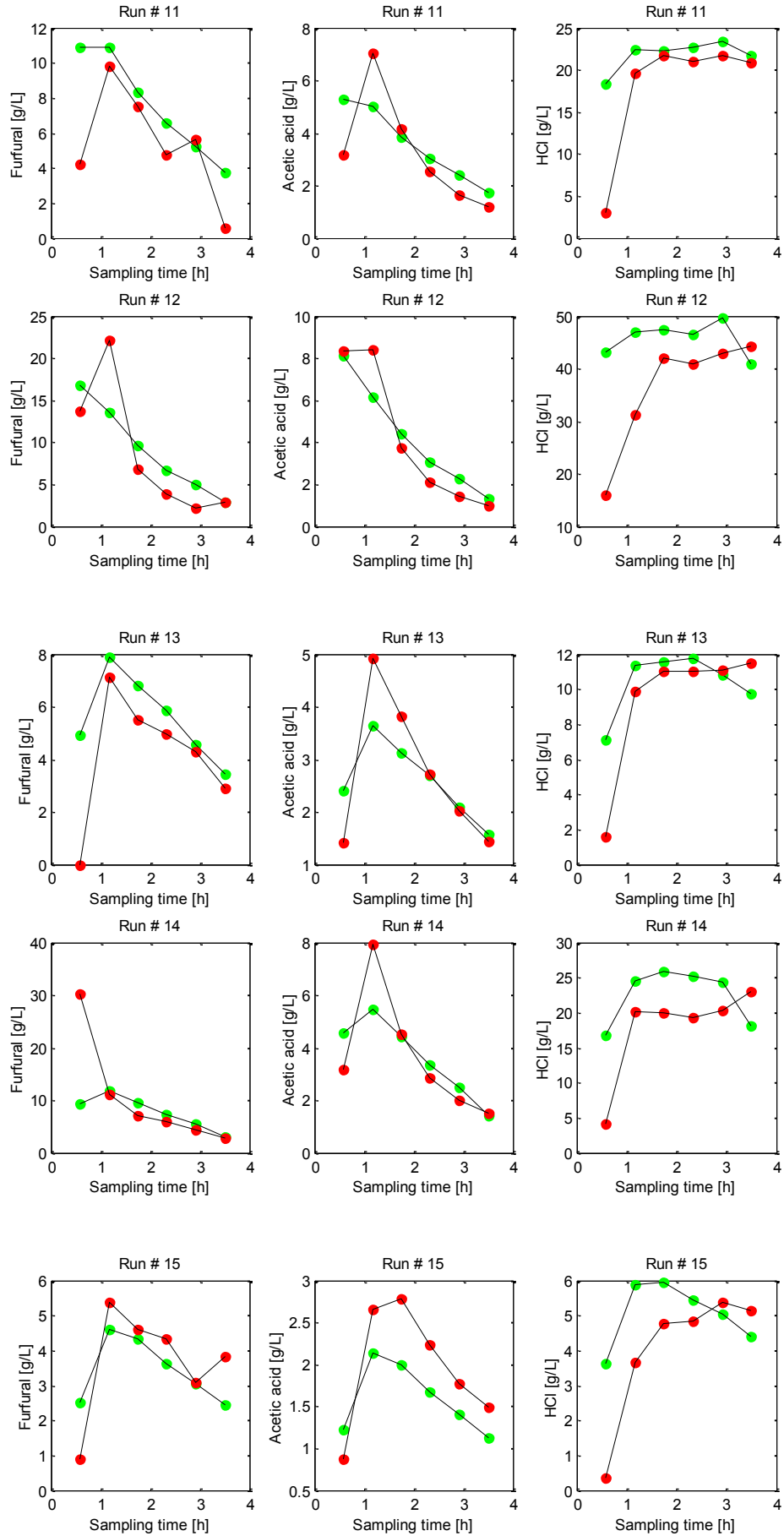


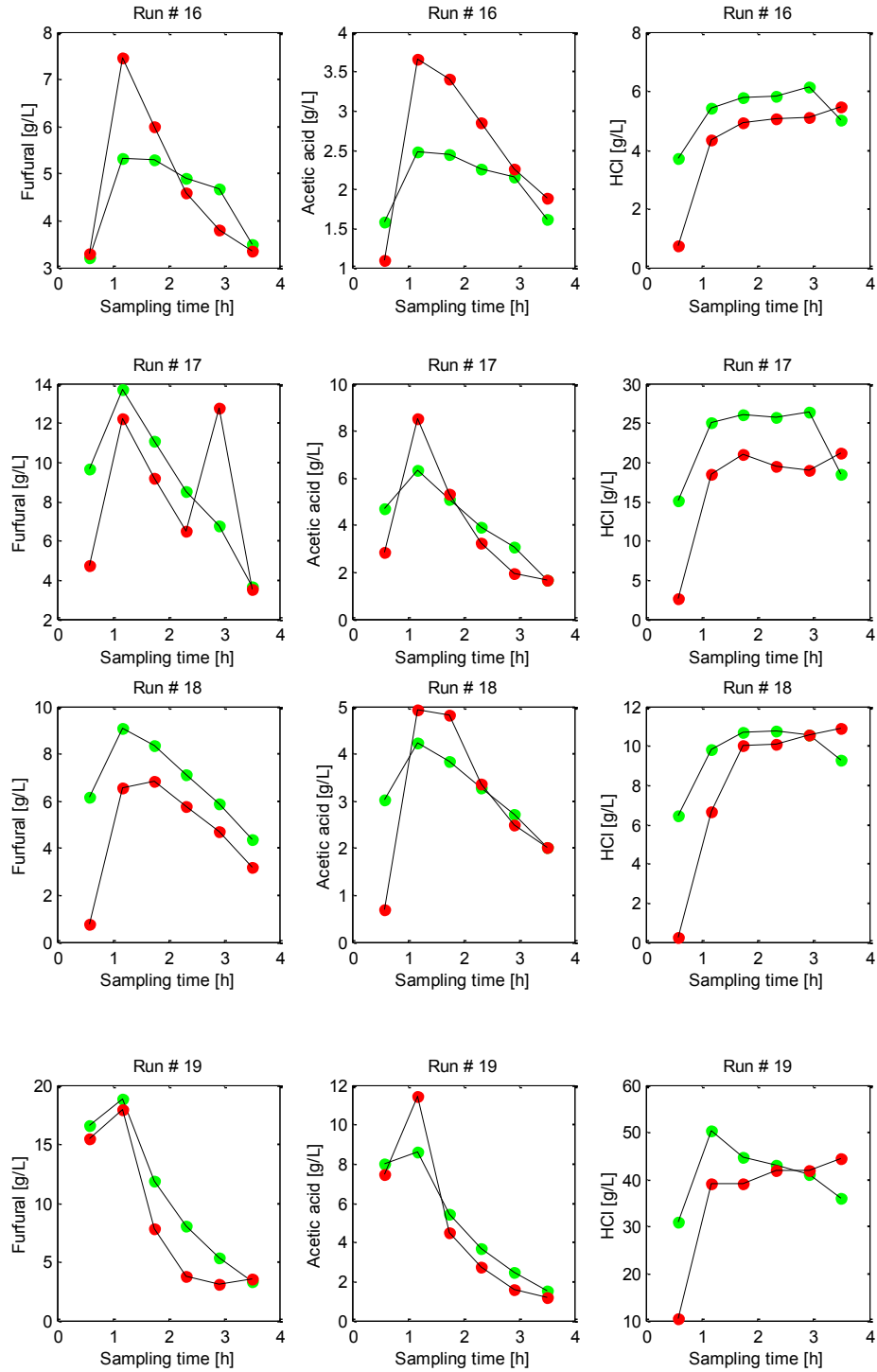
**Figure 30: Contribution of each run to the total error (performance index)**

Figure 30 shows that run 14 made the largest contribution to the error with 14% of the total error attributable to this run.









**Figure 31: Comparison of experimentally determined concentration versus time profiles (shown in red) and predicted profiles (shown in green) for furfural, acetic acid and hydrochloric acid for each run**

Figure 29 further demonstrates that different runs gave different qualities of fit of the data. The poor overall fit was most likely attributable to experimental error as a result of inaccuracies in temperature measurement and inaccuracies in the determination of the quantities in the product solution.

The profiles for each component of each run can be found in the Appendix J but the profiles for run 1 are shown in Figure 32 below for discussion purposes:

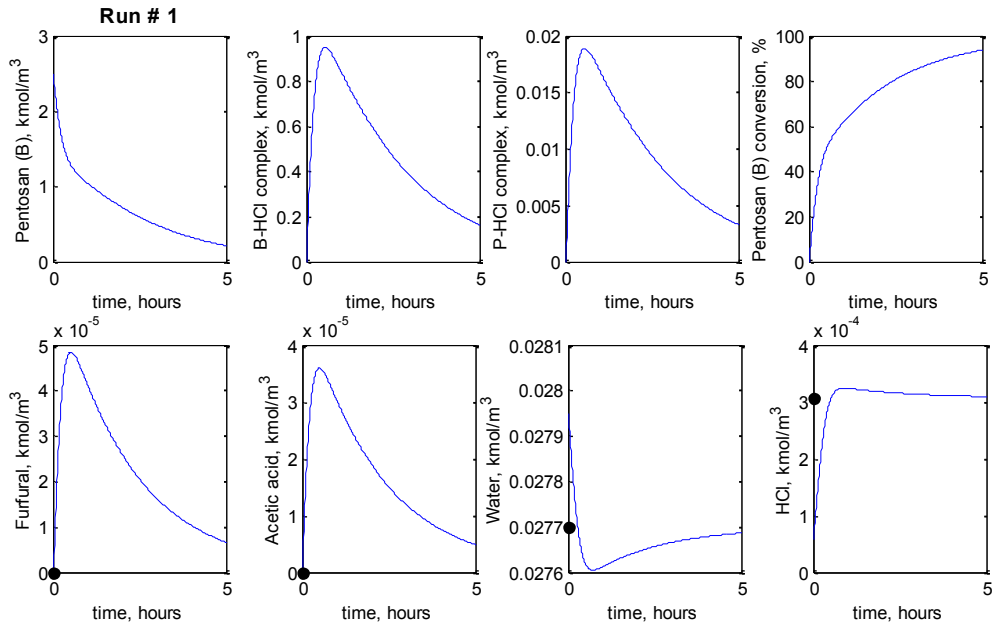


**Figure 32: Concentration profiles**

Figure 32 shows that the pentosan (B) undergoes an initial exponential decrease in concentration as the pentosan is complexed with the HCl. The pentosan-HCl (B-HCl) concentration increases rapidly following a more or less exponential trend until the concentration reaches a maximum at  $0.95 \text{ kmol/m}^3$  at which point the rate of increase in concentration starts to decrease. This decrease is a consequence of a reduction in the reactant concentration and as a result the reaction which converts the B-HCl complex to a pentose-HCl (P-HCl) complex begins to dominate over the rate of B-HCl production, eventually leading to a decrease in B-HCl concentration. The concentration of the P-HCl complex followed a similar trend, increasing to a maximum value then dropping off as it was consumed in the production of furfural. The furfural and acetic acid concentrations displayed similar trends to P-HCl and B-HCl respectively as a result of the production rates of these two components being dependent on the reactant concentration. The water concentration depleted rapidly initially as a result of its consumption in the hydrolysis reactions. The reason for the increase in water concentration after this was that as the hydrolysis reaction rate began to decrease and the production of furfural lead to an increase in the water concentration. It should be noted however that the change in water concentrations are very small. The HCl concentration was initially low as a result of the HCl becoming adsorbed onto the pentosan molecules, the value of the HCl increased until the pentosan molecules had reached saturation and thereafter the HCl concentration remained stable.



## **7. CONCLUSIONS AND RECOMMENDATIONS**

### **7.1. Conclusions**

- Furfural was produced by a gas-solid reaction using steam and hydrogen chloride gas passed through a bed of dried sunflower husks. This is the first documented evidence of such a case at a pilot scale and may provide reason to explore this process for a general processing option.
- A pilot plant rig was successfully set up using the available equipment to demonstrate that this process worked. This involved ensuring that temperatures were maintained at a high enough level so that no liquid phase was present in the reactor.
- The reaction system was modelled and was able to produce similar trends to those determined from the experimental work.
- The amount of furfural produced was dependent on the acid concentration as demonstrated by the experimental results and modelling showed that the reaction would also be dependent on the reaction temperature

### **7.2. Recommendations**

- A more rigorous study of the kinetics of the processes is required and a laboratory scale test method needs to be developed where parameters which affect the kinetics can be properly controlled. Key factors which require better control and measurement would be:
  - Gas flow rate
  - Temperature control
- Measurement of the furfural and other products should be more rigorous with the use of an HPLC.

## 8. REFERENCES

- The Kirk-Othmer Encyclopedia of Chemical Technology. Wiley.  
[www.EngineeringToolBox.com](http://www.EngineeringToolBox.com).
- (2003) Chemical Logic Steam Tab Companion. Burlington.
- AGUILAR, R., RAMIREZ, J. A., GARROTE, G. & VAZQUEZ, M. (2002) Kinetic study of the acid hydrolysis of sugar cane bagasse. *Journal of Food Engineering*, 55, 309-318.
- AGUZZI, A., FLUECKIGER, B. & ROSSI, M. J. (2003) The nature of the interface and the diffusion coefficient of HCl/ice and HBr/ice in the temperature range 190-205 K. *Physical Chemistry Chemical Physics*, 5, 4157-4169.
- AMINABHAVL, T. M. (1984) Use of Mixing Rules in the Analysis Mixtures. *J. Chem. Eng. Data*, 29, 54-55.
- ANTAL, M. J., LEESOMBOON, T., MOK, W. S. & ROCHARDS, G. N. (1991) Mechanism of the formation of 2-furaldehyde from D-Xylose. *Carbohydrate Research*, 217, 71-85.
- AZAROV, V. I., BUROV, A. V. & OBOLENSKAYA, A. V. (1999) *Chemistry of Wood and Synthetic Polymers*, Saint-Petersburg, LTA.
- BACELEO, D. E., JR., R. C. B. F& ISHIKAWA, Y. (1999) Ab Initio Monte Carlo Simulated Annealing Study of HCl(H<sub>2</sub>O)<sub>n</sub> (n = 3,4) Clusters. *Journal of Physical Chemistry A*, 10, 4631-4640.
- BOLTON, K. & PETTERSON, J. B. C. (2001) Ice-Catalyzed Ionization of Hydrochloric Acid. *Journal of the American Chemical Society*, 123, 7360-7363.
- BRAND, M. J. D. (1976) A general method for the solution of polynomial equations in H<sup>+</sup> ion concentration. *Journal of Chemical Education*, 53, 771.
- BROWNLEE, H. J. & MINER, C. S. (1948) Industrial development of furfural. *Industrial and Engineering Chemistry*, 40, 201 -
- BUTLER, J. N. (1998) *Ionic Equilibrium: Solubility and pH Calculations*, New York, Wiley-Interscience.
- CHAIKUMPOLLERT, O., METHACANON, P. & SUCHIVA, K. (2004) Structural elucidation of hemicelluloses from Vetiver grass. *Carbohydrate Polymers*, 57, 191-196.
- CUNNINGHAM, R. L., DETROY, R. W. & CARR, M. E. (1982) Thermal Hydropulping of Wheat Straw. *Transactions of the Illinois Academy of Sciences*, 75, 283-287.
- DIAS, A. S., PILLINGER, M. & VALENTE, A. A. (2005a) Dehydration of xylose into furfural over micro-mesoporous sulfonic acid catalysts. *Journal of Catalysis*, 229, 414-423.
- DIAS, A. S., PILLINGER, M. & VALENTE, A. A. (2005b) Liquid phase dehydration of D-xylose in the presence of Keggin-type heteropolyacids  
*Applied Catalysis A: General* 285, 126-131.
- FULLER, E. N., SCHETTLER, P. D. & GIDDINGS, J. C. (1966) *Ind. Eng. Chem*, 58, 18-27.
- GARROTE, G., DOMÍNGUEZ, H. & PARAJÓ, J. C. (2004) Production of Substituted Oligosaccharides by Hydrolytic Processing of Barley Husks. *Industrial and Engineering Chemistry Research*, 43, 1608-1614.
- GERNON, M. D., TRUMPFHELLER, C. M. & PICKER, B. A. (2005) Reactive amine catalysts for use in pucb foundry binder. IN OFFICE, U. P. A. T. (Ed.) USA.
- GERTNER, B. J. & HYNES, J. T. (1996) Molecular Dynamics Simulation of Hydrochloric Acid Ionization at the Surface of Stratospheric Ice. *Science*, 271.
- GLOVER, F. A. & GOULDEN, J. D. S. (1963) Relationship between Refractive Index and Concentration of Solutions. *Nature*, 200, 1165-1166.
- GUPTA, R. K. & DAS, S. K. (1997) Physical Properties of Sunflower Seed. *Journal of Agricultural Engineering Research*, 66, 1-8.
- HAGGLUND, E. (1951) *Chemistry of Wood*, New York, Academic Press Inc. Publishers.
- HART, H., CRAINE, L. E. & HART, D. J. (1999) *Organic Chemistry, A Short Course*, Boston, Houghton Mifflin Company.
- HIGGINS, F. J. & HO, G. E. (1982) Hydrolysis of Cellulose Using HCl: A Comparison Between Liquid Phase and Gaseous Phase Processes. *Agricultural Wastes*, 4, 97-116.

- HUGHES, E. E. & ACREE, S. F. (1938) Quantitative Formation of Furfural From Xylose. *Journal of Research of the National Bureau of Standards*, 21, 327-336.
- ISAKSON, M. J. & SITZ, G. O. (1999) Adsorption and Desorption of HCl on Ice. *Journal of Physical Chemistry A*, 103, 2044-2049.
- JOHNSON, D. K. (2003) Methods For Quantitative Analysis of Uronic Acids in Biomass. National Bioenergy Center, NREL.
- KLAUDITZ, W. (1941) *Holz Roh-u. Werkstoff*, 4, 314.
- LAVARACK, B. P., GRIFFIN, G. J. & RODMAN, D. (2002) The acid hydrolysis of sugarcane bagasse hemicellulose to produce xylose, arabinose, glucose and other products. *Biomass and Bioenergy*, 23, 367-380.
- LÁZARO, M., MARTÍCEZ-BENET, J. & PUIGJANER, L. (1986) Plant Design and Optimization for the Production of Furfural from Xylose Solutions. *Industrial and Engineering Process Design and Development*, 25, 687-693.
- LIAO, W., LIU, Y., LIU, C. & CHEN, S. (2004) Optimizing dilute acid hydrolysis of hemicellulose in a nitrogen-rich cellulosic material--dairy manure. *Bioresource Technology* 94, 33-41.
- MALONEY, M. T., CHAPMAN, T. W. & BAKER, A. J. (1985) Dilute Acid hydrolysis of Paper Birch: Kinetics Studies of Xyland and Acetyl Group Hydrolysis. *Biotechnology and Bioengineering*, 27, 355-361.
- MANSILLA, H., BAEZA, J., URZÚA, S., MATORANA, G., VILLASEÑOR, J. & DURÁN, N. (1998) Acid-Catalysed Hydrolysis of Rice Hull: Evaluation of Furfural Production. *Bioresource Technology*, 66, 189-193.
- MANTZ, Y. A., GEIGER, F. M., MOLINA, L. T., MOLINA, M. J. & TROUT, B. L. (2001) First-Principles Theoretical Study of Molecular HCl Adsorption on Hexagonal Ice (0001) Surface. *Journal of Physical Chemistry A*, 105, 7037 -7046.
- MCKILLIP, W. J. & ZEITSCH, K. J. (2002) *Ullmann's Encyclopedia of Industrial Chemistry - FURAN AND DERIVATIVES*, Weinheim. Germany, Wiley-VCH.
- MENSINGER, M. C., FELDKRICHNER, H. L., HILL, A. H., LAU, F. S., PUNWANI, D. V. & WANGEROW, J. R. (1990) Testing of Novel Catalytic Coal Gasification Concepts. Chicago, Institute of Gas Technology.
- MONTANE, D., SALVADÓ, J., TORRAS, C. & FARRIOL, X. (2002) High-temperature dilute-acid hydrolysis of olive stones for furfural production. *Biomass and Bioenergy*, 22, 295-304.
- MOREAU, C., DURAND, R., PEYRON, D., DUHAMET, J. & RIVALIER, P. (1998) Selective preparation of furfural from xylose over microporous solid acid catalysts. *Industrial Crops and Products* 7, 95-99.
- MYLERLY, R. S., NICHOLSON, M. D., KATZEN, R. & TAYLOR, J. M. (1981) The Forest Refinery. *Chemtech*, 11, 186-192.
- OTT, E., SPURLIN, H. M. & GRAFFLIN, M. W. (1952) *Cellulose and Cellulose Derivatives*, New York, Interscience Publishers Inc.
- OWEN, B. B., MILLER, R. C., MILNER, C. E. & COGAN, H. L. (1961) The Dielectric Constant of Water as a Function of Temperature and Pressure. *The Journal of Physical Chemistry*, 65, 2065-2070.
- PARAJÓ, J. C., ALONSO, J. L. & SANTOS, V. (1995) Kinetics of Catalyzed Organosolv Processing of Pine Wood. *Industrial and Engineering Chemistry Research*, 34, 4333-4342.
- PERCIVAL, E. G. V. (1953) *Structural Carbohydrate Chemistry*, London, J. Garnet Miller Ltd.
- PETERS, F. N. (1948) Furan Chemistry. *Industrial and Engineering Chemistry*, 40, 200.
- POLAKOVIC, M., KUDLACOVA, G., STEFUCA, V. & BALES, V. (2001) Determination of sucrose effective diffusivity and intrinsic rate constant of hydrolysis catalysed by Calcium alginate entrapped cells. *Chemical Engineering Science*, 56, 459-466.
- PRINGSHEIM, H. (1921) Ueber ein Verfahren zur Gewinnung von Essigsäure, Azeton (Methylalkohol) und Furfurol aus rohfaserhaltigen Naturstoffen. *Cellulosechemie*, 10, 123-124.

- RODRIGUEZ-CHONG, A., ALBERTO RAMIREZ, J., GARROTE, G. & VAZQUEZ, M. (2004) Hydrolysis of sugar cane bagasse using nitric acid: a kinetic assessment. *Journal of Food Engineering*, 61, 143-152.
- RUF, S., EMIG, G., SAUER, J., HIPPEL, L. V., HUTHMACHER, K. & VANHEERTUM, R. (1999) Formaldehyde production by dehydrogenation of methanol. Germany.
- SEADER, J. D. & HENLEY, E. J. (1998) *Separation Process Principals*, New Jersey, John Wiley & Sons.
- SKOOG, D. A., WEST, D. M. & HOLLER, F. J. (1997) *Fundamentals of Analytical Chemistry*, Orlando, Saunders College Publishing.
- SLAVIANSKII, A. K. E. A. (1962) *Chemical Technology of Wood*, Moscow, Goslesbumizdat.
- SPRINGER, E. L. & HARRIS, J. F. (1985) Procedures for Determining the Neutralising Capacity of Wood during Hydrolysis with Mineral Acid Solutions. *Industrial and Engineering Chemistry Product Research and Development*, 24, 485-489.
- SUN, J.-X., SUN, R., SUN, X.-F. & SU, Y. (2004a) Fractional and physico-chemical characterization of hemicelluloses from ultrasonic irradiated sugarcane bagasse. *Carbohydrate Research*, 339, 291-300.
- SUN, J. X., SUN, X. F., SUN, R. C. & SU, Y. Q. (2004b) Fractional extraction and structural characterization of sugarcane bagasse hemicelluloses. *Carbohydrate Polymers*, 56, 195-204.
- VIERHUIS, E., SCHOLS, H. A., BELDMAN, G. & VORAGEN, A. G. J. (2001) Structural characterization of xyloglucan and xylans present in olive fruit (*Olea europaea* cv koroneiki). *Carbohydrate Polymers*, 44, 51-62.
- VOEGELE, A. F., TAUTERMANN, C. S., LOERTING, T. & LIEDL, K. R. (2002) Reaction of  $\text{HOCl} + \text{HCl} + n\text{H}_2\text{O}$  and  $\text{HOCl} + \text{HBr} + n\text{H}_2\text{O}$ . *Journal of Physical Chemistry A*, 106, 7850-7857.
- VOSS, W., BAUER, R. & PFIRSCHKE, J. (1938) *Ann.*, 534.
- WELLS, J. & PRESTON, A. (1977) Method for the Manufacture of Furfural using Hydrogen Chloride. IN USPTO (Ed.) USA.
- WIN, D. T. (2005) Furfural - Gold from Garbage. *Assumption University Journal of Technology*.
- WISE, L. E. (1952) The Hemicelluloses. *Wood Chemistry*. Second Edition ed. New York, Reinhold Publishing Corporation.
- WONDU BUSINESS AND TECHNOLOGY SERVICES (2006) Furfural Chemicals and Biofuels from Agriculture. IN AUSTRALIAN GOVERNMENT (Ed.), Rural Industries Research and Development Corporation 06-127.
- YANG, R., ZHANG, C., FENG, H. & YANG, W. (2006) A Kinetic Study of Xylan Solubility and Degradation during Corn cob Steaming. *Biosystems Engineering*, 93, 375-382.
- ZEITSCH, K. J. (2000a) *The Chemistry and Technology of Furfural and its many By-Products*, Amsterdam, Elsevier.
- ZEITSCH, K. J. (2000b) Gaseous Acid Catalysis for the Production of Furfural. IN BUZZARD, J. (Ed.) Köln.
- ZEITSCH, K. J. (2001) Gaseous acid catalysis: An intriguing new process *Chemical Innovation*, 31, 41-44.

## APPENDIX A: CALCULATION METHODS FOR SUPERHEATER

In order to determine the exit temperature of the gas, the length of wire per metre of tube had to be determined. This was determined from the following equation:

$$L_{wire} = \frac{L_{tube}}{W} \sqrt{W^2 + [\pi \times (D \times T)]^2}$$

- where  $L_{wire}$  is the length of the wire  
 $L_{tube}$  is the length of the tube  
 $W$  is the width of the spacing (10mm)  
 $D$  is the tube diameter (5mm)  
 $T$  is the wire thickness (assumed to be 1mm)

The power per length of wire was then determined from:

$$P = \frac{V^2}{\frac{r \times L_{wire}}{L_{wire}}}$$

- where  $P$  is the power per meter of wire  
 $V$  is the voltage supplied  
 $r$  is the resistance of the wire per unit length (NiCr wire specification of 10Ω/m)

The glass temperature was then determined from the following equation:

$$T_g = \frac{m_g C_p T_{g,t-1} + P n L_{tube} dt + k \frac{A_g}{w l} dt T_a}{m_g C_p + k \frac{A_g}{w l} dt}$$

The vapour temperature inside the heated section of the tube was determined from:

$$T_v = \frac{F_v C_p T_{v,t-1} + P n d L + \left( k \frac{A_g}{w l} + U A_g \right) T_a}{F_v C_p + k \frac{A_g}{w l} + U A_g}$$

The temperature in the unheated section of the tube was

$$T_v = \frac{F_v C_p T_{v,t-1} + k \frac{A_g}{w l} T_a}{F_v C_p + k \frac{A_g}{w l}}$$

- where  $T$  is the temperature (K)

$m$  is the mass of the glass [kg]  
 $C_p$  is the heat capacity [J/(kg.K)]  
 $n$  is the ratio of the meters of wire per meter of tube  
 $dt$  is the time step [s]  
 $dL$  is the tube length step  
 $k$  is the thermal conductivity of the glass [W/(m°C)]  
 $A$  is the segment area [m<sup>2</sup>]  
 $U$  is the overall heat transfer coefficient  
 $w_1$  is the insulation thickness of the heated section [m]  
 $w_2$  is the insulation thickness of the un heated section [m]  
 the subscript  $g$  refers to glass  
 the subscript  $v$  refers to vapour

$$U = \frac{t_w}{k_g}$$

$U$  is determined by the thickness of the glass 'wall' ( $t_w$ ) divided by the thermal conductivity of the glass ( $k_g$ ).

### **MATLAB Code**

```

close all; clear all; clc
l = 0.3;
P = 10/1/1000;
n = 1.18;
dL = 0.001;
t = 200;
Fl(1) = 6.22e-6;
Fv = Fl(1);
T(1) = 110;
Tmax = 150;
L(1) = 0;
i = 1;
Lmax = l/n;

while L(i)<Lmax
    i = i+1;
    T(i) = T(i-1) + P*n*dL/(Fv*Cpv);
    L(i) = dL+L(i-1);
  
```

```
end
```

```
L'
```

```
T'
```

```
plot(L,T)
```

```
xlabel('length (m)')
```

```
ylabel('Temperature (degC)')
```

## APPENDIX B: FURTHER DETAIL ON CALIBRATIONS AND ASSAYS

### Refractometer calibration

A refractometer calibration curve relating the refractive indices of furfural, hydrochloric acid and acetic acid solutions with water to their concentrations on a mass fraction basis as well as a grams per litre basis was required.

In order to prepare the calibration curve, initial solutions of furfural, hydrochloric and acetic acid were made up as follows to achieve approximately 5%wt solutions of both the acids and an 8%wt solution of furfural. These solutions could then be diluted to produce different concentrations of each component for calibration.

**Table: Reagent purity and volume used**

Component	Reagent Concentration (%wt)	Volume of reagent used (ml)
Furfural	98%	7
HAc	96%	5
HCl	37%	15

A clean and dry 100ml volumetric flask was weighed and the volume of the reagent specified in the Table was added to each of the flasks. After the addition of the reagent the flask was weighed again in order to determine the mass of the reagent used. Distilled water was then added to fill the flask to the 100 ml mark. The diluted solution was then weighed in order to determine the total solution mass and hence be able to calculate the concentration in terms of mass percent.

In order to verify the concentrations of this starting solution, a weighed 10 ml sample of each of the acids was titrated with 1M NaOH. The indicator used for the hydrochloric acid titration was bromothymol blue which was yellow/orange in the acid solution and turned blue/green at the end point. Phenolphthalein was used as an indicator for the acetic acid titration. Phenolphthalein was clear in the acidic solution and turned pale pink at the end point. The titration results are shown in the following table:



**Table: Titrations to confirm acid concentrations**

Test	HCl				Hac			
	1	2	3	4	1	2	3	4
Volume (ml)	20	10	10	10	10	10	10	10
Mass (g)	20.5	10.3	10.3	10.3	10	10	9.9	10
Volume NaOH (ml)	36.35	18.66	18.27	18.08	8.46	8.45	8.43	8.42
Mass Acid (g)	1.33	0.68	0.67	0.66	0.51	0.51	0.51	0.51
Acid Mass %	6.5%	6.6%	6.5%	6.4%	5.1%	5.1%	5.1%	5.1%
Acid Concentration (g/L)	66.27	68.04	66.61	65.92	50.80	50.74	50.62	50.56
Acid Mass % (Ave)	6.5%				5.1%			
Acid Concentration (g/L) (Ave)	66.71				50.68			

The next step in preparing the calibration curve was to produce a range of concentrations by means of a serial dilution of this initial mixture. Five clean dry volumetric flasks of the following sizes were weighed and labelled<sup>1</sup>:

- 1 25 ml
- 2 25 ml
- 3 50 ml
- 4 100 ml
- 5 200 ml

To flask 1, 20 ml of the solution produced above was added and 10 ml was added to each of the subsequent flasks. The flasks were then weighed again to determine the mass of the original solution used. Distilled water was used to dilute each flask to the correct level. The flasks were weighed again to determine the total solution mass. This resulted in solutions of the following concentrations:

---

<sup>1</sup> Only flasks 2 to 5 were used for the two acid solutions because of their lower starting concentrations.

**Table: Hydrochloric acid concentrations**

<b>Hydrochloric Acid</b>	
<b>g/L</b>	<b>mass%</b>
65.3	6.37%
26.0	2.58%
13.1	1.30%
6.6	0.66%
3.3	0.33%

**Table: Acetic acid concentrations**

<b>Acetic Acid</b>	
<b>g/L</b>	<b>mass%</b>
49.9	5.01%
20.2	2.07%
10.1	1.02%
5.0	0.51%
2.5	0.25%

**Table: Furfural concentrations**

<b>Furfural</b>	
<b>g/L</b>	<b>mass%</b>
78.4	7.60%
61.2	6.21%
30.7	3.12%
16.1	1.60%
4.1	0.67%
3.9	0.39%

Refractive index readings at 20.0°C were then taken for each of these solutions to construct the calibration curves.

A linear regression was performed using MS Excel and linear equations were found to accurately describe the data. The intercept varied depending on the refractive index reading for distilled water on a particular day and it is therefore the gradient of the line which is of most significance for the calibration curve. These equations were subsequently used in the calculations but shifted up or down as prescribed by the water refractive index.

**Table: Calibration Curve Gradients**

	<b>Mass % curves</b>	<b>Concentration curves</b>
<b>HCl</b>	0.226	$2.19 \times 10^{-4}$
<b>HAc</b>	0.070	$7.05 \times 10^{-5}$
<b>Furfural</b>	0.194	$1.88 \times 10^{-4}$

The calibration curves were found to fit the data with a high degree of accuracy with the following  $R^2$  values:

**Table: Calibration Curve  $R^2$  values for a straight line fit**

	<b>Mass % curves</b>	<b>Concentration curves</b>
HCl	0.9997	0.9996
HAc	0.9962	0.9962
Furfural	0.9998	0.9991

These values indicated that the fitting of the data to a straight line was accurate.

### Size fraction pentosan analysis

After the material was screened as described in 4.2.2.1, each size fraction was analysed for pentosan as described in 4.2.2.2. The results are shown in the Table that follows and are summarised in the Table thereafter.

**Table: Size fraction pentosan concentrations**

Size (µm)	Moist Initial mass (g)	Absorbance	Xylan Mass (mg)	Dry initial mass(g)	% Pentosan	Averages	
-1400 +1000	0.3001	0.455	82.727	0.2654	31.17	31.49	
		0.467	84.909		31.99		
	0.3001	0.462	84.000	0.2654	31.65		
		0.455	82.727		31.17		
	0.2998	0.455	82.727	0.2626	31.50		32.03
		0.461	83.818		31.92		
0.3003	0.467	84.909	0.2630	32.28			
	0.469	85.273		32.42			
-1000 +750	0.2999	0.455	82.727	0.2682	30.85	30.57	
		0.450	81.818		30.51		
	0.3004	0.454	82.545	0.2686	30.73		
		0.446	81.091		30.19		
	0.3003	0.473	86.000	0.2682	32.06	32.60	
		0.452	82.182		30.64		
	0.2998	0.506	92.000	0.2678	34.35		
		0.491	89.273		33.34		
-750 +500	0.2997	0.466	84.727	0.2689	31.51	31.87	
		0.475	86.364		32.12		
	0.3003	0.477	86.727	0.2694	32.19		
		0.469	85.273		31.65		
	0.2999	0.427	77.636	0.2674	29.03	30.00	
		0.443	80.545		30.12		
0.3006	0.446	81.091	0.2681	30.25			
	0.451	82.000		30.59			
-500 +355	0.3001	0.455	82.727	0.2676	30.92	30.69	
		0.450	81.818		30.58		
	0.2996	0.454	82.545	0.2671	30.90		
		0.446	81.091		30.36		
	0.3001	0.463	84.182	0.2668	31.55	33.37	
		0.468	85.091		31.89		
0.2998	0.547	99.455	0.2665	37.31			
	0.480	87.273		32.74			
-250	0.5005	0.455	82.727	0.4366	18.95	18.80	
		0.450	81.818		18.74		
	0.5002	0.454	82.545	0.4364	18.92		
		0.446	81.091		18.58		
	0.5003	0.463	84.182	0.4383	19.20	20.31	
		0.468	85.091		19.41		
	0.4998	0.547	99.455	0.4379	22.71		
		0.480	87.273		19.93		

**Table: Summary of pentosan concentrations at different size fractions**

Size( $\mu\text{m}$ )	% Pentosan
1000-1400	31.2
710-1000	31.0
500-710	30.4
355-500	31.5
250 -	19.2

The Table above shows that the size fractions greater than 250 $\mu\text{m}$  had similar pentosan content which varied by only 1% from 30.4% to 31.5%. The -250 $\mu\text{m}$  fraction had a pentosan concentration over 10% lower than this at only 19.2%.

Samples of pure xylose were tested to check the method as shown below:

**Table: Test using pure xylose**

Size ( $\mu\text{m}$ )	Moist Initial mass (g)	Absorbance	Xylan Mass (mg)	Dry initial mass(g)	% Pentosan	Averages		
Test	0.088	0.659	119.818	0.088	136.84	139.39		
		0.666	121.091		138.29			
	0.090	0.686	124.727	0.090	139.09			
		0.707	128.545		143.35			
	0.089	0.089	0.766	139.273	0.089		157.16	153.21
			0.76	138.182			155.93	
0.088	0.088	0.747	135.818	0.088	153.57			
		0.711	129.273		146.17			

This showed that this method over-predicted the xylan concentration by 39 to 53%. For this reason, although the values were likely to give an indication of the trend of the difference in xylan concentration with size fraction, these values could not be used in the yield calculations and a test using new equipment and a new calibration curve was performed to confirm the pentosan concentration. Based on the errors from the previous tests, the actual pentosan concentration should be between 21% and 23%. It was suspected that the error arose due to a malfunction of the colorimeter and the test using the new equipment resulted in the following:

**Table: Re-determined pentosan concentrations**

Size ( $\mu\text{m}$ )	Moist Initial mass (g)	Absorbance	Xylan Mass (mg)	Dry initial mass(g)	% Pentosan	Averages		
710-500	0.3000	0.381	65.690	0.256	25.65	24.79		
		0.357	61.552		24.03			
	0.2999	0.2999	0.379	65.345	0.256		25.52	
			0.356	61.379			23.97	
	0.3000	0.3000	0.366	63.103	0.256		24.64	25.66
			0.381	65.690			25.65	
0.3000	0.3000	0.401	69.138	0.256	26.99			
		0.377	65.000		25.38			

The value of 25% pentosan shown in the above Table is a more realistic figure corresponding to the literature.

### **Calibration curve for pentosan analysis**

These calibration curves were prepared by performing the pentosan analysis on a series of known quantities of pure xylose and measuring the final solution absorbance. By converting the xylose mass to xylan mass, the relationship between absorbance and quantity of xylan present could be determined. This work was done by the laboratory staff at the university.

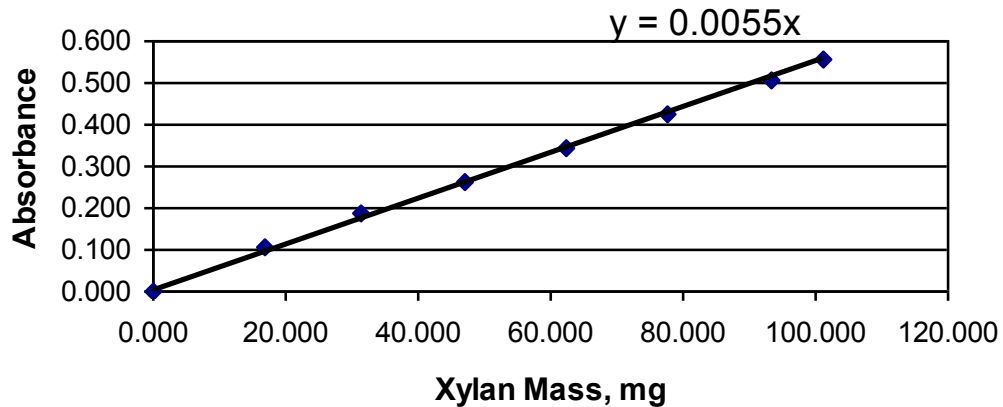


Fig 1: Calibration curve for original colorimeter

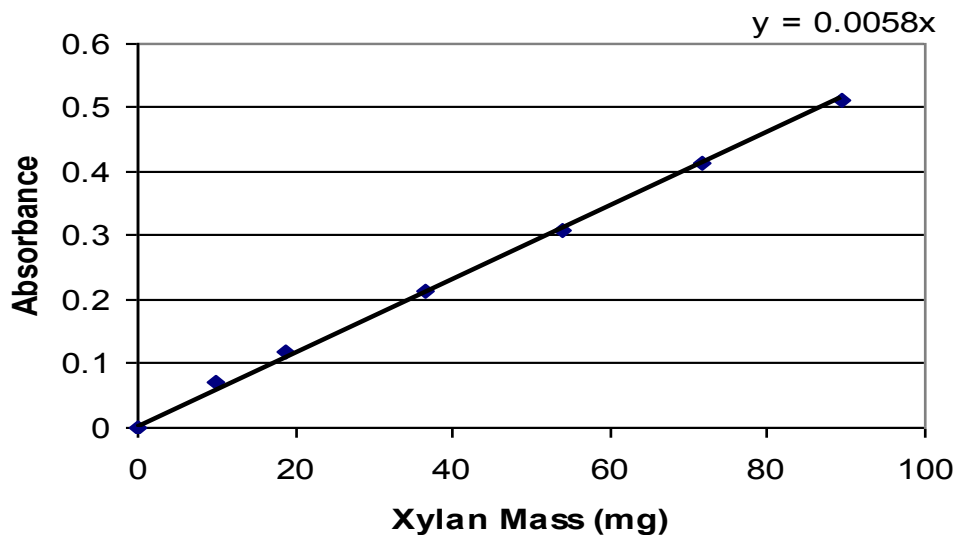


Fig 2: Calibration curve for new colorimeter

## APPENDIX C: TITRATION MATLAB CODE AND CURVES

### Theory for prediction of titration curves

In order to solve for the two acid titration curve the following equation was solved in MATLAB to determine the  $H^+$  concentration and hence pH at each volume addition.

Electro-neutrality requires the following equation (Brand, 1976):

$$[H^+] + [Na^+] - [Cl^-] - [Ac^-] + [OH^-] = 0$$

where  $[X]$  denotes the concentration of X in mol/L

$Ac^-$  indicates the acetate ion

In order to solve for  $H^+$ , the other ion concentrations must be determined; to this, they must be written in terms of measurable quantities.

The various equation components are therefore determined as follows:

The sodium ion concentration is calculated by mass balance:

$$[Na^+] = \frac{V_t \cdot c_{NaOH}}{V_s + V_t}$$

where  $V_t$  is the titration volume added (in L)

$V_s$  is the initial solution aliquot volume (in L)

$c_{NaOH}$  is the concentration of the sodium hydroxide solution (mol/L)

Since both  $[Cl^-]$  and  $[Ac^-]$  arise from acid dissociation, their values are calculated in the same manner and therefore the equation for their concentrations can be written for a generic acid, HA and applied to each:

$$c_{HA} = [HA] + [A^-]$$

$$\text{Since } K_{HA} = \frac{[H^+][A^-]}{[HA]} \Rightarrow [HA] = \frac{[H^+][A^-]}{K_{HA}}$$

$$c_{HA} = \frac{[H^+][A^-]}{K_{HA}} + [A^-] \Rightarrow c_{HA} = [A^-] \cdot \left( 1 + \frac{[H^+]}{K_{HA}} \right)$$

$$c_{HA} = [A^-] \cdot \left( \frac{K_{HA} + [H^+]}{K_{HA}} \right)$$

$$\therefore [A^-] = \frac{K_{HA} c_{HA}}{(K_{HA} + [H^+])}$$

$$\text{And } c_{HA} = \frac{V_s c_{HA,0}}{V_s + V_t}$$

$$\therefore [A^-] = \frac{K_{HA}}{(K_{HA} + [H^+])} \cdot \frac{V_s c_{HA,0}}{V_s + V_t}$$

where  $c_{HA}$  is the total acid concentration (mol/L) (the subscript '0' refers to initial)  
 $[HA]$  is the undissociated acid concentration (mol/L)  
 $[A^-]$  is the dissociated acid concentration (mol/L)  
 $K_{HA}$  is the acid equilibrium coefficient

The hydroxide ion concentration is determined from the water equilibrium coefficient:

$$[OH^-] = \frac{K_w}{[H^+]}$$

Therefore the mass balance equation can be rewritten as follows:

$$[H^+] + \frac{V_t \cdot c_{NaOH}}{V_s + V_t} - \frac{K_{HCl}}{(K_{HCl} + [H^+])} \cdot \frac{V_s c_{HCl,0}}{V_s + V_t} - \frac{K_{HAc}}{(K_{HAc} + [H^+])} \cdot \frac{V_s c_{HAc,0}}{V_s + V_t} + \frac{K_w}{[H^+]} = 0$$

This equation is then solved for a range of titration volume additions to produce a titration curve which is then used to determine the HCl and acetic acid concentrations.

The thermodynamic effects were accounted for by using the Davies equation to determine activity coefficients which could be used to adjust the  $K_i$  values. The Davies equation is (Butler, 1998):

$$\log \gamma = -Az_i^2 \left( \frac{\sqrt{I}}{1 + \sqrt{I}} \right) - bI$$

where  $A$  is a temperature dependent variable dependent on the dielectric constant of water

$I$  is the ionic strength

$b$  0.1, 0.2 or 0.3 (ion specific parameter)

The ionic strength is calculated using (Skoog et al., 1997):

$$I = \frac{1}{2} \sum_i^n c_i z_i^2$$

where  $c_i$  is the molar concentration of component  $i$   
 $z_i$  is the charge associated with component  $i$

The concentrations and hence the acid equilibrium constants could then be adjusted for any liquid equilibria non-idealities using the activity coefficients.

### **MATLAB code**

```

clc
clear all
format compact
format long

global Vt_exp pH_exp C0_NaOH C0_H2O Vs A z_H z_OH z_Ac z_Cl z_Na K_HAc
Kw K_HCl V11 pH11

conti = input('Contour plot (yes=1, no=0): ');
Nruns = 19;
Nsamp = 6;
for p = 1:Nruns
    for q = 1:Nsamp

        tC = 25;
        T = tC+273.15;

        Vs = 25/1000;

        pHdata

        t = num2str(10*p+q);
        eval(['Vt_exp = V_', t, ';'])
        eval(['pH_exp = pH_', t, ';'])
        eval(['par0 = par_', t, ';'])
        Kw = 10^(-4470.99/T+6.0875-0.01706*T);

        pK_HAc_exp = [4.756];
        K_HAc = 10^(-pK_HAc_exp);

        K_HCl = 10^6.21;
        % K_HCl = 10^3;

        z_H = 1;
        z_OH = 1;
        z_Ac = 1;
        z_Cl = 1;
        z_Na = 1;

        tC_e = [0, 25, 62, 83];
        e_exp = [88.2, 78.5, 66.4, 60.4]; % (Owen et al., 1961)
        e = interp1(tC_e, e_exp, tC, 'spline');
        A = 1.82e6*(e*T)^(-3/2);

        C0_NaOH = 1;
        rhow = (999.83952+tC*(16.952577+tC*(-7.9905127e-3+tC*...

```



```

        (-46.241757e-6+tC*(105.84601e-9-281.03006e...
        -12*tC)))))/(1+16.887236e-3*tC);
C0_H2O = rhow/18.02;

disp('Wait ...')

opt = optimset('TolX', 1e-6, 'TolFun', 1e-6);
par = fminsearch('ititra3', par0, opt);
c0_HAc = par(1);
c0_HCl = par(2);
IX = ititra3(par);

if conti,
    s = 0.1*round(10*c0_HAc);
    c0_HAc_x = [s-1:0.05:s+1];
    s = 0.1*round(10*c0_HCl);
    c0_HCl_x = [s-1:0.05:s+1];
    for i=1:length(c0_HAc_x),
        disp(i)
        for j=1:length(c0_HCl_x),
            par = [c0_HAc_x(i), c0_HCl_x(j)];
            index(j,i) = ititra3(par);
        end
    end
    figure(2)
    clf
    set(gcf, 'Position', [1, 31, 1280, 694])
    v = [3, 2.5, 2, 1.5, 1:-0.1:0.1];
    [h1, h2] = contour(c0_HAc_x, c0_HCl_x, index, v);
    clabel(h1, h2)
    hold on
    plot(c0_HAc, c0_HCl, 'r', 'MarkerSize', 40)
    plot(c0_HAc, c0_HCl, 'k')
    v = axis;
    text(c0_HAc+0.02*(v(4)-v(3)), c0_HCl, num2str(IX),
        'FontWeight', 'demi');
    xlabel('Acetic acid, g/L')
    ylabel('Hydrogen chloride, g/L')
    title(['Acetic acid = ', ...
        num2str(round(1000*c0_HAc)/1000), ...
        ' g/L, Hydrogen chloride = ', ...
        num2str(round(1000*c0_HCl)/1000), ' g/L'], ...
        'FontWeight', 'demi', 'FontSize', 14)
end

C0_HAc = c0_HAc/60.05;
C0_HCl = c0_HCl/36.46;

N0_HCl = C0_HCl*Vs;
N0_HAc = C0_HAc*Vs;
N0_Ac = 0;
N0_H = 0;
N0_Cl = 0;

Vtmax = 12;
Vt0 = [0:0.1:Vtmax]/1000;
for i=1:length(Vt0)
    Vt = Vt0(i);
    V = Vt+Vs;
    N0_H2O = C0_H2O*(Vs+Vt);

```

```

NO_OH = C0_NaOH*Vt;
f0 = (NO_H+NO_HAc+NO_HCl+NO_H2O)/V;
f1 = (NO_H2O+NO_OH)/V;
f2 = (NO_HAc+NO_Ac)/V;
f3 = (NO_HCl+NO_Cl)/V;
a(1) = 1;
a(2) = K_HCl+K_HAc+f1+f2+f3-f0;
a(3) = K_HCl*K_HAc+(K_HCl+K_HAc)* ...
      (f1-f0)+f2*K_HCl+f3*K_HAc-Kw;
a(4) = K_HCl*K_HAc*(f1-f0)-Kw*(K_HCl+K_HAc);
a(5) = -Kw*K_HCl*K_HAc;
r = roots(a);
j = find(imag(r)==0 & real(r)>0);
if length(j)>1,
    i
    r
    halt
end
C_H_id(i) = r(j);
C_H2O_id(i) = f1-Kw/C_H_id(i);
C_HAc_id(i) = f2/(1+K_HAc/C_H_id(i));
C_HCl_id(i) = f3/(1+K_HCl/C_H_id(i));
C_OH_id(i) = Kw/C_H_id(i);
C_Ac_id(i) = K_HAc*C_HAc_id(i)/C_H_id(i);
C_Cl_id(i) = K_HCl*C_HCl_id(i)/C_H_id(i);
pH_id(i) = -log10(C_H_id(i));
end

C_H = C_H_id;
C_Ac = C_Ac_id;
C_OH = C_OH_id;
C_Cl = C_Cl_id;
C_Na = C0_NaOH*Vt0./(Vt0+Vs);
pH = pH_id;

for i=1:length(Vt0)
    Vt = Vt0(i);
    V = Vt+Vs;
    NO_H2O = C0_H2O*(Vs+Vt);
    NO_OH = C0_NaOH*Vt;
    f0 = (NO_H+NO_HAc+NO_HCl+NO_H2O)/V;
    f1 = (NO_H2O+NO_OH)/V;
    f2 = (NO_HAc+NO_Ac)/V;
    f3 = (NO_HCl+NO_Cl)/V;
    k = 0;
    while 1,
        I = 0.5*(C_H(i)*z_H^2+C_Ac(i)*z_Ac^2+C_OH(i) ...
            *z_OH^2+C_Na(i)*z_Na^2+C_Cl(i)*z_Cl^2);
        s = sqrt(I);
        davis = -A*(s/(1+s)-0.2*I);
        g_H = 10^(z_H^2*davis);
        g_OH = 10^(z_OH^2*davis);
        g_Ac = 10^(z_Ac^2*davis);
        g_Cl = 10^(z_Cl^2*davis);

        K1w = Kw/(g_H*g_OH);
        K1_HAc = K_HAc/(g_H*g_Ac);
        K1_HCl = K_HCl/(g_H*g_Cl);
        a(1) = 1;
        a(2) = K1_HCl+K1_HAc+f1+f2+f3-f0;
        a(3) = K1_HCl*K1_HAc+(K1_HCl+K1_HAc)* ...

```

```

            (f1-f0)+f2*K1_HCl+f3*K1_HAc-K1w;
a(4) = K1_HCl*K1_HAc*(f1-f0)-K1w*(K1_HCl+K1_HAc);
a(5) = -K1w*K1_HCl*K1_HAc;
r = roots(a);
j = find(imag(r)==0 & real(r)>0);
if length(j)>1,
    i
    r
    halt
end
C_H(i) = r(j);
C_H2O(i) = f1-K1w/C_H(i);
C_HAc(i) = f2/(1+K1_HAc/C_H(i));
C_HCl(i) = f3/(1+K1_HCl/C_H(i));
C_OH(i) = K1w/C_H(i);
C_Ac(i) = K1_HAc*C_HAc(i)/C_H(i);
C_Cl(i) = K1_HCl*C_HCl(i)/C_H(i);
pH_old = pH(i);
pH(i) = -log10(g_H*C_H(i));
if abs(pH(i)-pH_old)<1e-8,
    break
end
k = k+1;
end
end

h = figure(1)
clf
set(gcf, 'Position', [1, 31, 1280, 694])
subplot(1,2,1)
plot(Vt_exp, pH_exp, '.r', 1000*Vt0, pH_id, '-g', ...
     1000*Vt0, pH, '-b')
xlabel('Titrant volume, mL')
title('pH', 'FontSize', 15);
text(1, 13, ['Acetic acid, ', ...
            num2str(round(1000*c0_HAc)/1000), ' g/L'], ...
     'FontWeight', 'demi')
text(1, 12.5, ['Hydrogen chloride, ', ...
              num2str(round(1000*c0_HCl)/1000), ' g/L'], ...
     'FontWeight', 'demi')

subplot(3,4,3)
semilogy(1000*Vt0, C_HAc_id, '-g', 1000*Vt0, C_HAc, '-b')
title('Acetic acid, g/L', 'FontSize', 9);
set(gca, 'XLim', [0, Vtmax])
set(gca, 'XTick', 0:2:Vtmax)
set(gca, 'FontSize', 9)

subplot(3,4,4)
semilogy(1000*Vt0, C_Ac_id, '-g', 1000*Vt0, C_Ac, '-b')
title('Acetate ion, g/L', 'FontSize', 9);
set(gca, 'XLim', [0, Vtmax])
set(gca, 'XTick', 0:2:Vtmax)
set(gca, 'FontSize', 9)

subplot(3,4,7)
semilogy(1000*Vt0, C_HCl_id, '-g', 1000*Vt0, C_HCl, '-b')
title('Hydrogen chloride, g/L', 'FontSize', 9);
set(gca, 'XLim', [0, Vtmax])
set(gca, 'XTick', 0:2:Vtmax)
set(gca, 'FontSize', 9)

```

```

subplot(3,4,8)
plot(1000*Vt0, C_Cl_id, '-g', 1000*Vt0, C_Cl, '-b')
title('Chloride ion, g/L', 'FontSize', 9);
set(gca, 'XLim', [0, Vtmax])
set(gca, 'XTick', 0:2:Vtmax)
set(gca, 'FontSize', 9)

subplot(3,4,11)
semilogy(1000*Vt0, C_OH_id, '-g', 1000*Vt0, C_OH, '-b')
xlabel('Titrate volume, mL', 'FontSize', 9)
title('Hydroxyl ion', 'FontSize', 9);
set(gca, 'XLim', [0, Vtmax])
set(gca, 'XTick', 0:2:Vtmax)
set(gca, 'FontSize', 9)

subplot(3,4,12)
plot(1000*Vt0, C_H2O_id, '-g', 1000*Vt0, C_H2O, '-b')
xlabel('Titrate volume, mL', 'FontSize', 9)
title('Water, g/L', 'FontSize', 9);
set(gca, 'XLim', [0, Vtmax])
set(gca, 'XTick', 0:2:Vtmax)
set(gca, 'FontSize', 9)

HAc(p,q) = par(1);
HCl(p,q) = par(2);

FileName = ['Run', num2str(p), 'Sample', num2str(q)];
saveas(h,FileName,'fig');
end
end

function index = ititra3(par)

global Vt_exp pH_exp C0_NaOH C0_H2O Vs A z_H z_OH z_Ac z_Cl z_Na K_HAc
Kw K_HCl

c0_HAc = par(1);
c0_HCl = par(2);
C0_HAc = c0_HAc/60.05;
C0_HCl = c0_HCl/36.46;

N0_HCl = C0_HCl*Vs;
N0_HAc = C0_HAc*Vs;
N0_Ac = 0;
N0_H = 0;
N0_Cl = 0;

for i=1:length(Vt_exp)
    Vt = Vt_exp(i)/1000;
    V = Vt+Vs;
    N0_H2O = C0_H2O*(Vs+Vt);
    N0_OH = C0_NaOH*Vt;
    f0 = (N0_H+N0_HAc+N0_HCl+N0_H2O)/V;
    f1 = (N0_H2O+N0_OH)/V;
    f2 = (N0_HAc+N0_Ac)/V;
    f3 = (N0_HCl+N0_Cl)/V;
    a(1) = 1;

```

```

a(2) = K_HCl+K_HAc+f1+f2+f3-f0;
a(3) = K_HCl*K_HAc+(K_HCl+K_HAc)*(f1-f0)+f2*K_HCl+f3*K_HAc-Kw;
a(4) = K_HCl*K_HAc*(f1-f0)-Kw*(K_HCl+K_HAc);
a(5) = -Kw*K_HCl*K_HAc;
r = roots(a);
j = find(imag(r)==0 & real(r)>0);
if length(j)>1,
    i
    r
    halt
end
C_H_id(i) = r(j);
C_H2O_id(i) = f1-Kw/C_H_id(i);
C_HAc_id(i) = f2/(1+K_HAc/C_H_id(i));
C_HCl_id(i) = f3/(1+K_HCl/C_H_id(i));
C_OH_id(i) = Kw/C_H_id(i);
C_Ac_id(i) = K_HAc*C_HAc_id(i)/C_H_id(i);
C_Cl_id(i) = K_HCl*C_HCl_id(i)/C_H_id(i);
pH_id(i) = -log10(C_H_id(i));
end

C_H = C_H_id;
C_Ac = C_Ac_id;
C_OH = C_OH_id;
C_Cl = C_Cl_id;
C_Na = C0_NaOH*Vt_exp/1000./(Vt_exp/1000+Vs);
pH = pH_id;

for i=1:length(Vt_exp)
    Vt = Vt_exp(i)/1000;
    V = Vt+Vs;
    N0_H2O = C0_H2O*(Vs+Vt);
    N0_OH = C0_NaOH*Vt;
    f0 = (N0_H+N0_HAc+N0_HCl+N0_H2O)/V;
    f1 = (N0_H2O+N0_OH)/V;
    f2 = (N0_HAc+N0_Ac)/V;
    f3 = (N0_HCl+N0_Cl)/V;
    while 1,
        I = 0.5*(C_H(i)*z_H^2+C_Ac(i)*z_Ac^2+C_OH(i) ...
            *z_OH^2+C_Na(i)*z_Na^2+C_Cl(i)*z_Cl^2);
        s = sqrt(I);
        davis = -A*(s/(1+s)-0.2*I);
        g_H = 10^(z_H^2*davis);
        g_OH = 10^(z_OH^2*davis);
        g_Ac = 10^(z_Ac^2*davis);
        g_Cl = 10^(z_Cl^2*davis);

        K1w = Kw/(g_H*g_OH);
        K1_HAc = K_HAc/(g_H*g_Ac);
        K1_HCl = K_HCl/(g_H*g_Cl);
        a(1) = 1;
        a(2) = K1_HCl+K1_HAc+f1+f2+f3-f0;
        a(3) = K1_HCl*K1_HAc+(K1_HCl+K1_HAc)* ...
            (f1-f0)+f2*K1_HCl+f3*K1_HAc-K1w;
        a(4) = K1_HCl*K1_HAc*(f1-f0)-K1w*(K1_HCl+K1_HAc);
        a(5) = -K1w*K1_HCl*K1_HAc;
        r = roots(a);
        j = find(imag(r)==0 & real(r)>0);
        if length(j)>1,
            i
            r

```

```

    halt
end
C_H(i) = r(j);
C_H2O(i) = f1-K1w/C_H(i);
C_HAc(i) = f2/(1+K1_HAc/C_H(i));
C_HCl(i) = f3/(1+K1_HCl/C_H(i));
C_OH(i) = K1w/C_H(i);
C_Ac(i) = K1_HAc*C_HAc(i)/C_H(i);
C_Cl(i) = K1_HCl*C_HCl(i)/C_H(i);
pH_old = pH(i);
pH(i) = -log10(g_H*C_H(i));
if abs(pH(i)-pH_old)<1e-7,
    break
end
end
end

s = pH-pH_exp;
index = sqrt(s*s'/length(s));

```

### **Comparison of graphically determined and regressed concentrations**

The figured generated by the code are shown for the first run.

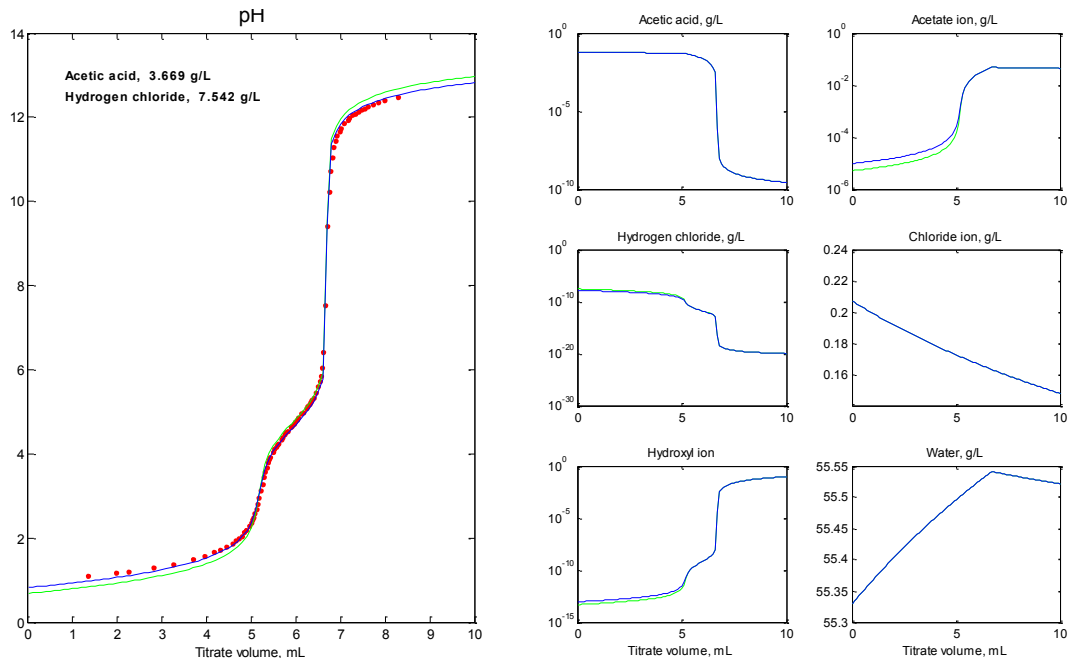


**Fig 3: Run 1 Sample 1**

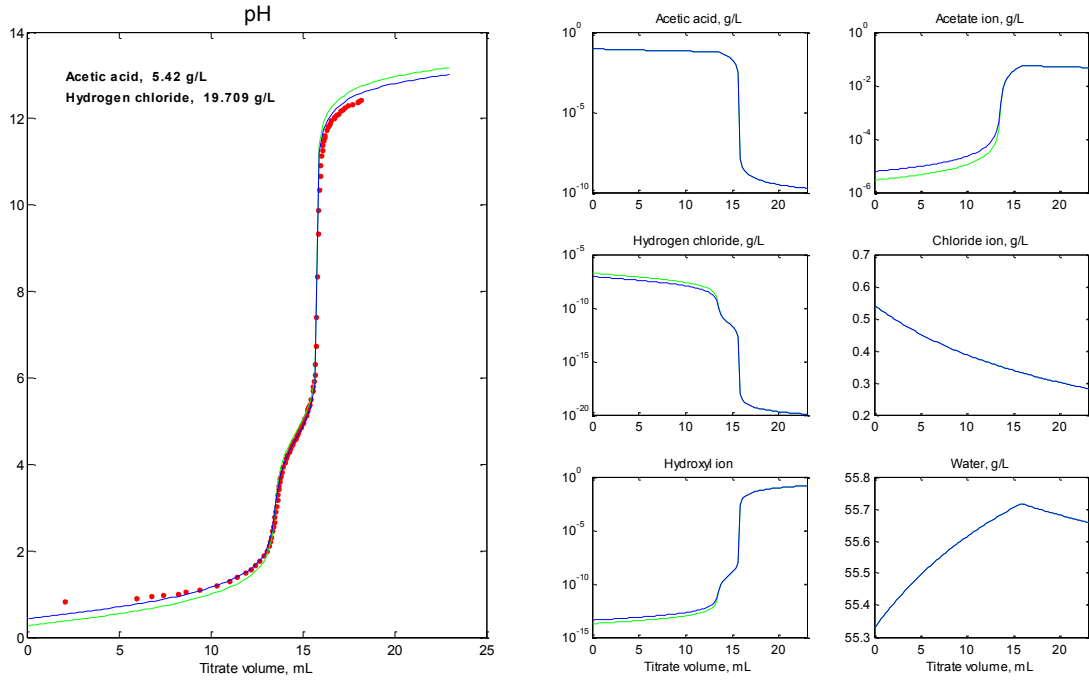


**Fig 4: Run 1 Sample 2**

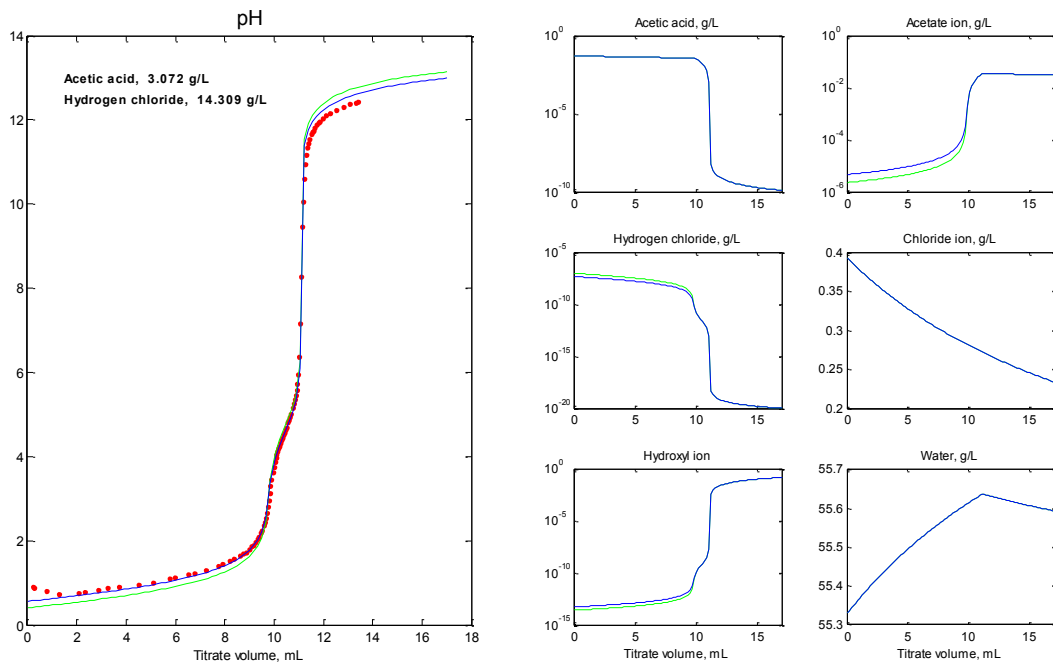


**Fig 5: Run 1 Sample 3**

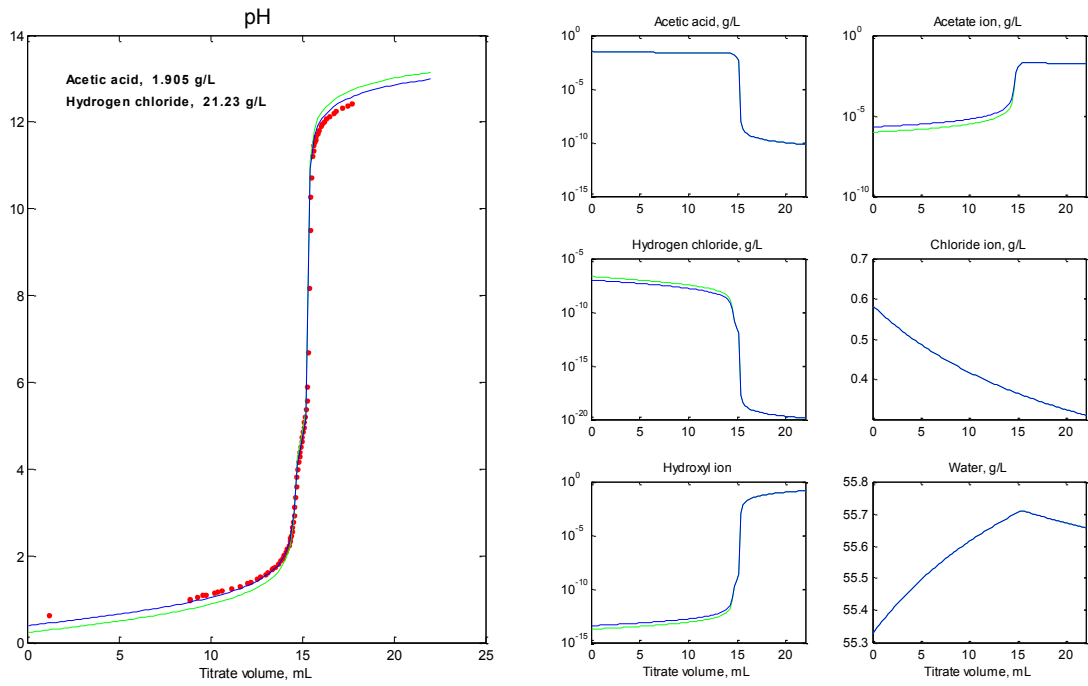


Fig 6: Run 1 Sample 4

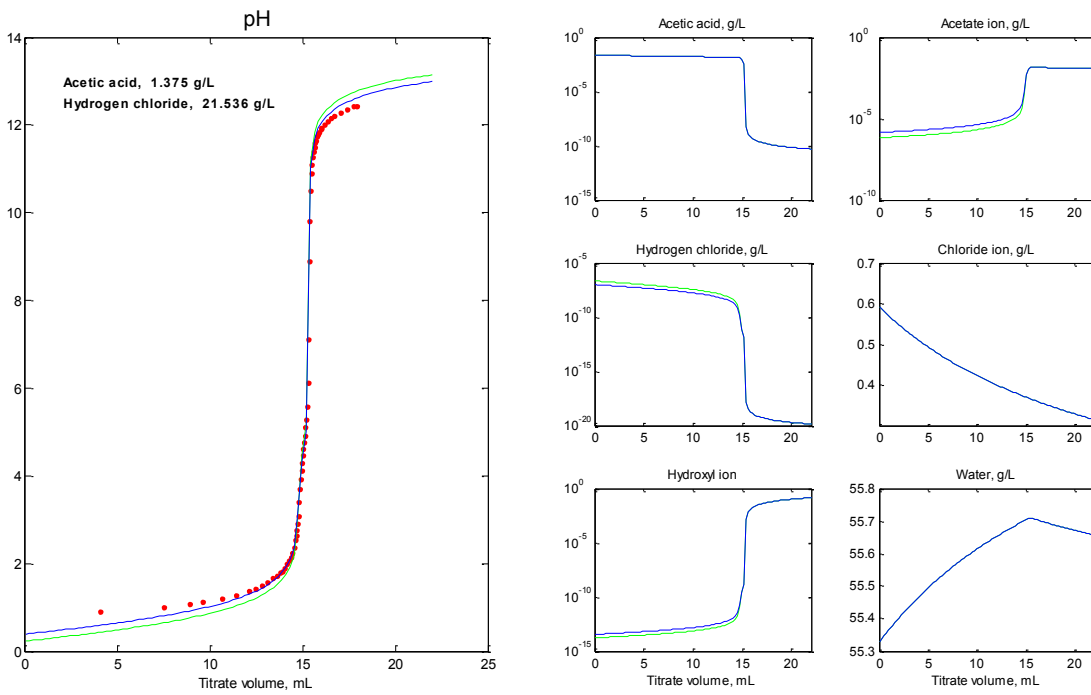
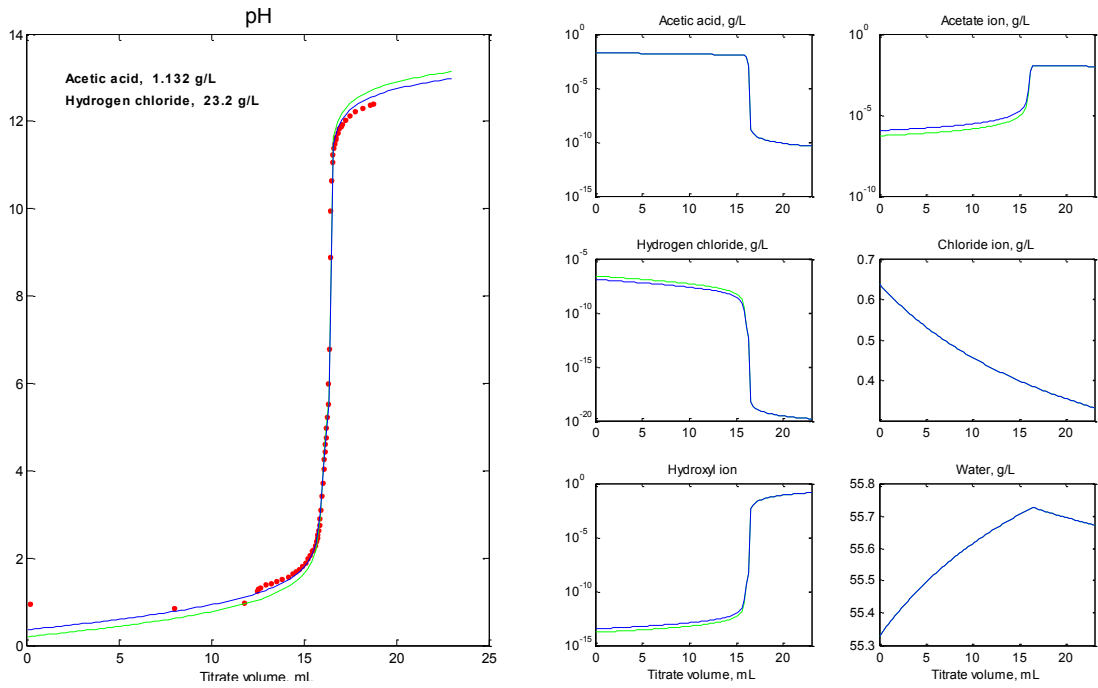


Fig 7: Run 1 Sample 5





**Fig 8: Run 1 Sample 6**

The following table summarises the HCl and acetic acid concentrations determined from both the model and graphically.

Run	Sample	Conc (g/L) [mod]		Conc (g/L) [graph]	
		HAc	HCl	HAc	HCl
1	1	3.67	7.54	3.58	7.58
	2	5.42	19.71	5.45	19.69
	3	3.07	14.31	3.05	14.32
	4	1.91	21.23	1.85	21.25
	5	1.38	21.54	1.87	21.32
	6	1.13	23.20	1.42	23.04
2	1	7.26	16.14	7.52	15.98
	2	6.85	38.79	7.28	38.50
	3	2.78	38.14	3.15	37.93
	4	1.85	44.26	2.14	44.06
	5	1.23	42.71	1.63	42.47
	6	1.10	46.13	1.61	45.95
3	1	1.56	1.54	1.39	1.62
	2	4.55	9.73	4.56	9.77
	3	3.28	10.21	3.24	10.21
	4	2.40	10.88	2.40	10.87
	5	1.64	10.92	1.68	10.94
	6	1.26	11.52	0.77	11.81
4	1	0.40	0.01	0.55	0.00
	2	2.32	3.32	2.69	3.22
	3	2.56	4.83	2.76	4.71
	4	2.15	5.02	2.26	4.90
	5	1.88	5.13	1.95	5.06
	6	1.34	5.30	1.66	5.13
5	1	7.17	17.38	7.28	17.21
	2	6.32	39.91	6.73	39.67
	3	2.77	40.11	3.12	39.81
	4	1.70	41.95	1.68	41.86
	5	1.11	41.52	1.68	41.27
	6	0.89	44.96	1.20	44.77
6	1	2.08	2.75	2.19	2.65
	2	4.27	10.64	4.54	10.50
	3	2.93	10.83	3.24	10.68
	4	2.09	11.14	2.31	11.00
	5	1.53	11.15	1.73	11.01
	6	1.23	11.47	1.23	11.51

Run	Sample	Conc (g/L) [mod]		Conc (g/L) [graph]	
		HAc	HCl	HAc	HCl
7	1	1.48	1.58	0.16	0.15
	2	4.22	9.66	0.43	0.93
	3	3.36	11.22	0.36	1.08
	4	2.60	10.86	0.27	1.06
	5	1.74	10.71	0.19	1.04
	6	1.53	11.16	0.16	1.09
8	1	3.42	3.59	3.58	3.50
	2	7.68	19.13	7.95	18.96
	3	4.29	20.60	4.61	20.42
	4	2.75	21.02	2.95	20.87
	5	1.83	20.91	2.16	20.72
	6	1.45	21.39	1.68	21.26
9	1	9.75	-5.57	0.62	0.00
	2	2.03	2.79	2.35	2.64
	3	2.91	5.04	2.98	4.93
	4	2.53	5.06	2.67	4.96
	5	2.35	5.27	2.59	5.13
	6	1.86	5.38	2.04	5.26
10	1	5.75	11.20	6.01	11.03
	2	8.39	37.34	8.82	37.03
	3	3.94	39.02	3.92	39.01
	4	2.12	41.80	2.23	41.74
	5	1.69	44.38	1.97	44.19
	6	1.43	47.65	1.66	47.53
11	1	3.15	3.00	3.27	2.96
	2	7.02	19.57	7.37	19.41
	3	4.17	21.72	4.40	21.56
	4	2.54	20.99	2.52	20.97
	5	1.65	21.63	1.68	21.57
	6	1.17	20.80	1.18	20.80
12	1	8.37	16.06	8.82	15.78
	2	8.42	31.45	8.77	30.92
	3	3.71	42.08	4.04	41.89
	4	2.10	41.00	2.11	40.94
	5	1.45	42.97	1.61	42.86
	6	1.01	44.32	1.08	44.26

Run	Sample	Conc (g/L) [mod]		Conc (g/L) [graph]	
		HAc	HCl	HAc	HCl
13	1	1.42	1.56	8.65	1.56
	2	4.93	9.87	4.83	9.89
	3	3.82	11.02	4.01	10.92
	4	2.73	11.03	2.74	10.98
	5	2.02	11.09	2.04	11.11
	6	1.44	11.52	1.56	11.45
14	1	3.04	4.19	3.07	4.21
	2	7.93	20.08	8.46	20.10
	3	4.64	19.98	4.54	19.98
	4	2.85	19.31	2.79	19.32
	5	2.02	20.31	2.09	20.30
	6	1.50	22.96	1.51	22.97
15	1	1.05	0.20	1.01	0.25
	2	2.66	3.65	2.71	3.62
	3	2.78	4.78	2.71	4.80
	4	2.24	4.84	2.26	4.84
	5	1.77	5.37	1.68	5.40
	6	1.49	5.15	1.35	5.19
16	1	1.89	0.76	1.90	0.77
	2	3.65	4.34	3.58	4.39
	3	3.40	4.91	3.29	4.96
	4	2.85	5.07	2.83	5.09
	5	3.36	5.11	2.35	5.10
	6	1.88	5.78	1.85	5.41
17	1	2.85	2.59	2.91	2.52
	2	8.53	18.51	8.82	18.32
	3	5.45	20.98	5.48	20.88
	4	3.21	19.40	3.22	19.35
	5	1.92	18.89	2.14	18.80
	6	1.64	21.16	1.61	21.18
18	1	0.68	0.25	0.74	0.19
	2	4.93	6.66	5.07	6.58
	3	4.83	10.00	4.92	9.96
	4	3.37	10.09	3.41	10.03
	5	2.48	10.54	2.47	10.49
	6	2.02	10.91	1.95	10.92
19	1	7.43	10.31	7.59	10.25
	2	11.40	39.21	12.78	38.36
	3	4.46	39.02	1.06	38.21
	4	2.72	41.93	2.71	41.84
	5	1.69	41.89	1.87	41.75
	6	1.17	44.37	1.10	44.39

## APPENDIX D: SUMMARISED RESULTS TABLES

### Run 1

#### Reaction Conditions

Pressure (bar)	1.013
Gas flow rate (kg/s)	3.27E-05
Particle size (m)	6.05E-04
Acid concentration (%m/m)	2.19
Temperature (°C)	162

#### Inputs

Mass of Raw Material (g)	18.2
%pentosan	29
Mass of Pentosan in Raw Material	5.3

Mass HCl (g)	8.8
--------------	-----

#### Product Samples

Number	1	2	3	4	5	6
Time (min)	35	35	35	35	35	35
Time (s)	2100	2100	2100	2100	2100	2100
Volume Collected (ml)	62.8	64.8	67.4	67.4	89	56.2
Mass Collected (g)	63	66	68	69	90	57
Titration aliquote volume (ml)	25	25	25	25	25	25
Tiration aliquot mass (g)	25	25	25	25	25	25
Titration volume endpoint 1 (ml)	5.20	13.5	9.82	14.6	14.6	15.8
Titration volume endpoint 2 (ml)	6.69	15.8	11.09	15.3	15.4	16.4
HCl Concentration (%m/m)	0.75	1.93	1.42	2.08	2.12	2.29
HAc Concentration (%m/m)	0.36	0.54	0.30	0.18	0.19	0.14
RI Total	1.3352	1.3389	1.3383	1.3381	1.3380	1.3382
RI HCl	0.0017	0.0044	0.0032	0.0047	0.0048	0.0052
RI Hac	0.0002	0.0004	0.0002	0.0001	0.0001	0.0001
RI Furfural	0.0010	0.0018	0.0026	0.0009	0.0008	0.0006
Furfural Concentration (%m/m)	0.49	0.94	1.34	0.47	0.41	0.33
HCl collected (g)	0.48	1.28	0.97	1.43	1.90	1.30
HAc collected (g)	0.22	0.35	0.21	0.12	0.17	0.08
Furfural collected (g)	0.31	0.62	0.91	0.33	0.37	0.19
Yield (%)	8	16	24	8	10	5
Furfural Production Rate (kmol/s)	1.54E-09	3.07E-09	4.51E-09	1.61E-09	1.81E-09	9.23E-10
Cumulative Yield (%)	8	24	48	56	66	71

**Run 2****Reaction Conditions**

Pressure (bar)	1.013
Gas flow rate (kg/s)	3.08E-05
Particle size (m)	6.05E-04
Acid concentration (%m/m)	4.29
Temperature (°C)	142

**Inputs**

Mass of Raw Material (g)	17.9
%pentosan	29
Mass of Pentosan in Raw Material	5.2

Mass HCl (g)	16.0
--------------	------

**Product Samples**

Number	1	2	3	4	5	6
Time (min)	35	35	35	35	35	35
Time (s)	2100	2100	2100	2100	2100	2100
Volume Collected (ml)	55	58.2	62	65	64	75.2
Mass Collected (g)	56	60	63	66	66	77
Titration aliquote volume (ml)	25	25	25	25	25	25
Tiration aliquot mass (g)	25	26	26	25	26	25
Titration volume endpoint 1 (ml)	10.96	26.4	26.01	30.21	29.12	31.51
Titration volume endpoint 2 (ml)	14.09	29.43	27.32	31.1	29.8	32.18
HCl Concentration (%m/m)	1.58	3.76	3.72	4.34	4.10	4.51
HAc Concentration (%m/m)	0.74	0.71	0.31	0.21	0.16	0.16
RI Total	1.3383	1.3438	1.3423	1.3432	1.3426	1.3432
RI HCl	0.0036	0.0085	0.0084	0.0098	0.0093	0.0102
RI Hac	0.0005	0.0005	0.0002	0.0001	0.0001	0.0001
RI Furfural	0.0020	0.0026	0.0015	0.0011	0.0010	0.0007
Furfural Concentration (%m/m)	1.05	1.35	0.77	0.55	0.53	0.37
HCl collected (g)	0.88	2.24	2.35	2.86	2.72	3.46
HAc collected (g)	0.41	0.42	0.20	0.14	0.10	0.12
Furfural collected (g)	0.59	0.81	0.49	0.36	0.35	0.28
Yield (%)	16	21	13	10	9	8
Furfural Production Rate (kmol/s)	2.91E-09	4.00E-09	2.43E-09	1.79E-09	1.75E-09	1.41E-09
Cumulative Yield (%)	16	37	50	59	69	76

**Run 3****Reaction Conditions**

Pressure (bar)	1.013
Gas flow rate (kg/s)	3.12E-05
Particle size (m)	6.05E-04
Acid concentration (%m/m)	1.13
Temperature (°C)	164

**Inputs**

Mass of Raw Material (g)	18.1
%pentosan	29
Mass of Pentosan in Raw Material	5.2

Mass HCl (g)	4.3
--------------	-----

**Product Samples**

Number	1	2	3	4	5	6
Time (min)	35	35	35	35	35	35
Time (s)	2100	2100	2100	2100	2100	2100
Volume Collected (ml)	59	62	62.2	62	65.6	72.4
Mass Collected (g)	60	62	63	63	70	74
Titration aliquote volume (ml)	25	25	25	25	25	25
Tiration aliquot mass (g)	25	25	25	26	27	26
Titration volume endpoint 1 (ml)	1.11	6.7	7	7.45	7.5	8.1
Titration volume endpoint 2 (ml)	1.69	8.6	8.35	8.45	8.2	8.42
HCl Concentration (%m/m)	0.16	0.98	1.00	1.06	1.02	1.16
HAc Concentration (%m/m)	0.14	0.46	0.32	0.23	0.16	0.08
RI Total	1.3331	1.3361	1.3358	1.3359	1.3357	1.3357
RI HCl	0.0004	0.0022	0.0023	0.0024	0.0023	0.0026
RI Hac	0.0001	0.0003	0.0002	0.0002	0.0001	0.0001
RI Furfural	0.0004	0.0013	0.0011	0.0011	0.0011	0.0008
Furfural Concentration (%m/m)	0.23	0.69	0.58	0.59	0.56	0.43
HCl collected (g)	0.10	0.61	0.63	0.67	0.72	0.86
HAc collected (g)	0.08	0.28	0.20	0.15	0.11	0.06
Furfural collected (g)	0.14	0.42	0.36	0.37	0.39	0.32
Yield (%)	4	11	10	10	10	8
Furfural Production Rate (kmol/s)	6.86E-10	2.10E-09	1.81E-09	1.85E-09	1.96E-09	1.59E-09
Cumulative Yield (%)	4	15	24	34	44	53

**Run 4****Reaction Conditions**

Pressure (bar)	1.013
Gas flow rate (kg/s)	3.00E-05
Particle size (m)	6.05E-04
Acid concentration (%m/m)	0.54
Temperature (°C)	161

**Inputs**

Mass of Raw Material (g)	18.2
%pentosan	29
Mass of Pentosan in Raw Material	5.3

Mass HCl (g)	2.0
--------------	-----

**Product Samples**

Number	1	2	3	4	5	6
Time (min)	35	35	35	35	35	35
Time (s)	2100	2100	2100	2100	2100	2100
Volume Collected (ml)	51.8	59.6	60	62.8	65.6	73.2
Mass Collected (g)	52	61	60	64	66	75
Titration aliquote volume (ml)	25	25	25	25	25	25
Tiration aliquot mass (g)	25	26	25	25	25	25
Titration volume endpoint 1 (ml)	0	2.21	3.23	3.36	3.47	3.52
Titration volume endpoint 2 (ml)	0.23	3.33	4.38	4.3	4.28	4.21
HCl Concentration (%m/m)	0.00	0.32	0.47	0.48	0.50	0.50
HAc Concentration (%m/m)	0.05	0.26	0.27	0.22	0.19	0.16
RI Total	1.3325	1.3341	1.3344	1.3344	1.3341	1.3341
RI HCl	0.0000	0.0007	0.0011	0.0011	0.0011	0.0011
RI Hac	0.0000	0.0002	0.0002	0.0002	0.0001	0.0001
RI Furfural	0.0002	0.0009	0.0009	0.0009	0.0006	0.0006
Furfural Concentration (%m/m)	0.11	0.47	0.44	0.44	0.30	0.31
HCl collected (g)	0.00	0.19	0.28	0.31	0.33	0.38
HAc collected (g)	0.03	0.16	0.17	0.14	0.13	0.12
Furfural collected (g)	0.06	0.28	0.27	0.28	0.20	0.23
Yield (%)	1	7	7	7	5	6
Furfural Production Rate (kmol/s)	2.85E-10	1.41E-09	1.32E-09	1.39E-09	1.00E-09	1.15E-09
Cumulative Yield (%)	1	9	16	23	28	34



**Run 5****Reaction Conditions**

Pressure (bar)	1.013
Gas flow rate (kg/s)	3.01E-05
Particle size (m)	6.05E-04
Acid concentration (%m/m)	4.29
Temperature (°C)	167

**Inputs**

Mass of Raw Material (g)	18.1
%pentosan	29
Mass of Pentosan in Raw Material	5.2

Mass HCl (g)	16.8
--------------	------

**Product Samples**

Number	1	2	3	4	5	6
Time (min)	35	35	35	35	35	35
Time (s)	2100	2100	2100	2100	2100	2100
Volume Collected (ml)	54.4	62	62.6	53.8	69.2	68
Mass Collected (g)	56	63	64	56	72	69
Titration aliquote volume (ml)	25	25	25	25	25	25
Tiration aliquot mass (g)	26	25	26	26	26	25
Titration volume endpoint 1 (ml)	11.8	27.2	27.3	28.7	28.3	30.7
Titration volume endpoint 2 (ml)	14.83	30	28.6	29.4	29	31.2
HCl Concentration (%m/m)	1.67	3.93	3.88	4.05	3.98	4.39
HAc Concentration (%m/m)	0.70	0.67	0.30	0.16	0.16	0.12
RI Total	1.3386	1.3445	1.3428	1.3427	1.3423	1.3431
RI HCl	0.0038	0.0089	0.0088	0.0091	0.0090	0.0099
RI Hac	0.0005	0.0005	0.0002	0.0001	0.0001	0.0001
RI Furfural	0.0022	0.0030	0.0016	0.0012	0.0011	0.0009
Furfural Concentration (%m/m)	1.16	1.53	0.85	0.64	0.56	0.46
HCl collected (g)	0.94	2.46	2.49	2.25	2.86	3.04
HAc collected (g)	0.40	0.42	0.20	0.09	0.12	0.08
Furfural collected (g)	0.65	0.96	0.54	0.36	0.40	0.32
Yield (%)	17	25	14	9	10	8
Furfural Production Rate (kmol/s)	3.22E-09	4.76E-09	2.70E-09	1.77E-09	1.98E-09	1.59E-09
Cumulative Yield (%)	17	42	56	66	76	85

**Run 6****Reaction Conditions**

Pressure (bar)	1.013
Gas flow rate (kg/s)	3.10E-05
Particle size (m)	6.05E-04
Acid concentration (%m/m)	1.14
Temperature (°C)	156

**Inputs**

Mass of Raw Material (g)	18
%pentosan	29
Mass of Pentosan in Raw Material	5.2

Mass HCl (g)	4.3
--------------	-----

**Product Samples**

Number	1	2	3	4	5	6
Time (min)	35	35	35	35	35	35
Time (s)	2100	2100	2100	2100	2100	2100
Volume Collected (ml)	68.8	63.2	63	62.6	63	63.2
Mass Collected (g)	69	65	64	64	64	65
Titration aliquote volume (ml)	25	25	25	25	25	25
Tiration aliquot mass (g)	25	26	26	26	25	26
Titration volume endpoint 1 (ml)	1.82	7.2	7.32	7.54	7.55	7.89
Titration volume endpoint 2 (ml)	2.73	9.09	8.67	8.5	8.27	8.4
HCl Concentration (%m/m)	0.26	1.02	1.05	1.08	1.09	1.13
HAc Concentration (%m/m)	0.22	0.44	0.32	0.23	0.17	0.12
RI Total	1.3336	1.3361	1.3361	1.3359	1.3357	1.3357
RI HCl	0.0006	0.0023	0.0024	0.0024	0.0025	0.0025
RI Hac	0.0001	0.0003	0.0002	0.0002	0.0001	0.0001
RI Furfural	0.0007	0.0013	0.0013	0.0012	0.0010	0.0009
Furfural Concentration (%m/m)	0.37	0.69	0.68	0.60	0.50	0.48
HCl collected (g)	0.18	0.66	0.67	0.69	0.69	0.73
HAc collected (g)	0.15	0.29	0.20	0.14	0.11	0.08
Furfural collected (g)	0.25	0.45	0.44	0.38	0.32	0.31
Yield (%)	7	12	12	10	8	8
Furfural Production Rate (kmol/s)	1.26E-09	2.21E-09	2.17E-09	1.90E-09	1.57E-09	1.53E-09
Cumulative Yield (%)	7	18	30	40	48	57

**Run 7****Reaction Conditions**

Pressure (bar)	1.013
Gas flow rate (kg/s)	2.74E-05
Particle size (m)	6.05E-04
Acid concentration (%m/m)	1.11
Temperature (°C)	146

**Inputs**

Mass of Raw Material (g)	18.2
%pentosan	29
Mass of Pentosan in Raw Material	5.3

Mass HCl (g)	3.7
--------------	-----

**Product Samples**

Number	1	2	3	4	5	6
Time (min)	35	35	35	35	35	35
Time (s)	2100	2100	2100	2100	2100	2100
Volume Collected (ml)	53	57	55	55	57	64
Mass Collected (g)	53	58	56	56	58	65
Titration aliquote volume (ml)	25	25	25	25	25	25
Tiration aliquot mass (g)	25	26	26	25	25	25
Titration volume endpoint 1 (ml)	1.01	6.52	7.59	7.38	7.28	7.59
Titration volume endpoint 2 (ml)	1.69	8.34	9.11	8.52	8.1	8.26
HCl Concentration (%m/m)	0.15	0.93	1.08	1.06	1.04	1.09
HAc Concentration (%m/m)	0.16	0.43	0.36	0.27	0.19	0.16
RI Total	1.3331	1.3360	1.3360	1.3359	1.3357	1.3355
RI HCl	0.0003	0.0021	0.0024	0.0024	0.0024	0.0025
RI Hac	0.0001	0.0003	0.0002	0.0002	0.0001	0.0001
RI Furfural	0.0004	0.0013	0.0010	0.0010	0.0009	0.0006
Furfural Concentration (%m/m)	0.19	0.67	0.50	0.50	0.45	0.32
HCl collected (g)	0.08	0.54	0.61	0.59	0.60	0.71
HAc collected (g)	0.09	0.25	0.20	0.15	0.11	0.10
Furfural collected (g)	0.10	0.39	0.28	0.28	0.26	0.21
Yield (%)	3	10	7	7	7	5
Furfural Production Rate (kmol/s)	4.91E-10	1.94E-09	1.39E-09	1.38E-09	1.28E-09	1.02E-09
Cumulative Yield (%)	3	13	20	27	34	39

**Run 8****Reaction Conditions**

Pressure (bar)	1.013
Gas flow rate (kg/s)	2.42E-05
Particle size (m)	6.05E-04
Acid concentration (%m/m)	2.15
Temperature (°C)	148

**Inputs**

Mass of Raw Material (g)	18.2
%pentosan	29
Mass of Pentosan in Raw Material	5.3

Mass HCl (g)	6.2
--------------	-----

**Product Samples**

Number	1	2	3	4	5	6
Time (min)	35	35	35	35	35	35
Time (s)	2100	2100	2100	2100	2100	2100
Volume Collected (ml)	46	49.2	51	48	52	57.2
Mass Collected (g)	46	49	51	49	52	58
Titration aliquote volume (ml)	25	25	25	25	25	25
Tiration aliquot mass (g)	25	25	25	26	25	25
Titration volume endpoint 1 (ml)	2.4	13	14	14.31	14.21	14.58
Titration volume endpoint 2 (ml)	3.89	16.31	15.92	15.54	15.11	15.28
HCl Concentration (%m/m)	0.35	1.89	2.03	2.03	2.07	2.12
HAc Concentration (%m/m)	0.36	0.79	0.46	0.29	0.22	0.17
RI Total	1.3341	1.3393	1.3389	1.3383	1.3380	1.3380
RI HCl	0.0008	0.0043	0.0046	0.0046	0.0047	0.0048
RI Hac	0.0002	0.0005	0.0003	0.0002	0.0001	0.0001
RI Furfural	0.0009	0.0023	0.0018	0.0013	0.0010	0.0010
Furfural Concentration (%m/m)	0.47	1.20	0.93	0.68	0.53	0.49
HCl collected (g)	0.16	0.93	1.04	1.00	1.08	1.22
HAc collected (g)	0.16	0.39	0.24	0.14	0.11	0.10
Furfural collected (g)	0.21	0.59	0.48	0.33	0.28	0.28
Yield (%)	6	15	12	9	7	7
Furfural Production Rate (kmol/s)	1.05E-09	2.94E-09	2.37E-09	1.66E-09	1.37E-09	1.41E-09
Cumulative Yield (%)	6	21	33	42	49	57

**Run 9****Reaction Conditions**

Pressure (bar)	1.013
Gas flow rate (kg/s)	2.52E-05
Particle size (m)	6.05E-04
Acid concentration (%m/m)	0.53
Temperature (°C)	141

**Inputs**

Mass of Raw Material (g)	18.1
%pentosan	29
Mass of Pentosan in Raw Material	5.2

Mass HCl (g)	1.5
--------------	-----

**Product Samples**

Number	1	2	3	4	5	6
Time (min)	35	35	35	35	35	35
Time (s)	2100	2100	2100	2100	2100	2100
Volume Collected (ml)	46	49.1	48.8	49.1	44.9	51
Mass Collected (g)	46	49	78	49	45	51
Titration aliquote volume (ml)	25	25	25	25	25	25
Tiration aliquot mass (g)	25	25	40	25	25	25
Titration volume endpoint 1 (ml)		1.81	3.38	3.4	3.52	3.61
Titration volume endpoint 2 (ml)	0.26	2.79	4.62	4.51	4.6	4.46
HCl Concentration (%m/m)	0.00	0.26	0.31	0.49	0.52	0.53
HAc Concentration (%m/m)	0.06	0.23	0.19	0.27	0.26	0.20
RI Total	1.3323	1.3338	1.3345	1.3344	1.3345	1.3342
RI HCl	0.0000	0.0006	0.0007	0.0011	0.0012	0.0012
RI Hac	0.0000	0.0002	0.0001	0.0002	0.0002	0.0001
RI Furfural	0.0000	0.0008	0.0014	0.0009	0.0009	0.0006
Furfural Concentration (%m/m)	0.00	0.41	0.71	0.44	0.44	0.29
HCl collected (g)	0.00	0.13	0.24	0.24	0.23	0.27
HAc collected (g)	0.03	0.12	0.15	0.13	0.12	0.10
Furfural collected (g)	0.00	0.20	0.55	0.22	0.20	0.15
Yield (%)	0	5	14	6	5	4
Furfural Production Rate (kmol/s)	9.09E-12	1.01E-09	2.72E-09	1.08E-09	9.80E-10	7.36E-10
Cumulative Yield (%)	0	5	20	25	31	35

**Run 10****Reaction Conditions**

Pressure (bar)	1.013
Gas flow rate (kg/s)	2.69E-05
Particle size (m)	6.05E-04
Acid concentration (%m/m)	4.22
Temperature (°C)	142

**Inputs**

Mass of Raw Material (g)	18.3
%pentosan	29
Mass of Pentosan in Raw Material	5.3

Mass HCl (g)	13.7
--------------	------

**Product Samples**

Number	1	2	3	4	5	6
Time (min)	35	35	35	35	35	35
Time (s)	2100	2100	2100	2100	2100	2100
Volume Collected (ml)	47.3	51.1	50.8	56.2	60.2	69
Mass Collected (g)	47	52	52	57	61	71
Titration aliquote volume (ml)	25	25	25	25	25	25
Tiration aliquot mass (g)	25	25	25	25	25	26
Titration volume endpoint 1 (ml)	7.56	25.39	26.75	28.62	30.3	32.59
Titration volume endpoint 2 (ml)	10.06	29.06	28.38	29.55	31.12	33.28
HCl Concentration (%m/m)	1.10	3.65	3.85	4.12	4.35	4.63
HAc Concentration (%m/m)	0.60	0.87	0.39	0.22	0.19	0.16
RI Total	1.3376	1.3438	1.3429	1.3426	1.3431	1.3439
RI HCl	0.0025	0.0082	0.0087	0.0093	0.0098	0.0105
RI Hac	0.0004	0.0006	0.0003	0.0002	0.0001	0.0001
RI Furfural	0.0025	0.0028	0.0017	0.0009	0.0009	0.0011
Furfural Concentration (%m/m)	1.31	1.42	0.88	0.46	0.48	0.58
HCl collected (g)	0.52	1.89	1.98	2.35	2.66	3.28
HAc collected (g)	0.28	0.45	0.20	0.13	0.12	0.11
Furfural collected (g)	0.62	0.74	0.45	0.26	0.30	0.41
Yield (%)	16	19	12	7	8	11
Furfural Production Rate (kmol/s)	3.07E-09	3.65E-09	2.23E-09	1.30E-09	1.46E-09	2.05E-09
Cumulative Yield (%)	16	35	47	54	61	72

**Run 11****Reaction Conditions**

Pressure (bar)	1.013
Gas flow rate (kg/s)	2.5E-05
Particle size (m)	6.05E-04
Acid concentration (%m/m)	2.2
Temperature (°C)	163

**Inputs**

Mass of Raw Material (g)	18.3
%pentosan	29
Mass of Pentosan in Raw Material	5.3

Mass HCl (g)	6.9
--------------	-----

**Product Samples**

Number	1	2	3	4	5	6
Time (min)	35	35	35	35	35	35
Time (s)	2100	2100	2100	2100	2100	2100
Volume Collected (ml)	40	55.5	55.2	53.2	52	54.4
Mass Collected (g)	40	56	56	53	56	54
Titration aliquote volume (ml)	25	25	25	25	25	25
Tiration aliquot mass (g)	25	25	25	25	27	25
Titration volume endpoint 1 (ml)	2.03	13.31	14.78	14.38	14.79	14.26
Titration volume endpoint 2 (ml)	3.39	16.38	16.61	15.43	15.49	14.75
HCl Concentration (%m/m)	0.30	1.93	2.14	2.09	2.01	2.08
HAc Concentration (%m/m)	0.33	0.73	0.44	0.25	0.16	0.12
RI Total	1.3340	1.3390	1.3388	1.3381	1.3379	1.3372
RI HCl	0.0007	0.0044	0.0048	0.0047	0.0045	0.0047
RI Hac	0.0002	0.0005	0.0003	0.0002	0.0001	0.0001
RI Furfural	0.0008	0.0019	0.0015	0.0009	0.0010	0.0001
Furfural Concentration (%m/m)	0.42	0.97	0.75	0.47	0.52	0.06
HCl collected (g)	0.12	1.08	1.19	1.12	1.12	1.13
HAc collected (g)	0.13	0.41	0.24	0.13	0.09	0.06
Furfural collected (g)	0.17	0.54	0.42	0.25	0.29	0.03
Yield (%)	4	14	11	6	8	1
Furfural Production Rate (kmol/s)	8.31E-10	2.70E-09	2.07E-09	1.24E-09	1.45E-09	1.60E-10
Cumulative Yield (%)	4	18	29	36	43	44

**Run 12****Reaction Conditions**

Pressure (bar)	1.013
Gas flow rate (kg/s)	2.41E-05
Particle size (m)	6.05E-04
Acid concentration (%m/m)	4.38
Temperature (°C)	152

**Inputs**

Mass of Raw Material (g)	18.3
%pentosan	29
Mass of Pentosan in Raw Material	5.3

Mass HCl (g)	13.0
--------------	------

**Product Samples**

Number	1	2	3	4	5	6
Time (min)	35	35	35	35	35	35
Time (s)	2100	2100	2100	2100	2100	2100
Volume Collected (ml)	40	53.2	50.8	50.8	48	56.8
Mass Collected (g)	40	53	52	52	49	58
Titration aliquote volume (ml)	25	25	25	25	25	25
Tiration aliquot mass (g)	25	25	25	25	25	25
Titration volume endpoint 1 (ml)	10.82	21.2	28.72	28.07	29.39	30.35
Titration volume endpoint 2 (ml)	14.49	24.85	30.4	28.95	30.06	30.8
HCl Concentration (%m/m)	1.56	3.09	4.11	4.04	4.24	4.36
HAc Concentration (%m/m)	0.87	0.88	0.40	0.21	0.16	0.11
RI Total	1.3389	1.3440	1.3430	1.3422	1.3423	1.3426
RI HCl	0.0035	0.0070	0.0093	0.0091	0.0096	0.0098
RI Hac	0.0006	0.0006	0.0003	0.0001	0.0001	0.0001
RI Furfural	0.0026	0.0043	0.0013	0.0007	0.0004	0.0005
Furfural Concentration (%m/m)	1.35	2.21	0.67	0.38	0.21	0.28
HCl collected (g)	0.63	1.64	2.13	2.08	2.06	2.51
HAc collected (g)	0.35	0.47	0.21	0.11	0.08	0.06
Furfural collected (g)	0.55	1.18	0.35	0.20	0.10	0.16
Yield (%)	14	31	9	5	3	4
Furfural Production Rate (kmol/s)	2.71E-09	5.84E-09	1.73E-09	9.74E-10	5.12E-10	7.94E-10
Cumulative Yield (%)	14	45	54	59	61	66



**Run 13****Reaction Conditions**

Pressure (bar)	1.013
Gas flow rate (kg/s)	2.61E-05
Particle size (m)	6.05E-04
Acid concentration (%m/m)	1.14
Temperature (°C)	153

**Inputs**

Mass of Raw Material (g)	18.6
%pentosan	29
Mass of Pentosan in Raw Material	5.4

Mass HCl (g)	3.6
--------------	-----

**Product Samples**

Number	1	2	3	4	5	6
Time (min)	35	35	35	35	35	35
Time (s)	2100	2100	2100	2100	2100	2100
Volume Collected (ml)	48	52.6	54.8	53.6	58.7	63.7
Mass Collected (g)	48	53	54	53	58	64
Titration aliquote volume (ml)	25	25	25	25	25	25
Tiration aliquot mass (g)	25	25	25	25	25	25
Titration volume endpoint 1 (ml)	1.07	6.78	7.49	7.53	7.62	7.85
Titration volume endpoint 2 (ml)	4.67	8.79	9.16	8.67	8.47	8.5
HCl Concentration (%m/m)	0.16	0.99	1.10	1.10	1.13	1.14
HAc Concentration (%m/m)	0.87	0.48	0.41	0.28	0.21	0.16
RI Total	1.3331	1.3361	1.3360	1.3358	1.3357	1.3354
RI HCl	0.0004	0.0022	0.0025	0.0025	0.0026	0.0026
RI Hac	0.0006	0.0003	0.0003	0.0002	0.0001	0.0001
RI Furfural	0.0000	0.0014	0.0011	0.0010	0.0009	0.0006
Furfural Concentration (%m/m)	-0.02	0.71	0.56	0.50	0.44	0.29
HCl collected (g)	0.07	0.52	0.60	0.59	0.65	0.73
HAc collected (g)	0.42	0.25	0.22	0.15	0.12	0.10
Furfural collected (g)	-0.01	0.37	0.30	0.27	0.25	0.19
Yield (%)	0	10	8	7	6	5
Furfural Production Rate (kmol/s)	-5.86E-11	1.86E-09	1.50E-09	1.32E-09	1.25E-09	9.18E-10
Cumulative Yield (%)	0	9	17	24	30	35

**Run 14****Reaction Conditions**

Pressure (bar)	1.013
Gas flow rate (kg/s)	2.46E-05
Particle size (m)	6.05E-04
Acid concentration (%m/m)	2.21
Temperature (°C)	150

**Inputs**

Mass of Raw Material (g)	18.4
%pentosan	29
Mass of Pentosan in Raw Material	5.3

Mass HCl (g)	6.5
--------------	-----

**Product Samples**

Number	1	2	3	4	5	6
Time (min)	35	35	35	35	35	35
Time (s)	2100	2100	2100	2100	2100	2100
Volume Collected (ml)	44.2	50.4	47.9	48.4	50.2	65.6
Mass Collected (g)	44	51	48	49	51	66
Titration aliquote volume (ml)	25	25	25	25	25	25
Tiration aliquot mass (g)	25	25	25	25	25	25
Titration volume endpoint 1 (ml)	2.89	13.78	13.7	13.25	13.92	15.75
Titration volume endpoint 2 (ml)	4.17	17.3	15.59	14.41	14.79	16.38
HCl Concentration (%m/m)	0.42	1.97	1.99	1.91	2.01	2.29
HAc Concentration (%m/m)	0.31	0.83	0.45	0.28	0.21	0.15
RI Total	1.3392	1.3393	1.3383	1.3378	1.3377	1.3380
RI HCl	0.0009	0.0045	0.0045	0.0043	0.0045	0.0052
RI Hac	0.0002	0.0006	0.0003	0.0002	0.0001	0.0001
RI Furfural	0.0058	0.0021	0.0014	0.0011	0.0008	0.0005
Furfural Concentration (%m/m)	3.01	1.10	0.70	0.59	0.42	0.28
HCl collected (g)	0.19	1.01	0.96	0.94	1.02	1.51
HAc collected (g)	0.14	0.43	0.22	0.13	0.10	0.10
Furfural collected (g)	1.34	0.56	0.34	0.29	0.21	0.18
Yield (%)	34	14	9	7	6	5
Furfural Production Rate (kmol/s)	6.63E-09	2.79E-09	1.67E-09	1.43E-09	1.06E-09	9.00E-10
Cumulative Yield (%)	34	49	58	65	71	75

**Run 15****Reaction Conditions**

Pressure (bar)	1.013
Gas flow rate (kg/s)	2.83E-05
Particle size (m)	6.05E-04
Acid concentration (%m/m)	0.54
Temperature (°C)	152

**Inputs**

Mass of Raw Material (g)	18.5
%pentosan	29
Mass of Pentosan in Raw Material	5.4

Mass HCl (g)	1.9
--------------	-----

**Product Samples**

Number	1	2	3	4	5	6
Time (min)	35	35	35	35	35	35
Time (s)	2100	2100	2100	2100	2100	2100
Volume Collected (ml)	49	50.8	54.1	59.8	65.9	73.6
Mass Collected (g)	49	51	54	60	66	78
Titration aliquote volume (ml)	25	25	25	25	25	25
Tiration aliquot mass (g)	25	25	25	25	25	26
Titration volume endpoint 1 (ml)	0.17	2.48	3.29	3.32	3.7	3.56
Titration volume endpoint 2 (ml)	0.59	3.61	4.42	4.26	4.4	4.12
HCl Concentration (%m/m)	0.02	0.36	0.48	0.49	0.54	0.49
HAc Concentration (%m/m)	0.10	0.27	0.27	0.23	0.17	0.13
RI Total	1.3324	1.3342	1.3343	1.3342	1.3340	1.3340
RI HCl	0.0001	0.0008	0.0011	0.0011	0.0012	0.0011
RI Hac	0.0001	0.0002	0.0002	0.0002	0.0001	0.0001
RI Furfural	0.0002	0.0010	0.0009	0.0008	0.0006	0.0007
Furfural Concentration (%m/m)	0.09	0.54	0.46	0.44	0.31	0.36
HCl collected (g)	0.01	0.18	0.26	0.29	0.36	0.38
HAc collected (g)	0.05	0.14	0.15	0.14	0.11	0.10
Furfural collected (g)	0.04	0.27	0.25	0.26	0.20	0.28
Yield (%)	1	7	6	7	5	7
Furfural Production Rate (kmol/s)	2.18E-10	1.36E-09	1.23E-09	1.29E-09	1.00E-09	1.40E-09
Cumulative Yield (%)	1	8	14	21	26	34

**Run 16****Reaction Conditions**

Pressure (bar)	1.013
Gas flow rate (kg/s)	2.09E-05
Particle size (m)	6.05E-04
Acid concentration (%m/m)	0.54
Temperature (°C)	152

**Inputs**

Mass of Raw Material (g)	18.3
%pentosan	29
Mass of Pentosan in Raw Material	5.3

Mass HCl (g)	1.4
--------------	-----

**Product Samples**

Number	1	2	3	4	5	6
Time (min)	35	35	35	35	35	35
Time (s)	2100	2100	2100	2100	2100	2100
Volume Collected (ml)	34	41.8	44.2	45	43.6	52.2
Mass Collected (g)	34	42	44	48	44	52
Titration aliquote volume (ml)	25	25	25	25	25	25
Tiration aliquot mass (g)	25	25	25	27	25	25
Titration volume endpoint 1 (ml)	0.53	3.01	3.4	3.49	3.5	3.71
Titration volume endpoint 2 (ml)	1.32	4.5	4.77	4.67	4.48	4.48
HCl Concentration (%m/m)	0.08	0.44	0.49	0.48	0.51	0.54
HAc Concentration (%m/m)	0.19	0.36	0.33	0.27	0.24	0.19
RI Total	1.3331	1.3348	1.3346	1.3342	1.3342	1.3341
RI HCl	0.0002	0.0010	0.0011	0.0011	0.0012	0.0012
RI Hac	0.0001	0.0002	0.0002	0.0002	0.0002	0.0001
RI Furfural	0.0006	0.0015	0.0012	0.0008	0.0007	0.0006
Furfural Concentration (%m/m)	0.33	0.75	0.60	0.43	0.38	0.33
HCl collected (g)	0.03	0.18	0.22	0.23	0.22	0.28
HAc collected (g)	0.06	0.15	0.15	0.13	0.10	0.10
Furfural collected (g)	0.11	0.31	0.26	0.21	0.17	0.17
Yield (%)	3	8	7	5	4	5
Furfural Production Rate (kmol/s)	5.54E-10	1.54E-09	1.31E-09	1.02E-09	8.21E-10	8.65E-10
Cumulative Yield (%)	3	11	18	23	27	32

**Run 17****Reaction Conditions**

Pressure (bar)	1.013
Gas flow rate (kg/s)	2.16E-05
Particle size (m)	6.05E-04
Acid concentration (%m/m)	2.19
Temperature (°C)	151

**Inputs**

Mass of Raw Material (g)	18.1
%pentosan	29
Mass of Pentosan in Raw Material	5.2

Mass HCl (g)	
--------------	--

**Product Samples**

Number	1	2	3	4	5	6
Time (min)	35	35	35	35	35	35
Time (s)	2100	2100	2100	2100	2100	2100
Volume Collected (ml)	40.8	43.6	42.3	42	41	56.8
Mass Collected (g)	41	44	42	42	47	57
Titration aliquote volume (ml)	25	25	25	25	25	25
Tiration aliquot mass (g)	25	25	25	25	28	25
Titration volume endpoint 1 (ml)	1.73	12.56	14.32	13.27	12.89	14.52
Titration volume endpoint 2 (ml)	2.94	16.23	16.6	14.61	13.78	15.19
HCl Concentration (%m/m)	0.25	1.83	2.10	1.94	1.66	2.11
HAc Concentration (%m/m)	0.29	0.88	0.55	0.32	0.19	0.16
RI Total	1.3338	1.3392	1.3390	1.3380	1.3382	1.3377
RI HCl	0.0006	0.0041	0.0047	0.0044	0.0037	0.0048
RI Hac	0.0002	0.0006	0.0004	0.0002	0.0001	0.0001
RI Furfural	0.0009	0.0024	0.0018	0.0013	0.0022	0.0007
Furfural Concentration (%m/m)	0.48	1.22	0.92	0.65	1.12	0.35
HCl collected (g)	0.10	0.80	0.88	0.81	0.77	1.20
HAc collected (g)	0.12	0.38	0.23	0.14	0.09	0.09
Furfural collected (g)	0.19	0.53	0.39	0.27	0.52	0.20
Yield (%)	5	14	10	7	14	5
Furfural Production Rate (kmol/s)	9.59E-10	2.63E-09	1.92E-09	1.35E-09	2.59E-09	9.85E-10
Cumulative Yield (%)	5	19	29	36	50	55

**Run 18****Reaction Conditions**

Pressure (bar)	1.013
Gas flow rate (kg/s)	2.08E-05
Particle size (m)	6.05E-04
Acid concentration (%m/m)	1.11
Temperature (°C)	161

**Inputs**

Mass of Raw Material (g)	18.3
%pentosan	29
Mass of Pentosan in Raw Material	5.3

Mass HCl (g)	
--------------	--

**Product Samples**

Number	1	2	3	4	5	6
Time (min)	35	35	35	35	35	35
Time (s)	2100	2100	2100	2100	2100	2100
Volume Collected (ml)	33.9	44	45.3	45.2	46.4	51.3
Mass Collected (g)	32	43	44	44	47	52
Titration aliquote volume (ml)	25	25	25	25	25	25
Tiration aliquot mass (g)	24	24	24	24	25	25
Titration volume endpoint 1 (ml)	0.13	4.51	6.83	6.88	7.19	7.49
Titration volume endpoint 2 (ml)	0.44	6.62	8.88	8.3	8.22	8.3
HCl Concentration (%m/m)	0.02	0.68	1.02	1.03	1.04	1.09
HAc Concentration (%m/m)	0.08	0.52	0.50	0.35	0.24	0.19
RI Total	1.3324	1.3353	1.3361	1.3358	1.3355	1.3353
RI HCl	0.0000	0.0015	0.0023	0.0023	0.0023	0.0025
RI Hac	0.0001	0.0004	0.0003	0.0002	0.0002	0.0001
RI Furfural	0.0002	0.0013	0.0014	0.0011	0.0009	0.0006
Furfural Concentration (%m/m)	0.08	0.68	0.70	0.59	0.46	0.32
HCl collected (g)	0.01	0.29	0.45	0.45	0.49	0.56
HAc collected (g)	0.03	0.22	0.22	0.15	0.11	0.10
Furfural collected (g)	0.03	0.29	0.31	0.26	0.22	0.16
Yield (%)	1	7	8	7	6	4
Furfural Production Rate (kmol/s)	1.25E-10	1.43E-09	1.53E-09	1.29E-09	1.08E-09	8.04E-10
Cumulative Yield (%)	1	8	16	23	29	33

**Run 19****Reaction Conditions**

Pressure (bar)	1.013
Gas flow rate (kg/s)	2.07E-05
Particle size (m)	6.05E-04
Acid concentration (%m/m)	4.33
Temperature (°C)	162

**Inputs**

Mass of Raw Material (g)	18.2
%pentosan	29
Mass of Pentosan in Raw Material	5.3

Mass HCl (g)	10.8
--------------	------

**Product Samples**

Number	1	2	3	4	5	6
Time (min)	35	35	35	35	35	35
Time (s)	2100	2100	2100	2100	2100	2100
Volume Collected (ml)	38.8	39	42	42.9	44.9	49.9
Mass Collected (g)	39	40	43	43	46	51
Titration aliquote volume (ml)	25	25	25	25	25	25
Tiration aliquot mass (g)	25	26	26	25	25	26
Titration volume endpoint 1 (ml)	7.03	26.3	26.2	28.69	28.63	30.44
Titration volume endpoint 2 (ml)	10.19	31.62	26.64	29.82	29.41	30.9
HCl Concentration (%m/m)	1.03	3.76	3.74	4.14	4.11	4.34
HAc Concentration (%m/m)	0.76	1.25	0.10	0.27	0.18	0.11
RI Total	1.3380	1.3449	1.3422	1.3424	1.3422	1.3427
RI HCl	0.0023	0.0085	0.0084	0.0093	0.0093	0.0098
RI Hac	0.0005	0.0009	0.0001	0.0002	0.0001	0.0001
RI Furfural	0.0030	0.0034	0.0015	0.0007	0.0006	0.0007
Furfural Concentration (%m/m)	1.55	1.76	0.76	0.38	0.30	0.34
HCl collected (g)	0.40	1.50	1.60	1.80	1.87	2.22
HAc collected (g)	0.29	0.50	0.04	0.12	0.08	0.06
Furfural collected (g)	0.60	0.70	0.33	0.16	0.14	0.18
Yield (%)	16	18	9	4	4	5
Furfural Production Rate (kmol/s)	2.98E-09	3.47E-09	1.63E-09	8.07E-10	6.88E-10	8.71E-10
Cumulative Yield (%)	16	34	42	47	50	55





## Refractive Index and Mass balance sheet

Date: 18/06/2007 Run no: 4

Sample no:	H2O	* 1	2	3	4	5	6
Mass of Empty Flask		115,2	99,5	94,0	109,6	115,5	100,3
Mass of Full Flask		178,3	166,5	162,1	178,3	205,1	156,9
Volume of sample		62,8	64,8	67,4	67,4	89,0	56,2
Sample Time (min)		87	72	107	152	187	202
RI1	1,3323	1,3352	1,3358	1,3353	1,3381	1,3380	1,3382
RI2	1,3323	1,3352	1,3389	1,3353	1,3380	1,3380	1,3382

start from 2 min

Titration Data

Reaction no. 4  
 Titrations:  
 Aliquot Volume 25ml

Date: 18/06/2007  
 NaOH conc 1N

Analyst: Ronelle

Sample: 1				Sample: 2			
Vol (ml)	pH	Vol (ml)	pH	Vol (ml)	pH	Vol (ml)	pH
0	6.98	4.37	5.22	0	0.94	15.30	5.32
1.34	1.08	4.40	5.28	2.03	0.93	15.36	5.338
1.96	1.18	4.43	5.34	5.02	0.91	15.44	5.51
2.28	1.21	4.48	5.46	6.71	0.94	15.51	5.69
3.84	1.30	4.54	5.61	7.38	0.97	15.55	5.780
4.29	1.38	4.58	5.73	8.19	1.01	15.59	5.93
4.74	1.50	4.61	5.85	8.58	1.04	15.62	6.08
4.99	1.58	4.63	6.06	9.35	1.10	15.66	6.31
5.21	1.66	4.66	6.402	10.29	1.21	15.70	6.74
5.35	1.72	4.70	6.753	10.98	1.30	15.73	7.42
5.49	1.79	4.74	9.41	11.40	1.39	15.77	8.35
5.61	1.87	4.78	10.22	11.87	1.50	15.81	8.93
5.68	1.93	4.81	10.72	12.17	1.58	15.85	9.88
5.75	1.99	4.85	11.05	12.36	1.66	15.89	10.35
5.83	2.05	4.89	11.29	12.64	1.77	15.93	10.67
5.88	2.14	4.93	11.45	12.85	1.87	15.96	10.92
5.92	2.19	4.96	11.56	13.01	2.00	16.00	11.14
6.00	2.30	5.01	11.67	13.12	2.11	16.04	11.26
6.03	2.347	5.05	11.74	13.20	2.21	16.08	11.38
6.06	2.43	5.12	11.85	13.28	2.32	16.12	11.49
6.09	2.49	5.20	11.94	13.34	2.46	16.15	11.51
6.12	2.59	5.24	11.99	13.38	2.56	16.19	11.62
6.15	2.69	5.31	12.05	13.42	2.66	16.28	11.73
6.18	2.81	5.36	12.09	13.46	2.79	16.36	11.780
6.21	2.95	5.43	12.13	13.50	2.90	16.39	11.84
6.24	3.14	5.51	12.18	13.53	3.03	16.46	11.89
6.30	3.28	5.58	12.21	13.58	3.17	16.55	11.95
6.31	3.44	5.66	12.25	13.61	3.29	16.68	12.02
6.34	3.57	5.71	12.30	13.65	3.42	16.72	12.04
6.38	3.67	5.88	12.35	13.67	3.50	16.82	12.09
6.41	3.79	6.03	12.40	13.71	3.59	16.90	12.12
6.44	3.86	6.32	12.47	13.75	3.67	17.05	12.188
6.47	3.93			13.78	3.73	17.14	12.21
6.53	4.05			13.83	3.82	17.30	12.25
6.56	4.12			13.91	3.94	17.47	12.30
6.60	4.17			14.01	4.05	17.66	12.34
6.62	4.21			14.09	4.15	17.96	12.39
6.65	4.24			14.15	4.22	18.01	12.41
6.71	4.33			14.23	4.29	18.13	12.43
6.74	4.38			14.30	4.36		
6.79	4.456			14.37	4.43		
6.82	4.51			14.41	4.46		
6.86	4.55			14.49	4.53		
6.93	4.63			14.51	4.59		
6.96	4.67			14.65	4.66		
6.99	4.71			14.71	4.72		
7.02	4.75			14.79	4.79		
7.07	4.82			14.87	4.85		
7.09	4.87			14.91	4.89		
7.17	4.95			15.00	4.97		
7.21	4.99			15.05	4.9505		
7.28	5.078			15.16	5.14		
7.36	5.123			15.23	5.22		
7.37	5.18			15.26	5.27		

Titration Data

Reaction no. 4  
 Titrations:  
 Aliquot Volume 25ml

Date: 18/06/2007  
 NaOH conc 1N

Analyst: Ronelle

Sample: 3				Sample: 4			
Vol (ml)	pH	Vol (ml)	pH	Vol (ml)	pH	Vol (ml)	pH
0.00	0.95	8.33	4.57	0.00	0.91	15.35	8.188
0.21	0.91	8.37	4.63	1.15	0.63	15.40	7.52
0.49	0.87	8.42	4.68	8.81	0.97	15.43	10.27
0.79	0.81	8.48	4.81	8.85	1.01	15.46	10.72
1.30	0.73	8.52	4.87	9.24	1.06	15.53	11.21
2.08	0.75	8.56	4.93	4.55	1.09	15.58	11.37
		8.60	5.01	7.68	1.10	15.61	11.46
+0.23	0.79	8.68	5.16	10.15	1.16	15.65	11.59
0.19	0.83	8.72	5.25	10.35	1.18	15.69	11.60
1.18	0.87	8.76	5.35	10.60	1.20	15.73	11.66
1.65	0.90	8.79	5.46	11.09	1.26	15.81	11.74
2.43	0.96	8.83	5.57	11.356	1.31	15.88	11.82
3.03	1.01	8.87	5.72	11.96	1.387	16.00	11.92
3.71	1.09	8.90	5.74	12.15	1.40	16.08	11.96
3.89	1.12	8.95	6.37	12.48	1.477	16.16	12.02
4.45	1.20	8.98	6.7.16	12.70	1.51	16.30	12.08
4.69	1.23	9.01	8.27	12.97	1.58	16.47	12.14
5.14	1.30	9.06	9.37	13.09	1.62	16.68	12.21
5.66	1.37	9.10	10.06	13.32	1.7269	16.84	12.25
5.85	1.44	9.14	10.61	13.36	1.72	17.15	12.33
6.14	1.51	9.18	10.94	13.49	1.74	17.47	12.39
6.29	1.56	9.22	11.16	13.65	1.882	17.71	12.43
6.55	1.65	9.27	11.33	13.77	1.88		
6.67	1.70	9.30	11.43	13.89	1.95		
6.79	1.73	9.35	11.53	13.98	2.01		
6.92	1.79	9.42	11.66	14.06	2.08		
7.02	1.86	9.47	11.71	14.15	2.16		
7.07	1.90	9.51	11.74	14.22	2.25		
7.16	1.96	9.55	11.82	14.30	2.34		
7.24	2.03	9.66	11.88	14.33	2.40		
7.31	2.10	9.73	11.94	14.37	2.47		
7.39	2.19	9.77	11.97	14.41	2.56		
7.44	2.25	9.89	12.03	14.44	2.65		
7.51	2.37	10.03	12.10	14.48	2.78		
7.55	2.44	10.21	12.16	14.52	2.94		
7.59	2.54	10.43	12.23	14.56	3.14		
7.63	2.66	10.73	12.31	14.59	3.36		
7.67	2.80	11.00	12.37	14.64	3.61		
7.71	2.46	11.24	12.41	14.67	3.81		
7.74	3.12	11.32	12.43	14.72	3.99		
7.78	3.330			14.76	4.16		
7.82	3.46			14.81	4.28		
7.88	3.62			14.84	4.40		
7.92	3.75			14.88	4.51		
7.96	3.86			14.93	4.63		
7.99	3.96			14.97	4.74		
8.03	4.04			15.02	4.86		
8.06	4.12			15.06	4.97		
8.10	4.19			15.09	5.08		
8.14	4.25			15.12	5.20		
8.17	4.32			15.17	5.37		
8.21	4.38			15.22	5.57		
8.26	4.45			15.26	5.71		
8.30	4.51			15.30	6.68		

Titration Data

Reaction no. 4 Date: 12/06/2007 Analyst: Rozelle  
 Titrations: \_\_\_\_\_  
 Aliquot Volume 25ml NaOH conc 1N

Sample: 5				Sample: 6			
Vol (ml)	pH	Vol (ml)	pH	Vol (ml)	pH	Vol (ml)	pH
0.00	1.03	11.94	11.93	6.00	6.94	9.11	11.94
4.07	0.91	12.10	12.00	6.17	6.96	9.27	12.04
7.34	0.99	12.26	12.08	7.93	6.85	9.50	12.13
9.84	1.07	12.46	12.16			9.80	12.23
5.54	1.13	12.60	12.21	7.82	6.98	10.20	12.31
6.57	1.21	12.76	12.29	4.53	1.26	10.61	12.38
7.35	1.28	13.31	12.35	4.56	1.29	10.83	12.41
8.02	1.37	13.67	12.42	4.66	1.32		
8.37	1.43	13.84	12.44	4.99	1.39		
8.71	1.50			5.25	1.42		
9.00	1.56			5.56	1.46		
9.31	1.66			5.83	1.51		
9.52	1.72			6.18	1.58		
9.72	1.79			6.43	1.64		
9.84	1.83			6.62	1.69		
9.95	1.90			6.78	1.75		
10.08	1.98			6.95	1.83		
10.19	2.07			7.15	1.90		
10.28	2.14			7.27	1.98		
10.37	2.24			7.39	2.06		
10.46	2.37			7.51	2.17		
10.53	2.53			7.65	2.20		
10.58	2.63			7.63	2.28		
10.61	2.76			7.72	2.39		
10.65	2.91			7.76	2.45		
10.68	3.08			7.80	2.54		
10.73	3.41			7.84	2.64		
10.77	3.69			7.88	2.75		
10.80	3.92			7.92	2.91		
10.85	4.12			7.97	3.11		
10.89	4.30			8.01	3.42		
10.93	4.47			8.05	3.73		
10.96	4.62			8.10	4.05		
11.00	4.75			8.12	4.26		
11.03	4.91			8.16	4.45		
11.07	5.10			8.19	4.61		
11.11	5.28			8.23	4.77		
11.15	5.57			8.26	4.98		
11.20	5.81			8.31	5.22		
11.24	6.11			8.34	5.53		
11.27	6.40			8.38	5.80		
11.31	6.80			8.41	6.78		
11.37	10.49			8.45	8.89		
11.40	10.90			8.49	9.96		
11.43	11.10			8.55	10.66		
11.46	11.26			8.58	11.06		
11.51	11.40			8.61	11.25		
11.55	11.49			8.66	11.40		
11.59	11.58			8.71	11.50		
11.64	11.65			8.74	11.58		
11.72	11.74			8.78	11.64		
11.76	11.78			8.86	11.74		
11.82	11.84			8.94	11.83		
11.90	11.90			9.03	11.88		

## APPENDIX F: STATISTICAL ANALYSIS

The hypothesis to be tested is:

$$H_0: \mu_1 = \mu_2 = \dots = \mu_{12} = 0$$

$$H_1: \mu_{ij} \neq 0 \text{ for at least one } j$$

If  $H_0$  were rejected, it would mean that at least one of the factors or the interaction effect would be greater than zero and therefore significant.

$$SS_A = \frac{a \sum_{i=1}^a \left( \sum_{j=1}^b y_{ij} \right)^2 - \left( \sum_{i=1}^a \sum_{j=1}^b y_{ij} \right)^2}{a \cdot b \cdot n}$$

$$SS_B = \frac{b \sum_{j=1}^b \left( \sum_{i=1}^a y_{ij} \right)^2 - \left( \sum_{i=1}^a \sum_{j=1}^b y_{ij} \right)^2}{a \cdot b \cdot n}$$

$$SS_I = \frac{a \cdot b \sum_{i=1}^a \left( \sum_{j=1}^b y_{ij}^2 \right) - \left( \sum_{i=1}^a \sum_{j=1}^b y_{ij} \right)^2}{a \cdot b \cdot n} - SS_A - SS_B$$

In the above equations:  $SS$  is the sum of squares

$y_{ij}$  is the yield for a given acid concentration (i) and temperature (j)

$a$  is the number of acid conditions tested (in this case 4)

$b$  is the number of temperature conditions tested (in this case 3)

$n$  is the number of replicates at each condition (in this case 1)

Since there are only replicates of some of the data points, a separate matrix was formed to determine the sum of squares of errors and the total sum of squares. These two values were determined from the following two equations:

$$SS_E = \sum_i \sum_k^n \left( yR_{ik} - \overline{yR}_i \right)^2$$

$$SS_T = \sum_i \left( \overline{yR}_i - \overline{\overline{yR}} \right)^2$$

where  $\overline{yR}_i$  is the average of the replicates for a particular set of conditions

And  $\overline{\overline{yR}}$  is the average of all values in the replicate matrix.

From this

$$F_o = \frac{SS_T/v_1}{SS_E/v_2} = \frac{MS}{MS_E}$$

The  $F_0$  test statistic was then compared to  $F_{\alpha, v_1, v_2}$  where  $\alpha$  is the level of significance i.e. the probability of rejecting a true null hypothesis;  $v_1$  is the numerator degrees of freedom and  $v_2$  is the denominator degrees of freedom which may be calculated as follows:

$$v_1 = a - 1 \text{ or } b - 1$$

$$v_2 = a(n - 1) \text{ or } b(n - 1)$$

If the  $F_0$  test statistic was found to be greater than  $F_{\alpha, v_1, v_2}$  the  $H_0$  could be rejected and this would indicate that the factor in question was significant.

## APPENDIX G: MATLAB CODES FOR MODELLING

```

close all; clear all

format short e

global MB MF MA MW MH P R n0_B Ct0 q0 F0 n0_B a VS0 VB0 VG k1 K k2 k3
C q SG SS runs
global t cF_pred cF_exp cA_pred cA_exp cH_pred cH_exp aH_exp k10 K0
k20 k30 E1R DHR E2R E3R rhoB

% Runs chosen for parameter estimation
runs = [1:19]; % Here, for example, all the runs were included

est = input('Estimation (yes=1, no=0): ');
if ~est,
    load model % the last best estimated parameters are loaded for
the results viewing
end

% Starting point for the parameter estimation
% This can be modified but some care is advised (typically, no more
than 1-2 parameters at a time)
k10 = 300;
K0 = 2500;
k20 = 30;
k30 = 0.25;
E1R = 2000;
DHR = 200;
E2R = 3000;
E3R = 8000;

R = 8.314;

MF = 96.09;
MA = 60.05;
MW = 18.02;
MH = 36.461;
MB = 165.049;

species = ['Pentosan (B) ',
          'B-HCl complex',
          'P-HCl complex',
          'Furfural ',
          'Acetic acid ',
          'Water ',
          'HCl '];

data

P = 1.01325e5;

rhoB = 1443; % kg/m3, mass density of raw material
rhoW = 0.5091; % kg/m3, mass density of superheated steam at 1 bar
and T

```

```

% Mean particle dimensions [m]
dp0 = 605e-6;
r0 = dp0/2;
Lp = 9.5/1000;

% Initial mass of solids [kg]
m0 = 0.018;
% Initial amount of pentosan [kmol]
n0_B = 0.286*m0/MB;

% Volume of solids [m3]
VS0 = m0/rhoB;
VB0 = 0.286*VS0;

D = 0.05; % Reactor bed diameter, m
L = 0.1; % Reactor bed length, m
a = 3400; % Specific particle surface area, m2/m3
e = 0.32; % Bed porosity

% Stoichiometry matrices
SG = [ 0 0 1
       0 0.74 0
       0 -1.74 3
       -1 0 1 ];

SS = [-1 0 0
       1 -1 0
       0 1 -1 ];

if est,
    par0 = [k10, K0, k20, k30, E1R, DHR, E2R, E3R ];
    par = fminsearch('index', par0)
    %par = [-37.01, 1624, 24.63, 350.5, 23461, 1224, -8.6225, -3717];

    % par_min = 1e-4*par0; par_min(6) = -100000;
    % par_max = 1e4*par0; par_max(6) = 100000;
    % par = fmincon('index', par0, [], [], [], [], par_min, par_max)
end

I = index(par)
m = 3; f = 0;
MS = 18;
for j=1:length(runs),
    i = runs(j);
    s = num2str(i);
    if i<10,
        s = ['0', s];
    end
    eval(['Sample = Samples_', s, ';'])
    t = Sample(:,1); % hour

    if m==3,
        f = f+1;
        figure(f)
        clf
        set(gcf, 'Position', [1, 31, 1280, 694])
        m = 1;
    end
    subplot(2,3,3*(m-1)+1)
    plot(t, cF_pred(j,:), '.g', 'MarkerSize', MS)

```



```

hold on
plot(t, cF_pred(j,:), '-k')
plot(t, cF_exp(j,:), '.r', 'MarkerSize', MS)
plot(t, cF_exp(j,:), '-k')
xlabel('Sampling time [h]')
ylabel('Furfural [g/L]')
title(['Run # ', num2str(i)])

subplot(2,3,3*(m-1)+2)
plot(t, cA_pred(j,:), '.g', 'MarkerSize', MS)
hold on
plot(t, cA_pred(j,:), '-k')
plot(t, cA_exp(j,:), '.r', 'MarkerSize', MS)
plot(t, cA_exp(j,:), '-k')
xlabel('Sampling time [h]')
ylabel('Acetic acid [g/L]')
title(['Run # ', num2str(i)])

subplot(2,3,3*(m-1)+3)
plot(t, cH_pred(j,:), '.g', 'MarkerSize', MS)
hold on
plot(t, cH_pred(j,:), '-k')
plot(t, cH_exp(j,:), '.r', 'MarkerSize', MS)
plot(t, cH_exp(j,:), '-k')
xlabel('Sampling time [h]')
ylabel('HCl [g/L]')
title(['Run # ', num2str(i)])
m = m+1;
end

m = length(runs);
figure(ceil(m/2)+2)
clf
set(gcf, 'Position', [1, 31, 1280, 724])
for i=1:m,
    s = num2str(runs(i));
    h(i) = uicontrol('style', 'pushbutton', 'position', [30, 30+35...
*(i-1), 30, 30],...
    'string', s, 'callback', ['Run = ', s, ';
simula']);
end

```

```

function I = index(par)

global exptl MB MF MA MW MH P R n0_B Ct0 q0 F0 k1 K k2 k3 C q runs
global t cF_pred cF_exp cA_pred cA_exp cH_pred cH_exp aH_exp k10 K0
k20 k30 E1R DHR E2R E3R

data

k10 = par(1);
K0 = par(2);
k20 = par(3);
k30 = par(4);
E1R = par(5);
DHR = par(6);
E2R = par(7);
E3R = par(8);

I = 0;
I1 = [];
for jj=1:length(runs),
    i = runs(jj);
    tC = Operas(i,1);           % °C
    G = Operas(i,2);           % kg/hour
    a0_H = Operas(i,3);        % mass percent
    T = tC+273.15;
    s = 1/T-1/298.15;
    k1 = k10*exp(-E1R*s);
    K = K0*exp(-DHR*s);
    k2 = k20*exp(-E2R*s);
    k3 = k30*exp(-E3R*s);

    s = num2str(i);
    if i<10,
        s = ['0', s];
    end
    eval(['Sample = Samples_', s, ';'])
    t = Sample(:,1);           % hour
    VL = Sample(:,2);          % mL
    cF_exptl = Sample(:,3);    % g/L
    cA_exptl = Sample(:,4);    % g/L
    cH_exptl = Sample(:,5);    % mass percent
    N(i) = length(t);

    % Inlet flow rates [kmol/h]:
    F0_W = (1-a0_H/100)*G/MW;
    F0_H = (a0_H/100)*G/MH;%a0_H/(100-a0_H)*G/MH;
    Ftot0 = F0_W+F0_H;
    y0_H = F0_H/Ftot0;

    % Total molar gas concentration [kmol/m3]
    Ct0 = P/(1000*R*(tC+273.15));

    % Inlet vol. flow rate of feed [m3/h]
    q0 = Ftot0/Ct0;

    % Initial conditions [kmol/m3]
    F0 = [0; 0; F0_W; F0_H];

```

```

% Numerical integration of ODEs using a variable-order method
% for stiff ODEs: Shampine & Reichelt, SIAM J. Sci. Comput,
18, 1 (1997)
% - Max. size of the integration step [h]
hmax = 0.01;
% - Integration tolerance
tol = 1e-7;
opt = odeset('MaxStep', hmax, 'RelTol', tol);
u0 = [n0_B, zeros(1,6)];
[t1, u1] = ode15s('balances', [0, t'], u0, opt);
for j=1:length(t1),
    RHS = balances(t1(j), u1(j,:));
    Cplot(j,:) = C';
    qplot(j) = q;
end
XB = 100*(n0_B-u1(:,1))/n0_B; % percent
nF = u1(2:end,4)-u1(1:end-1,4); % kmol
cF = 1e6*MF*nF./VL; % g/L
nA = u1(2:end,5)-u1(1:end-1,5); % kmol
cA = 1e6*MA*nA./VL; % g/L
nH = u1(2:end,7)-u1(1:end-1,7); % kmol
cH = 1e6*MH*nH./VL; % g/L

dcF = (cF-cF_exptl)/mean(cF_exptl);
dcA = (cA-cA_exptl)/mean(cA_exptl);
dcH = (cH-cH_exptl)/mean(cH_exptl);
I1(jj) = dcF'*dcF+dcA'*dcA+dcH'*dcH;
I = I+I1(jj);
cF_pred(jj,:) = cF';
cA_pred(jj,:) = cA';
cH_pred(jj,:) = cH';
cF_exp(jj,:) = cF_exptl';
cA_exp(jj,:) = cA_exptl';
cH_exp(jj,:) = cH_exptl';
end
I = sqrt(I/sum(N));

figure(ceil(length(runs)/2)+1)
clf
set(gcf, 'Position', [1, 31, 1280, 694])

shy = 0.15;
h = subplot(1,3,1);
po = get(h, 'Position');
set(h, 'Position', po+[0,shy,0,0])
plot(cF_exp, cF_pred, '.r', 'MarkerSize', 16)
hold on
axis([0, 25, 0, 25]);
v = axis;
plot(v(1:2), v(3:4), '-k')
axis('square')
xlabel('Furfural, exptl. [g/L]')
ylabel('Furfural, pred. [g/L]')
h = text(0, 31, ['I = ', num2str(I)]);
set(h, 'Color', 'b', 'FontWeight', 'demi', 'FontSize', 14)

h = subplot(1,3,2);
po = get(h, 'Position');
set(h, 'Position', po+[0,shy,0,0])
plot(cA_exp, cA_pred, '.b', 'MarkerSize', 16)
hold on

```

```

axis([0, 10, 0, 10]);
v = axis;
plot(v(1:2), v(3:4), '-k')
axis('square')
xlabel('Acetic acid, exptl. [g/L]')
ylabel('Acetic acid, pred. [g/L]')
s = setstr(10);
h = title(['k_{10} = ', num2str(k10), ';   K_0 = ', num2str(K0), ';
k_{20} = ', num2str(k20), ...
          ';   k_{30} = ', num2str(k30), ';   E_1/R = ',
num2str(E1R), ';   DH/R = ', num2str(DHR), ...
          ';   E_2/R = ', num2str(E2R), ';   E_3/R = ',
num2str(E3R), s]);

h = subplot(1,3,3);
po = get(h, 'Position');
set(h, 'Position', po+[0,shy,0,0])
plot(cH_exp, cH_pred, '.g', 'MarkerSize', 16)
hold on
axis([0, 30, 0, 30]);
v = axis;
plot(v(1:2), v(3:4), '-k')
axis('square')
xlabel('HCl, exptl. [g/L]')
ylabel('HCl, pred. [g/L]')

for i=1:length(runs),
    if i==1,
        aa = num2str(runs(i));
    else
        aa = str2mat(aa, num2str(runs(i)));
    end
end
h = axes('Position', [0.13 0.06 0.775 0.32]);
bar(1:length(runs), 100*I1/sum(I1))
ylabel('Contribution to total error, %', 'FontSize', 12)
colormap(cool)
set(h, 'XTick', 1:length(runs))
set(h, 'XTickLabel', aa)
drawnow

if all(par([1:5,7:8])>0),
    save model par
end

```

```

function RHS = balances(t, n)

    global Ct0 q0 F0 n0_B a VS0 VB0 VG k1 K k2 k3 C q SG SS MB rhoB

    % Solid-phase components, kmol
    % n(1) - Pentosan (B)
    % n(2) - B-HCl complex
    % n(3) - P-HCl complex (P - pentose)

    % Gas-phase components, kmol
    % n(4) - total collected furfural
    % n(5) - total collected acetic acid
    % n(6) - total collected water
    % n(7) - total collected HCl

    % Gas-phase components, kmol/m3
    % C(1) - Furfural
    % C(2) - Acetic acid
    % C(3) - Water
    % C(4) - HCl

    ntot = sum(n(1:3));
    VB = ntot*MB/rhoB;
    VS = VS0-VB0+VB;

    c_B = max([0, n(1)/VS]);
    c_BH = max([0, n(2)/VS]);
    c_PH = max([0, n(3)/VS]);

    L1 = [ 0      0      0      k1*c_B
           0      0      k2*c_BH  0
           0      0      0      0      ];

    L0 = [ -k1/K*c_BH;  0;  k3*c_PH];

    q = q0;
    while 1,
        C = inv(q*eye(4)-SG*L1*VS)*(F0+SG*L0*VS);
        r = L1*C+L0;
        RG = SG*r;
        q1 = q0+sum(RG)*VS/Ct0;
        if abs((q1-q)/q1)<1e-9,
            q = q1;
            break
        end
        q = q1;
    end
    C = inv(q*eye(4)-SG*L1*VS)*(F0+SG*L0*VS);
    r = L1*C+L0;
    RG = SG*r;
    RS = SS*r;
    RHS = [RS*VS; C*q];

```

## APPENDIX H: INITIAL MODEL DEVELOPMENT

### Physical Description of the Process

A stream of superheated hydrogen chloride and steam entered from the top of the reactor. The reactor itself consists of a haphazardly packed bed of needle shaped oat hulls consisting of structural components (lignin) and pentosan chains. The pentosan monomers in the pentosan chain reacted with the steam to produce free pentose molecules. The pentose molecules were then converted to furfural by a complex dehydration mechanism. Both the hydrolysis and the dehydration appear to be catalysed by the HCl (as is assumed to be the case in the liquid phase). The occurrence of side reactions cannot be excluded between the intermediate products of the dehydration step as well as reactions of the furfural and the intermediate products with the lignin.

### The unreacted core model

The needle shaped particles are approximated by thin cylinders. All particles are assumed to be identical (uniform particle size distribution). The reaction is assumed to take place only at the reaction front which the boundary separating the fresh unreacted solid material from the residual material that has already reacted. At any moment two distinct regions can be defined within the particle: one area in which the reaction has already taken place called the 'ash layer' and another unreacted area called the 'unreacted core'. The ash layer contains no solid reactant (pentosan) while the inner core contains no reaction product (pentose). A model of this nature is commonly referred to as the unreacted core model.

### Reaction-Diffusion Model of the Ash Layer

The ash layer is the zone which requires mathematical modelling in order to determine the water concentration at the reaction front. Initially the ash layer does not exist as no reaction has occurred and therefore for the first instant the water molecules instantaneously reach the unreacted material and react with pentosan. The result of the reaction is a net generation of water which therefore begins to diffuse back to the gas phase through the newly formed ash layer. It is assumed that both diffusion and ash layer formation occur in the radial direction only and that axial effects can be neglected. This assumption is due to a large height-to-diameter aspect ratio. A diagrammatic description of the process in the particle is given below:

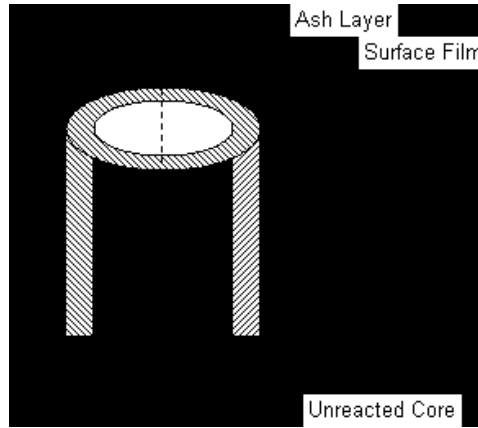


**Figure: Unreacted Core Model**

The radial diffusion of water is assumed to obey the first Fick's Law:

$$N_w = -D_w \frac{dC_w}{dr} \quad 48$$

where  $N_w$  is the molar flux of water and

$D_w$  is the diffusivity of water through the ash which is assumed to be porous

As the time constant for the diffusion process is very much smaller than that of the overall reaction, the diffusion process may be assumed to reach steady-state despite the overall reaction being an unsteady-state process and therefore a steady state mass balance equation may be developed as follows:

$$(2\pi r L N_w)_r - (2\pi r L N_w)_{r+dr} = 0 \quad 49$$

Then if one divides by  $dr$  and takes the limit as  $dr \rightarrow 0$ , equation 49 becomes:

$$\frac{d(rN_w)}{dr} = 0 \quad 50$$

If one applies Fick's Law (Equation 48) to Equation 50:

$$\frac{d}{dr} \left( r \frac{dC_w}{dr} \right) = 0 \quad 51$$

Equation 51 has to satisfy the following boundary conditions:

1. At the particle surface, where  $r = r_0$ , there is an interface between the gas surface film and the particle and the boundary condition is defined by the process of gas transfer through the film:

$$-D_W \left. \frac{dC_W}{dr} \right|_{r=r_0} = k_{gW} (C_W(r_0) - C_{W,g}) \quad 52$$

2. Then at the ash-core interface where  $r = r_c$ , the water is produced by the reaction and the boundary condition becomes:

$$-D_W \left. \frac{dC_W}{dr} \right|_{r=r_c} = R_W(r_c) = 2k_1(C_H)C_W(r_c) \quad 53$$

The subscript 'g' refers to the conditions in the bulk gas phase and  $k_{gW}$  is the gas phase mass transfer coefficient [m/s] for water.

The analytical solution to this two point boundary value problem is given in dimensionless form:

$$y(x_c) = 1 + \frac{Sh \ln x - 1}{1 - Sh \ln x_c - \frac{\alpha}{x_c}} \quad 54$$

where:

$$x = \frac{r}{r_0} \quad (\text{dimensionless radius}) \quad 55$$

$$y = \frac{C_W}{C_{Wg}} \quad (\text{dimensionless water concentration}) \quad 56$$

$$Sh = \frac{k_{gW} \cdot r_0}{D_W} \quad (\text{Sherwood number}) \quad 57$$

$$\alpha = \frac{k_{gW}}{2k_1(C_H)} \quad 58$$

The value of  $y$  at  $r = r_c$  ( $x = x_c$ ) is the value that is of particular interest:

$$y(x_c) = \frac{\alpha}{x_c Sh \ln x_c - x_c + \alpha} \quad 59$$



## APPENDIX I: DIFFUSION CALCULATION

The mass transfer coefficient for the bed was determined using the following correlation (Seader and Henley, 1998) for flow through a bed of spheres and utilising the equivalent spherical diameter to account for the needle shaped particles:

$$N_{Sh} = \frac{k_g D_e}{D_A} = 2 + 1.1 N_{Re}^{0.6} N_{Sc}^{1/3}$$

where: 
$$N_{Re} = \frac{D_e G}{\mu} \quad \text{(Reynolds Number)}$$

$$N_{Sc} = \frac{\mu}{\rho D_A} \quad \text{(Schmidt Number)}$$

$k_g$  is the gas phase mass transfer coefficient [m/s]

$D_e$  is the equivalent spherical diameter [m]

$D_A$  is the Diffusivity of component A (water) [m<sup>2</sup>/s]

$G$  is the superficial gas mass velocity [kg/(m<sup>2</sup>s)]

$\mu$  is the viscosity of the gas phase [Pa.s]

$\rho$  is the density of the gas phase [kg/m<sup>3</sup>]

The equivalent spherical diameter is determined as:

$$D_e = \phi D_p$$

In this equation  $\phi$  is the sphericity of the particle which is defined as the ratio of the surface area of a sphere of the same volume as the particle to the surface area of the particle.  $D_p$  is the diameter of the particle.

In order to solve this equation for the mass transfer coefficient, the diffusivity,  $D_{AB}$ , in the gas phase can be determined from the empirical equation developed by Fuller et al (1966):

$$D_{AB} = D_{BA} = \frac{0.00143T^{1.75}}{PM_{AB}^{1/2} \left[ \left( \sum v_A \right)^{1/3} + \left( \sum v_B \right)^{1/3} \right]^2}$$

where:  $D_{AB}$  is in cm<sup>2</sup>/s

$P$  is in atm

$T$  is in K

$$M_{AB} = \frac{2}{\left(\frac{1}{M_A}\right) + \left(\frac{1}{M_B}\right)}$$

$M_i$  is the molar mass of component  $i$

And  $\sum_v$  is the summation of atomic and structural diffusion volumes from tables

If one inputs the values for the HCl water system at 1 atm and a temperature of 160°C, the equation for  $D_{AB}$  becomes:

$$D_{AB} = D_{BA} = \frac{0.00143(160 + 273.15)^{1.75}}{(1) \left( \frac{2}{\frac{1}{18.02} + \frac{1}{36.461}} \right)^{1/2} \left[ (9.44)_{A}^{1/3} + (21.48)_{B}^{1/3} \right]^2} = 6.97 \cdot 10^{-5} \text{ m}^2 / \text{s}$$

The sphericity of the particles was determined to be 0.35 for the particles:

$$D_e = (0.35)(614 \cdot 10^{-6}) = 2.15 \cdot 10^{-4}$$

The Reynolds and Schmidt numbers could be evaluated:

$$N_{Re} = \frac{(1.82 \cdot 10^{-4})(0.011)}{(1.46 \cdot 10^{-5})} = 0.16$$

$$N_{Sc} = \frac{(1.46 \cdot 10^{-5})}{(0.51)(6.97 \cdot 10^{-5})} = 0.41$$

Using all these values to input into the Sherwood number correlation resulted in a Sherwood number of 2.27.

Solving the Sherwood number equation for  $k_{gW}$  resulted in:

$$k_{gW} = \frac{N_{Sh} \cdot D_A}{D_e} = \frac{(2.25)(6.97 \cdot 10^{-5})}{(1.82 \cdot 10^{-4})} = 0.74 \text{ m} / \text{s}$$

## APPENDIX J: MODEL RESULTS – PROFILES FOR EACH RUN

